A New Design of the University of Manitoba Cyclotron for D^- ion Acceleration and A Study for the Beam Extraction from the Princeton University AVF Cyclotron

by

YUNXIANG HUANG

A thesis submitted to the Faculty of Graduate Studies of the University of Manitoba in partial fulfillment of the requirements of the degree of

DOCTOR OF PHILOSOPHY

ISBN 0-315-47942-6

A NEW DESIGN OF THE UNIVERSITY OF MANITOBA CYCLOTRON FOR D⁻ion ACCELERATION AND A STUDY FOR THE BEAM EXTRACTION FROM THE PRINCETON UNIVERSITY AVF CYCLOTRON

BY

YUNXIANG HUANG

A thesis submitted to the Faculty of Graduate Studies of
the University of Manitoba in partial fulfillment of the requirements
of the degree of

DOCTOR OF PHILOSOPHY

Synopsis

Two independent cyclotron upgrading projects are treated separately: a redesign of the University of Manitoba cyclotron for D^- ion acceleration and a study of the beam extraction from the Princeton University AVF cyclotron. These two projects are described in part 1 and part 2 of this thesis, respectively.

The first part includes an analysis of the magnetic field mapping data that was previously obtained from the University of Manitoba cyclotron, as well as systematic beam orbit dynamics study based on the improved magnetic field and the newly designed central dee-tips for D^- ion acceleration. These studies show that after the upgrade program is finished, it will be possible to obtain in the University of Manitoba cyclotron a D^- ion beam with substantial improvement in the available maximum energy, beam quality and transmission efficiency.

The second part of this thesis first describes the extensive modifications that were made in the computer program that was previously used. The modified program can now be used over the full energy range of an AVF cyclotron. Then the upgraded computer code is utilized to carry out simulative calculation for the reference particle and the beam in phase space, from the ion source through the electro-static deflector of the Princeton University AVF cyclotron. On the basis of these studies, all the parameters for the extraction system are optimized, and suggestions for further improvements are proposed.

Acknowledgements

Although only one name appears on the title page of this dissertation, a number of other people contributed to this work in very substantial ways, both technical and non-technical.

Most importantly, I shall always be extremely grateful to my advisor, Professor Saewoong Oh for his infinite encouragement and guidance. Professor Oh taught me very much about accelerator physics. He was a very thoughtful and very kind teacher and I have benefited greatly in very many ways by working with him during the past four years. Dr. Moohyun Yoon was extremely helpful, enthusiastic, as well as generous in sharing his knowledge. I am very grateful to Dr. Yoon for all his assistance and friendship.

For their constant and generous help during all the years of my stay at the University of Manitoba, I am grateful to all the members of the machine development group of the cyclotron laboratory: Professor J.S.C. McKee of the Director of the Cyclotron Laboratory, Mr. Irv Gusdal, Vladimir Drenchuk, Jim Anderson and their other colleagues. Dr. Tony Smith spent much time to introduce me to the VAX/750 computer; I would like to thank him deeply.

I was fortunate to have the chance to participate in the upgrading program of the Princeton University cyclotron. I am very grateful to Professor Frank Calaprice and Professor Arthur McDonald for providing me with this opportunity and for supporting me during my stay at the Princeton University. I also obtained a great deal of very valuable assistance from Dr. Richard Kouzes, who not only helped me to master the Data General MV 10000 Computer but also read carefully the second part of this thesis and suggested many improvements. Dr. Yitzhak Sharon spent a lot of time in reading the original manuscript of this thesis and in further improving my English. He also gave me other advice whenever it was needed. Therefore, I would like to thank him. The late Dr. William Moore, as well as Steve Kidner and Fred Loeser, have all been most helpful in familiarizing me with the intricacies of the Princeton cyclotron.

Finally, I wish to express my deepest and warmest gratitude to my wife, Shuzhen Li. While I was writing this thesis, she single-handedly took care of the entire housework and also assisted very greatly with the dissertation drawings and typing, in addition to her own research work in the Biochemistry Department of the Princeton University.

Table of Contents

Part II A Design Study for the Beam Extraction from the Princeton University AVF Cyclotron

Chapter

Introduction

The principle of the cyclotron was proposed in 1930 by Ernest O. Lawrence of the University of California ([LAW30]). In 1932, Lawrence and Livingston in their paper described the first prototype model which produced a proton beam of over 1 MeV energy at the Berkeley Laboratory. This early success stimulated interest in many laboratories around the world, hence more cyclotrons were built during the next two decades.

However, the conventional cyclotron is limited in energy by contradictory requirements on the magnetic field. To provide beam stability (focusing) along the direction of the magnetic field (axial direction), the field must decrease with radius. But to keep the beam in phase with a constant frequency accelerating voltage on the dees, the field must increase with radius to compensate for the relativistic increase in the mass of particles.

The discovery of phase stability by Veksler and McMillan in 1945 allowed the phase requirements to be satisfied by modulating the frequency of the accelerating voltage. A magnetic field fall-off is introduced in this "synchrocyclotron" to provide axial focusing. This principle has been used to accelerate protons up to energies of 700 MeV at the University of California. Unfortunately, the duty cycle in this type of machine is only about 1% of that of the conventional fixed-frequency cyclotron.

An alternate solution to the energy limitation was proposed by Thomas in 1938 ([THO38]). He suggested that the phase requirement be satisfied by having the average magnetic field increase with radius. A new type of axial focusing would be provided by an azimuthally varying magnetic field (AVF). This would more

than compensate for the defocusing due to the increasing average field. In the 1950's several "Thomas cyclotron" were built at Berkeley and Los Alamos. This demonstrated that for protons, the Thomas principle could be used to increase the energy of fixed-frequency cyclotrons from 20 MeV up to several hundred MeV. Another suggestion, made in 1955 by Kerst ([KER55]), was that spiral sectors of strong magnetic field would give more axial focusing than the straight sectors, and therefore a spiral-ridge cyclotron emerged.

Since the 1950's, the advent of the relativistic cyclotron gave an impetus to build new cyclotrons in many laboratories around the world. The University of Manitoba cyclotron and the Princeton University cyclotron (whose upgrading studies form the two main constituents of this thesis) were built in the early and in the late 1960's, respectively. From then until the present time, they have been continuously devoted to fundamental subatomic physics investigations.

In the two decades that have passed since these two cyclotrons were built, there has been a significant advance in cyclotron technology, progress that was in part due to the appearance of solid-state electronic devices and the emergence of powerful computers. The solid-state based instrumentation made it possible to carry out precise mappings and analyses of the cyclotron magnetic field. The powerful new generation of computers enabled one to calculate the RF electric field distribution inside a cyclotron and then to trace particle trajectories from the ion source to the extraction radius, under the influence of this calculated electric field and the measured magnetic field. The accuracy of these calculations is much better than what could be obtained at the time when these first-generation AVF cyclotrons became operational.

In a separate development, nuclear physics experiments became more and more sophisticated during the same time span, resulting in a need for beams of higher intensity and better quality. In response to this demand, together with the availability of enormously more advanced cyclotron technology in the 1980's, many laboratories around the world began to embark upon ambitious upgrading programs for their cyclotrons.

The University of Manitoba Cyclotron Laboratory was no exception. In fact, members of the machine development group at this laboratory started investigating the possibility of such an upgrading as early as 1976, when they carried out exploratory magnetic field mappings. Later, in 1982, more elaborate field mappings [DER83] based on computer-aided technology were performed with much higher precision. The result was quite encouraging; it convinced them that a substantial improvement in beam quality would be achieved by upgrading the cyclotron. This finally led to a decision to initiate an extensive and intensive improvement program for the cyclotron, a project which was started in 1984. The author was engaged in design studies for a new central region of the cyclotron for the acceleration of D^- ions, and in a beam dynamic investigation based on this new central region geometry.

The Princeton University AVF Cyclotron Laboratory also turned its attention to the type of improvements described earlier. A proposal to upgrade the facility has been submitted to the National Science Foundation. The objective of the modifications to the existing accelerator system is to provide beams of a wider variety, with substantial improvements in intensity and energy resolution.

For this purpose, a design of a new central region of the accelerator has been

developed by Professor Oh and Dr. Yoon. The design, coupled with a new design study of the extraction system as well as improvements to the power supply system and the use of a higher dee voltage, is expected to enhance beam intensity by about a factor of four. This also enables single turn extraction to be accomplished, providing the excellent energy resolution and brightness needed for high resolution experiments.

The initial beam dynamics study by Professor Oh and Dr. Yoon was limited to the central region. The author's task was to extend the above study to the full energy range of the accelerator and to carry out a redesign investigation of the beam extraction system.

This thesis consists of two independent parts under the following headings:

(1) A redesign of the University of Manitoba cyclotron for the acceleration of D^- ions, and,

(2) A study of beam extraction from the Princeton University AVF cyclotron.

The first part begins with a brief historical background of the University of Manitoba cyclotron is presented. Then the magnetic field analysis before and after the upgrading program is given. It is then followed by comprehensive investigations of the particle dynamics of the D^- ions in the newly designed central region based on the improved magnetic field. This part contains an introduction to the electric field distribution calculation, determinations of some important engineering parameters, an inspection of the beam stability in both radial and axial motions, and finally a computer simulation study of positive beam extraction from the cyclotron. This part concludes with a presentation of the expected improvement in performance of

the cyclotron for the acceleration of D^- ions after the upgrade.

The second part of this thesis deals with the upgrading program of the Princeton University cyclotron. It starts with an introduction to the Princeton University cyclotron, followed by a description of the modifications of the old computer programs. These modifications were necessary for the project. Considerable amount of space in connection with the new design, is devoted to the discussion of the investigation of the beam extraction system. Finally, a summary is given in which optimized values of important parameters for the extraction system are presented and some possible future improvements are also suggested.

Part I

A New Design
of
the University of Manitoba Cyclotron
for D^- Ion Acceleration

Chapter 1

Historical Background

The University of Manitoba cyclotron is a four-sector, spiral-ridge, variable energy machine, which was originally designed to accelerate an H^- beam whose energy could range from 20 to 50 MeV [STA62]. The unique feature of this cyclotron is the method that is employed in it for trimming the magnetic field. Here, unlike other machines, the field is trimmed by individually controlling the permeability of 64 blocks of Invar alloy ([PIC40], [BUR65], [BUR66]). These blocks are placed, eight at a time, sandwiched between each hill piece and the corresponding pole piece (8 blocks/hill piece $\times$ 2 hill pieces/hill $\times$ 4 hills). The radial profile of the magnetic field can be shaped by adjusting the temperatures of the Invar blocks (which are arranged underneath each hill piece, successively, in eight radial positions along the radius of the cyclotron.)

In 1976, D^- ions were also successfully accelerated and extracted from the Manitoba cyclotron. Polarized D^- ions were subsequently successfully accelerated in 1980. However, deuteron beams were rarely accelerated after that time, due to low beam intensity and beam instability. In addition, the maximum D^- ion beam energy that was reached was only 19 MeV. From the existing cyclotron design parameters, on the other hand, one expected to achieve variable- energy deuteron extraction with up to 23 MeV. The main problem here was the loss of vertical focusing in some regions of the cyclotron, and the isochronism was also poor. In addition, there were some other problems which also contributed to fluctuations in the beam current that was available from the cyclotron. These problems included,

among others, very small energy gain per turn, dee movements due to a mechanical backlash, RF heating of the dee system, etc. These problems are described in detail in ref. ([HUA84]), ([CDG83]), ([BRU82]).

The above facts, plus the specific problems which were related to the acceleration of H^- ions ([MYT86]), led us to believe that the upgrading of the Manitoba cyclotron was an urgent task. Additionally, as time passed, the nuclear physics experiments became more and more sophisticated, requiring beams of increasingly higher quality and versatility. Hence, the need to upgrade the cyclotron performance to meet the above demands became acute. Consequently, two exploratory studies were carried out in 1976 and 1982. Based on the above, major upgradings were carried out in 1984, as is described in detail by Dr. Yoon in his Ph.D dissertation([MYT86]).

Prior to the 1984 upgrading program, the D^- ions were injected at 5.5 KeV and then accelerated by application of 14.24 MHz rf to a pair of diametrically placed dees which was operated in the push-pull mode at a peak voltage of 14.5 KV. These parameter values, however, were by no means the optimum values, having been chosen to keep the D^- ions in the same trajectory as the H^- ions. Until the completion of the 1984 major upgrading program, this was the only option available for accelerating D^- ions.

An extensive upgrading of the cyclotron in 1984 totally changed the cyclotron parameters for D^- ion acceleration. The main features were:

1. The presence of two separate dee-tips in the central regions; one for H^- ions and another for D^- ions. These were built to be mechanically interchangeable

without too much inconvenience. It was not possible to compromise the central region design so that one central region geometry would serve for both modes of operation, and still maintain the required beam quality.

2. The dee frequency was changed from 14.24 MHz in a push-pull mode to about 30.50 MHz in a push-push mode. The change in frequency, coupled with an improved magnetic field, was expected to increase the available maximum energy of the deuteron beam to 27 MeV from 19 MeV.

3. The D^- ion injection energy was increased to about 15 keV(from 5.5 keV) and the dee voltage to 40 kV(from 14.5 kV). These changes, together with the change to an RF push-push mode, greatly increased the energy gain of the D^- ions, resulting in much better beam stability, beam reproducibility and transmission efficiency.

The construction of the new dee-tips and the new central region for D^- ions was started in-house in 1984, during an intensive major cyclotron upgrading project. The design was based on the data that was obtained during the exploratory cyclotron magnetic field mapping program which was carried out in 1982. During the 1984 field mapping and shimming program, however, the magnetic field of the cyclotron underwent an extensive reshaping([GUS84]). The cyclotron flutter field was effectively extended inward, towards the center of the cyclotron, to improve the vertical focusing in this region. This extension, however, resulted in the radial broadening of the bump magnetic field of the cyclotron.

To take this broadening effect into account, and to investigate the effectiveness of the parameter changes, the dee-tips and central region were redesigned and the beam orbit dynamics were restudied.

The first part of this thesis (chapters 1-5) describes the author's work within the context of the upgrading project of the University of Manitoba cyclotron. This work involved the analyses of the field mapping data, the redesign studies for a new central region for the D^- ion acceleration, and a detailed study of the beam orbit dynamics.

Chapter 2

The Magnetic Field for the Acceleration of D^- Ions

2.1 The magnetic field mapping method

In the University of Manitoba cyclotron, to measure and improve the magnetic field distribution, field mapping programs were carried out in 1976,1982 and 1984. In the last mapping program, a "flip coil" (which consisted of an assembly of 52 coils, equally spaced along the radius of the cyclotron), was utilized. As the coils were moved along the azimuthal direction on the median plane and flipped, the current induced in them flowed to chopper-stablized integrators. A digital voltmeter measured the individual integrated voltages through the multiplexer. All the data and control signals passed through interfaces onto a LSI-11/23 microcomputer. Once a mapping had been started, this computer controlled all the measuring events and recorded the field measurements at uniform intervals of azimuth angle. The resulting raw field values were transferred to the VAX-11/750 computer for analysis.

After that, the fields were Fourier-analyzed to sort out their intrinsic harmonic components. The resulting magnetic field in the median plane(z=0) of the cyclotron can be expanded as

$$B_z(r,\theta) = B_0(r) + \sum_{n=1}^{\infty}(A_n(r)\cos(nN\theta) + B_n(r)\sin(nN\theta)) \quad , \qquad (2.1)$$

where $B_0(r)$ is the average field at radius r, and N is the number of magnet sectors. Here, $A_n(r)$ and $B_n(r)$ represent the amplitude of the n^{th} harmonic components of the magnetic field.

Note that components attributable to the field imperfection have been omitted in eq.(2.1) because the field mappings were performed only over one complete sector of the cyclotron. This automatically eliminated any possibility of recovering the imperfection field components from the measurements.

The analysis was carried out by using the code MAPANL which was developed at the University of Manitoba (henceforth denoted by U. of M.) cyclotron laboratory. The basic algorithm of MAPANL was introduced in the work of Gordon and Welton ([GOR59], [WEL59]), who developed methods to find the equilibrium orbit and to calculate ν, ν_r, ν_z, *etc.* as functions of the energy. With the particle energy as an input, the program integrates the equations of motion over one magnetic field period(90°), using the azimuthal angle(θ) as the independent variable. Since the equilibrium orbit, by definition, is smoothly closed upon itself, the initial values of r and p_r are the same as the final values of these variables along the equilibrium orbit. The determination of an equilibrium orbit then reduces to the determination of the initial values of r and p_r.

The radial equations of motion are integrated numerically, to obtain r and p_r through a process of successive iterations and to determine the transfer matrices over one period. Once r and p_r have been found, all the equations, including the axial equations, are subsequently integrated. Then the knowledge of transfer matrices for the radial and axial motions enables us to calculate ν_r and ν_z by using the following two relations ([LIV61]):

$$\nu_r = \frac{1}{\theta_0}\cos^{-1}\left(\frac{J_{11}+J_{22}}{2}\right), \qquad \nu_z = \frac{1}{\theta_0}\cos^{-1}\left(\frac{K_{11}+K_{22}}{2}\right) \quad . \tag{2.2}$$

Here, θ_0 is 2π divided by the number of sectors; J_{ij}, K_{ij} are the corresponding

elements of the radial and axial transfer matrices, respectively. From the above equations, it is apparent that the motion stays bounded if $J_{11}, J_{22}, K_{11}, K_{22}$ are real and if the absolute value of the trace of each of the transfer matrices is less than two.

The revolution frequencies, ν_r and ν_z, can be easily evaluated after all the integrations over one period have been carried out with respect to the independent variable θ. The time t is also integrated as a function of θ. Several references ([GOR59], [WEL59]) provide the explicit forms of the equations of motion as well as more details about the computational procedures.

By repeating the above procedures for different input energies, one can obtain curves of ν, ν_z and ν_r, as functions of r.

These three curves were then investigated to obtain improved shapes and locations for shims to be placed inside the cyclotron. On the basis of these three curves, we could also choose a better set of temperature settings for the Invar blocks for the succeeding mapping. The shims, after being machined, were placed in the indicated position inside the cyclotron for the next set of field mappings.

2.2 Analysis of the mapping data

Figs. 2.1, 2.2 and 2.3 show the field properties before the upgrade of the magnetic field. These figures provide the D^- particle's revolution frequency (ν) as well as the axial (ν_z) and radial (ν_r) focusing frequencies. Each of these frequencies, (the three most important characteristics of the cyclotron magnetic field), is plotted as a function of the radius of the D^- ion beam.

Ideally, ν should be a constant all along the radius, so that the isochronism in the acceleration of the D^- ions can be maintained. However, Fig. 2.1 indicates that it fluctuates considerably.

A particularly conspicuous fluctuation is seen to occur at a radius of approximately 10 cm. This fluctuation is caused by a premature termination of the central bump magnetic field. Such a bump pulls the flux from the surrounding area, and therefore tends to leave a shadow just outside the bump.

A departure from isochronism results in a phase oscillation of the particles during acceleration. Let us now utilize the following notation: we define ϕ to be the phase of a particle with respect to the RF voltage, N the turn number, ω_{RF} the angular oscillation frequency of the electric field, $\omega(E)$ the particle's revolution frequency at the energy E, h the integral harmonic ratio. We also let E_1 denote the maximum energy gain per turn [which is a function of the charge number, the total number of dees, the dee voltage, the harmonic mode, and the dee angle that depends on the turn number]. One can then formulate the expressions for the phase change per turn and for the energy gain per turn as,

$$\frac{d\phi(E)}{dN} = 2\pi\left(\frac{\omega_{RF}}{\omega(E)} - h\right) \qquad and \qquad \frac{dE}{dN} = E_1 \cos\phi(E) \qquad . \tag{2.3}$$

From these equations, it is straightforward to derive a formula for the phase oscillation as a function of energy. The result is given by

$$\sin\phi(E) = \sin\phi_0 + \frac{2\pi h}{E_1}\int_{E_i}^{E}\left(\frac{\omega_{RF}}{h\omega(E)} - 1\right)dE \qquad , \tag{2.4}$$

where ϕ_0 and E_i, respectively, are the RF phase and the beam energy at the center

Figs. 2.1, 2.2, 2.3 Results of the magnetic field mapping that was carried out before 1984. For each plot, the horizontal axis denotes the radius of D^- ion in centimeters, and the vertical axis represents the D^- ion's revolution frequency (fig. 2.1), axial focusing frequency (fig. 2.2) and radial focusing frequency (fig. 2.3) in figs. 2.1, 2.2, and 2.3, respectively.

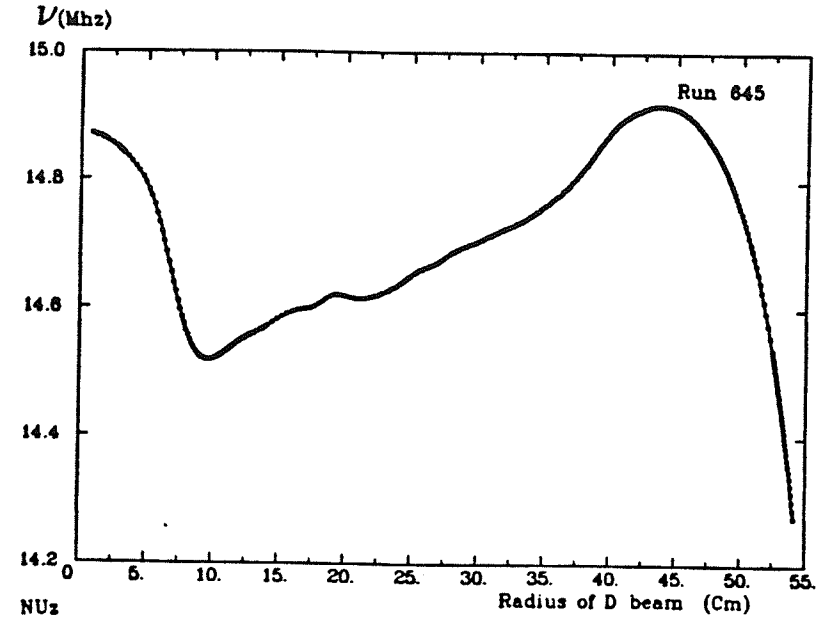
ν(Mhz)
15.0
14.8
14.6
14.4
14.2
Run 645
0
5.
10.
15.
20.
25.
30.
35.
40.
45.
50.
55.
Radius of D beam (Cm)

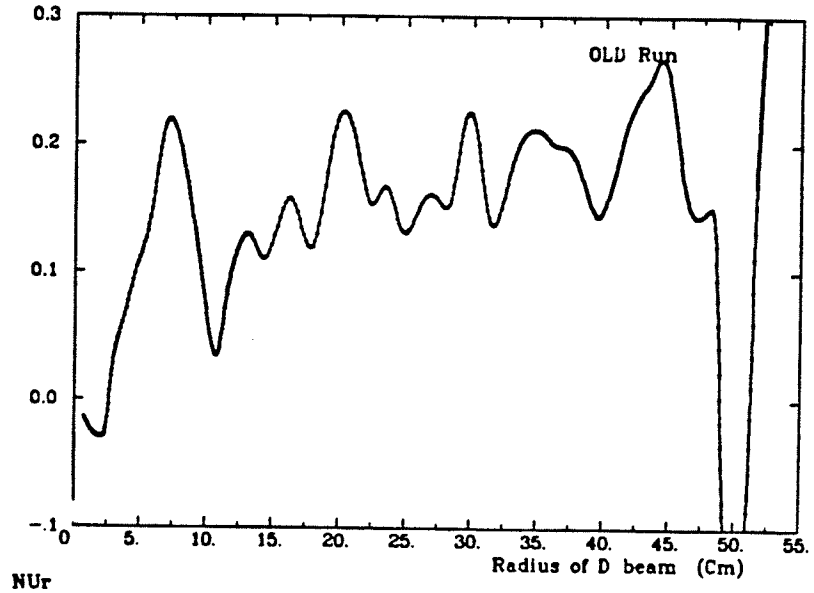
NUz
0.3
0.2
0.1
0.0
-.1
OLD Run
0
5.
10.
15.
20.
25.
30.
35.
40.
45.
50.
55.
Radius of D beam (Cm)

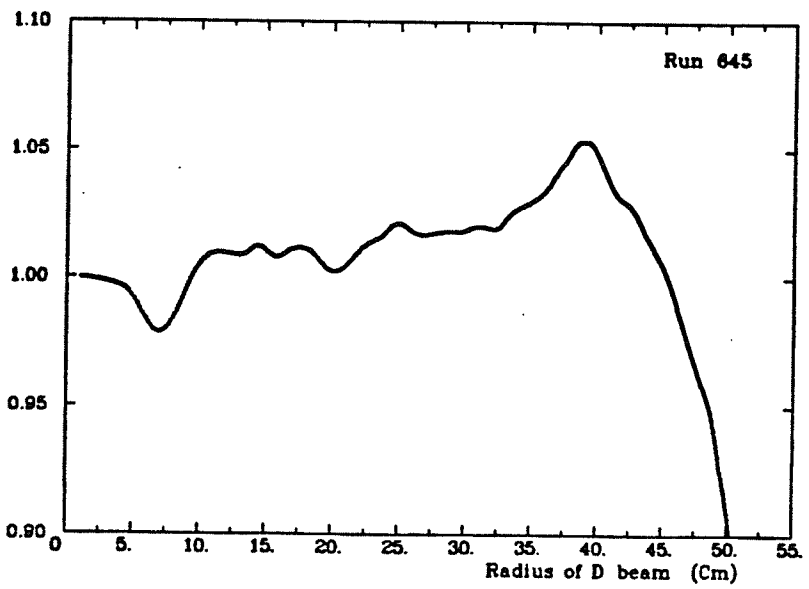
NUr
1.10
1.05
1.00
0.95
0.90
Run 645
0
5.
10.
15.
20.
25.
30.
35.
40.
45.
50.
55.
Radius of D beam (Cm)

of the first gap (between the mirror and the dee-tips in the case of the U of M cyclotron).

We now apply the above equation to fig. 2.1 and substitute the following values: ϕ_0=+8°, h=1, ω_{RF}=2π × 14.24 MHz, E_i=5.5 keV and E_1 ranging from 25 keV to 48 keV, depending on the turn number. The result that we obtain is shown in fig. 2.4.

From this figure, we notice that the phase excursion keeps increasing along the radius. The figure indicates that when the particle's energy reaches 19 MeV (r=40 cm), the phase has already become −80°. Therefore, with the field configuration that leads to fig. 2.4, it is no longer possible to accelerate a D^- particle with an energy that is higher than 20 MeV. Moreover, these large phase excursions cause the beam to undergo a great number of turns to reach 19 MeV, and the turn separation in this energy region is, in fact, almost unrecognizable. It is therefore expected that there will be a large spread in the number of turns among the particles extracted from the cyclotron. This kind of spread may lead to a deterioration in beam quality (*e.g.*, to a large energy spread or to a large beam center spread, *etc.*).

Let us now turn our attention to the axial motion, Fig. 2.2. A large dip is seen to fall to zero at r= 48 cm and then for larger radii, ν_z acquires an imaginary value, indicating that the axial motion experiences a defocusing force. The axial displacement, z, when ν_z varies adiabatically, is given by [LIV61](assume no acceleration):

$$z = \frac{const}{\sqrt{\nu_z B_0}} e^{\pm i \int \nu_z \omega dt} \quad , \tag{2.5}$$

where B_0 (=$\omega M/q$) is the average magnetic field, and ω is the cyclotron angular

frequency. This expression indicates that the motion in the z direction grows exponentially when ν_z is imaginary with a growth rate $(\Delta z/\Delta r)$ that is proportional to $\pm i\nu_z$, where $i = \sqrt{-1}$. Therefore, most of the ions are expected to be lost in passing through this region, by hitting the dee structures. Even for those that are not lost, many will have a large oscillation amplitude.

Fig. 2.2 shows that there is a large defocusing effect between r=48 and 51 cm. This effect was eventually traced to the presence of a large magnetic shim placed at the leading edge of each valley at this radius and further outward(It turned out that the presence of this shim affected the shape of the spiral so much that the sense of the direction of the spiral reversed in this region). The sudden rise in ν_r, starting at r=48 cm in fig. 2.3, results from the effect of this shim. This is the most serious imperfection of the U of M cyclotron that had to be corrected.

The above two effects, the defect in the axial focusing and the serious phase excursion, were together sufficient to prevent the D^- ion beam from reaching energies above 19 MeV instead of achieving the intended design goal of 22.5 MeV.

It is now therefore clear that the magnetic field in the U of M cyclotron had serious imperfections before 1984. These problems could be corrected only by reoptimizing the cyclotron field through a series of field mapping and shimming programs, and such a project was started in November 1983.

2.3 The improvement of the magnetic field after upgrade

The results of the 1984 field mapping for the D^- ions are depicted in fig. 2.5, 2.6 and 2.7. These graphs indicate that the serious shortcomings of the field, as mentioned earlier, have now disappeared. The improvement in the isochronism can

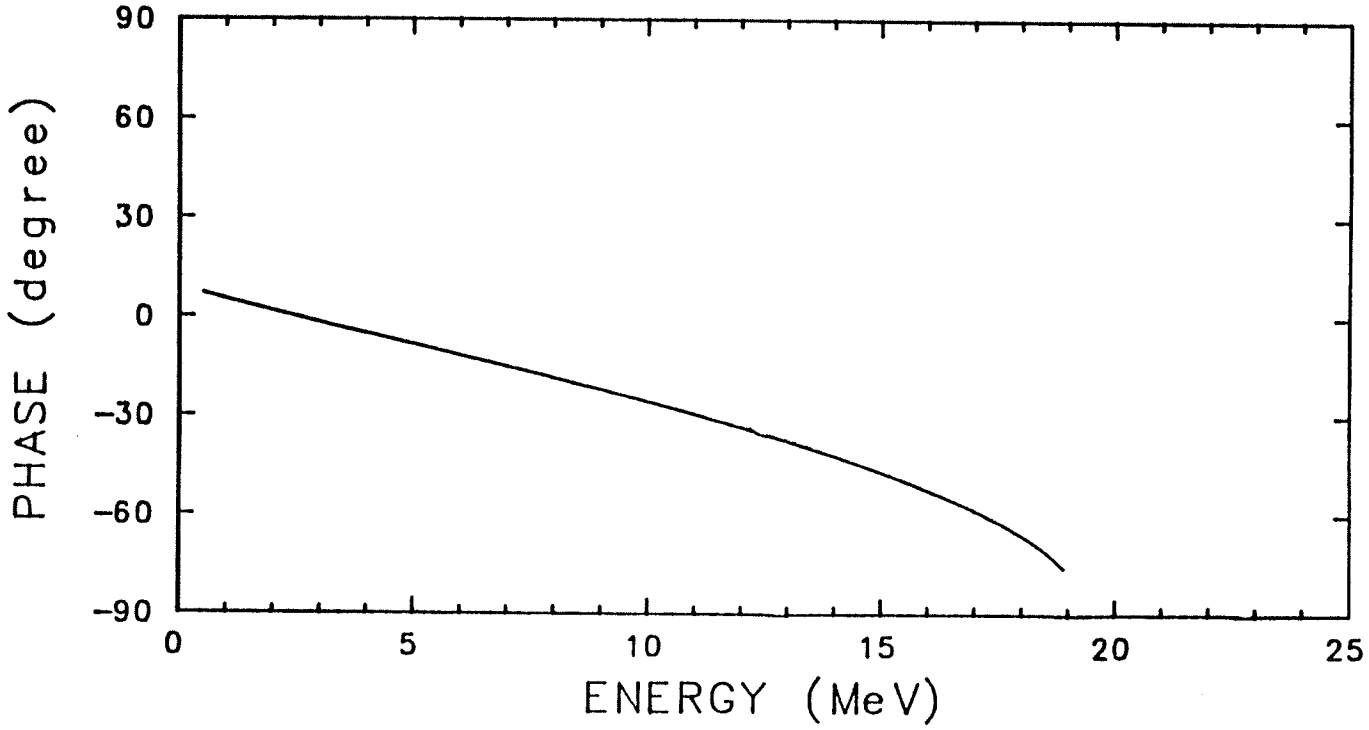

Fig. 2.4 The phase excursion of the D^- particle as a function of the energy(up to 19 MeV) for a typical magnetic field that was measured before the 1984 updrade.

be clearly seen by comparing fig. 2.5 with fig. 2.1. The width of the fluctuations in ν, between 13 and 40 cm, is now within 30 kHz(60 kHz with the second-harmonic mode of acceleration).

The axial focusing frequency, ν_z, has also improved significantly, as can be seen by comparing fig. 2.6 with fig. 2.2. To obtain these results, the Invar temperatures were set at T_1=40, T_2=50, T_3=154, T_4=95, T_5=230, T_6=105, T_7=180, T_8=230 °C, (the main magnet current set at 3350 A), as well as placing three sets of shims in the valley. The first set of shims, a very large one, extends from the 40 cm radius to the outer edge of pole-tips, and is placed on the trailing edge of the valley. The second set of shims is of medium size, and is centered around the 20 cm radius. The third set is a small one, and is located at a radius of approximately 8 cm. This last set of shims was introduced in order to reduce the slope of ν in this region and to extend the central bump field further out, while at the same time improving the behaviors of ν_z in this region.

An improvement in axial focusing can also be seen clearly from fig. 2.6. The disappearances of the axial focusing at radii of 10 and 48 cm (see fig. 2.2) have clearly been corrected. Furthermore, ν_z is now seen to increase smoothly throughout the entire region.

The radial contour maps of the new magnetic field in the median plane of the cyclotron for the D^- ions are depicted in figs. 2.8.

Figs. 2.5, 2.6, 2.7 Results of the magnetic field mapping that was carried out in 1984. For each plot, the horizontal axis denotes the radius of D^- ion in centimeters, and the vertical axis represents the D^- ion's revolution frequency (fig. 2.5), axial focusing frequency (fig. 2.6) and radial focusing frequency (fig. 2.7).

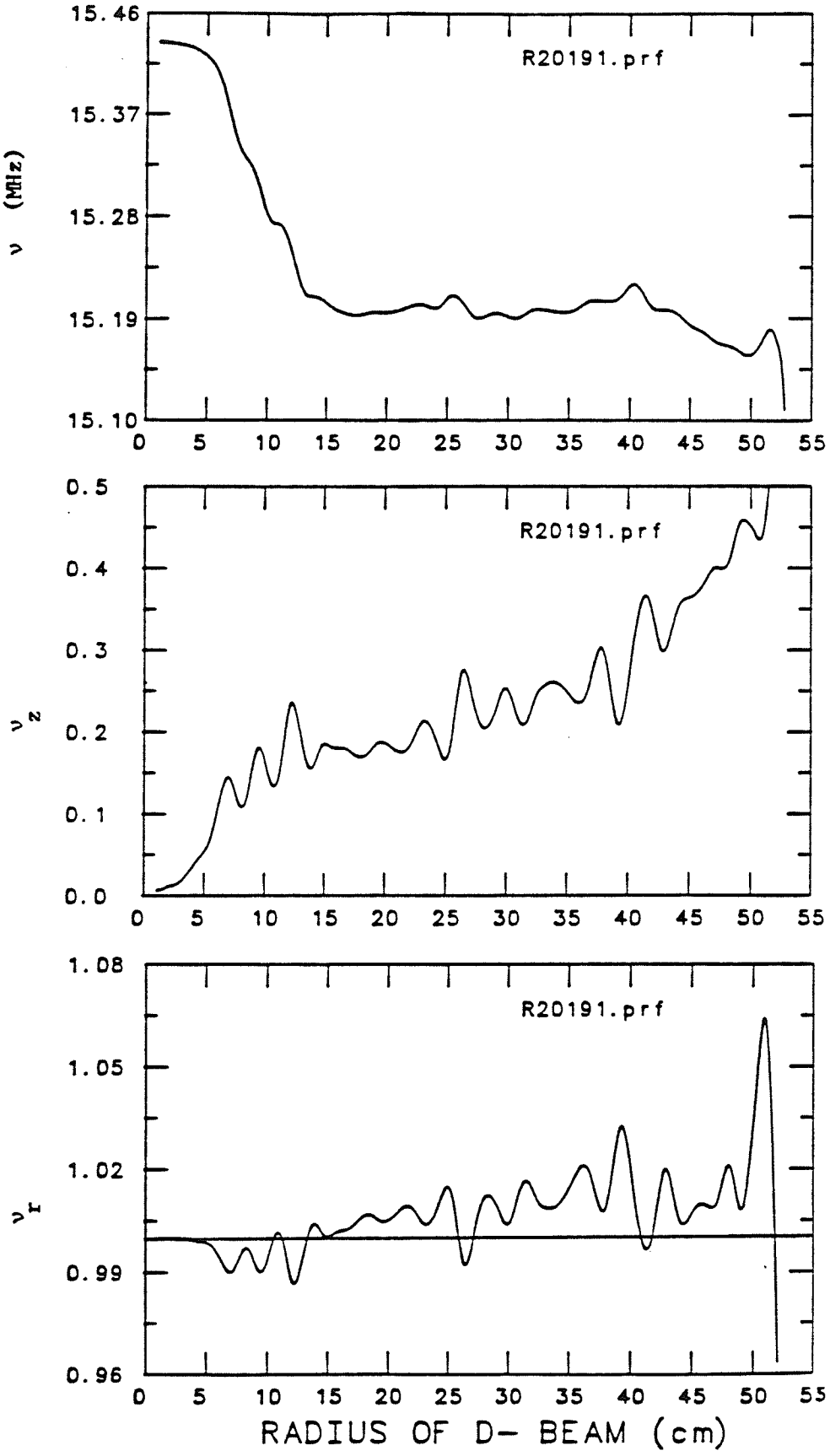
R20191.prf
15.46
15.37
15.28
15.19
15.10
ν (MHz)
0 5 10 15 20 25 30 35 40 45 50 55
R20191.prf
0.5
0.4
0.3
0.2
0.1
0.0
ν z
0 5 10 15 20 25 30 35 40 45 50 55
R20191.prf
1.08
1.05
1.02
0.99
0.96
ν r
0 5 10 15 20 25 30 35 40 45 50 55
RADIUS OF D- BEAM (cm)

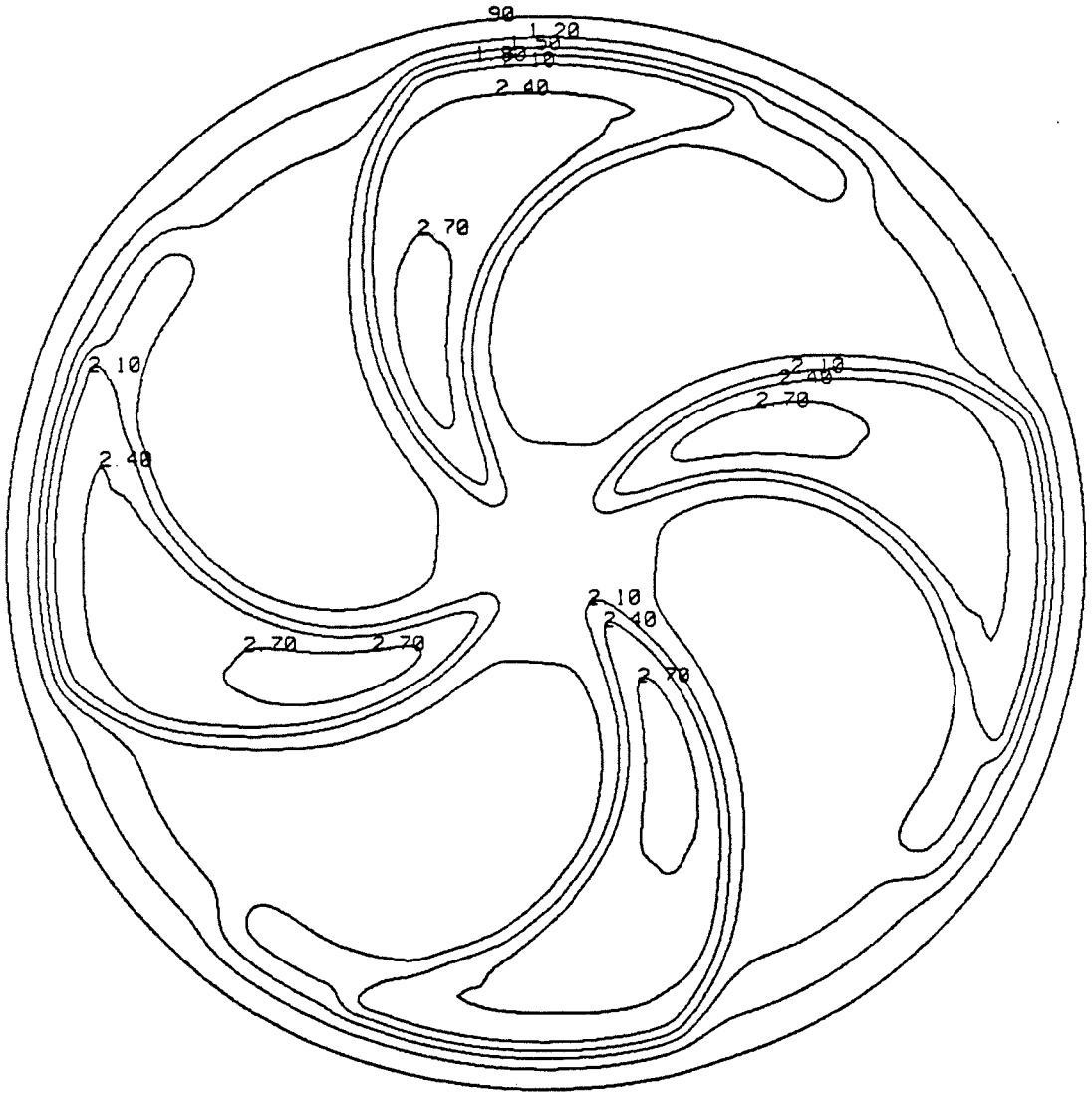

Fig. 2.8 The radial contour map of the D^- field for the new central region of the University of Manitoba cyclotron.

Chapter 3

The Electric Field Calculation for D^- Ion Acceleration

Knowledge of the distributions of both the electric field and the magnetic field inside a cyclotron is one of the fundamental prerequisites for successful investigations of the beam orbit dynamics. For the U of M cyclotron, the magnetic field distribution can be obtained from the measured data, an approach which was described in chapter 2. However, the data for the electric field distribution in this cyclotron was not available. For a simple dee structure ($e.g., \theta_D$=180°), the electric field distribution may be obtained in a closed form by utilizing the Schwartz-Cristoffel transformation method [MUR53]. However, the dee structure of the sector-focused cyclotron is, in general, too complicated for analytical calculations of the electric field distribution to be possible. One could also try to obtain this distribution by direct measurements in the median plane of model electrodes; for example, by using the electrolytic tank (or trough) method ([REI65], [ZIN69]). Yet, this method also has the following significant drawback, and hence can not be utilized in our design studies of the new central region; more specifically, whenever a change in the geometry is necessary, this method requires an actual re-machining of the model electrode, a very expensive and time-consuming procedure. Furthermore, a significant error may also occur during the measurement process due to various reasons(See, for instance, the description in Septier's book [SEP67, Chapter1.2]. The accuracy of the result obtained from this method seems to be no better than 5%.

On the other hand, a numerical solution of Laplace equation, by using the successive over-relaxation (SOR) method, enables us to obtain an accurate static

electric potential distribution. When applied to a cyclotron, this method assumes that the real dynamic field is approximated by a "quasi-static" field, a static field with a uniform potential over the entire dee structure that varies sinusoidally with time. The SOR method has a number of advantages over other methods of obtaining the electric field distributions, being more accurate (it can be better than 0.1% for a static field), inexpensive, and less time-consuming [LOU71]. We therefore employed this method to obtain the electric potential distribution in the central region of the U of M cyclotron. The detailed theory of the SOR method can be found elsewhere ([NEL69a], [NEL69b], [LOU71], [CHE81]). Consequently, in the following pages, only a very brief review of the SOR method is given and instead we shall emphasize its application to the calculation of the electric potential in the U of M cyclotron's central region.

3.1 A summary of the successive over-relaxation method

The numerical solution of the Laplace equation can be obtained by approximating this differential equation by a set of difference equations. For the actual computation, the region of interest is divided into a number of cubic meshes. The potential at each node is then calculated iteratively, by averaging the potentials at adjacent nodes, until the potential converges. To make the convergence faster, the successive over-relaxation coefficient α, a numerical factor which usually lies between one and two, is employed. The potential at node (i,j,k) at the n^{th} iteration is then given by the expression

$$\phi_{ijk}^{n} = \phi_{ijk}^{n-1} + \alpha[\frac{1}{6}(\phi_{i-1}^{n} + \phi_{i+1}^{n-1} + \phi_{j-1}^{n} + \phi_{j+1}^{n-1} + \phi_{k-1}^{n} + \phi_{k+1}^{n-1}) - \phi_{ijk}^{n-1}]. \quad (3.1)$$

The optimum value of α depends on the dimensions of the meshes and it is given

by [FOR60]

$$\alpha = 2 - 2\pi\sqrt{\frac{1}{3}(\frac{1}{p^2} + \frac{1}{q^2} + \frac{1}{r^2})}, \tag{3.2}$$

where (p, q, r) is the dimension of the meshes in the i, j, k directions, respectively.

3.2 Computational details

In our design studies of the new central region of the U of M cyclotron, the mesh dimensions and the value of α were taken to be (256,256,15) and 1.5, respectively. We see from eq. (3.2) that the optimum theoretical value of α for these mesh dimensions is 1.7573. However, it should be noted that the formal derivation of eq. (3.2) was carried out by imposing fixed Dirichlet or Neumann conditions on the boundary planes while all the interior points were free to vary [FOR60]. The real situation does not quite correspond to this picture; the potentials in many interior points are also fixed. Therefore, the effective mesh dimensions (p, q, r) are smaller than the real dimensions, making the value of α smaller than the one that is predicted by eq. (3.2). Since the design investigations of our new central region required studies of many trial geometries, in order to find the best geometry, it appears to be too time-consuming to search for the optimum value of α that corresponds to each new geometry. Therefore, in our investigations, no such effort was made; instead, the value of α was fixed, at α=1.5, throughout the calculation, thereby greatly simplifying the computations. With this value of α, the total number of iterations that are required to achieve an average fractional change in the potential (per iteration) of 10^{-6} was found to be about 120.

In order to be able to start numerical calculation, we initially assign an arbitrary(uniform) potential to each point in the "empty" space of our region (*i.e.*, to

each point which is neither on the outside boundary nor on the electrode boundary). This value of the potential was taken to be half the sum of the maximum and minimum potential values that are assigned by us to the electrodes in the region. Dirichlet conditions are imposed on the boundary region. In order to carry out the actual SOR calculation, the FORTRAN packages RLX3D were developed at the U of M Cyclotron Laboratory [OH83]. The packages consist of several independent main programs. These include the program for initializing the potential, the main relaxation program, and the program for expanding the region by reducing the mesh size. More detailed descriptions of the structures of these programs can be found in the reference just quoted above.

The accuracy of the calculation of the electric potential depends upon the mesh size. As was mentioned earlier, the effect of the electric field on the motion of a particle is most important during the first few turns. Therefore, meshes of 0.25 mm were taken to cover this region, which are sufficiently small. As the particle moves toward the outer region, coarser meshes can be utilized. In order to cover the entire acceleration range of the cyclotron, as well as to include all the ground shields, the RLX3D program starts with 4 mm meshes. Then, in sequence, the program carries out the SOR calculation, reduces the mesh size by half and re-calculates the potential, *etc.*, until the calculation with meshes of 0.25 mm is performed. Of all this, the fields obtained from the 4 mm grids were not used in the particle tracing. The data that were actually used in the beam dynamics studies involved meshes which ranged from 2 mm down to 0.25 mm.

Chapter 4

The D^- Beam Orbit Dynamics

4.1 Introduction

In the beginning of this thesis we noted that the idea of an azimuthally varying field (AVF) led to the development of a sector-focused cyclotron, for which the axial focusing term from this AVF component was found to be independent of the requirement of isochronism. To be more specific, we will now look into the expression for the axial betatron oscillation in an AVF cyclotron. In the limit of small flutter amplitudes of the magnetic field, this frequency is given approximately by [LIV61]

$$(\nu_z)^2 = \gamma + F(R) + 2F(R)\tan^2\xi + F(R)n^2/N^2 \qquad , \tag{4.1.1}$$

where γ is a field index defined by $\gamma = -(r/B)(dB/dr)$ and ξ describes the spiral angle of the magnetic field [LIV61]. The flutter function, F, is a measure of the azimuthally varying part of the magnetic field, and is defined by

$$\begin{aligned} F &= \frac{\langle B^2\rangle - \langle B\rangle^2}{\langle B\rangle^2}, \qquad where \qquad \langle\cdots\rangle \equiv \frac{1}{2\pi}\int_0^{2\pi}\cdots d\theta \\ B &= B(r,\theta,z=0) = \langle B\rangle + \sum_{n=1}^{\infty} B_n(r)\cos nN(\theta - \delta_n(r)), \end{aligned} \tag{4.1.2}$$

where N is the total number of identical sectors (which is 4 for the U of M cyclotron).

Eq. (4.1.1) is derived through a linear analysis of orbits in an AVF field. The successive terms on the right-hand side of that equation represent contributions from four different focusing effects as follows:

Term 1: Focusing or defocusing by the gradient of the radial field.

Term 2: Thomas (or Sector) focusing.

Term 3: Focusing by the edge fields of a spiral boundary.

Term 4: Alternating-gradient focusing arising from the change in the actual field index between hills and valleys. Usually, this is a small effect.

Therefore, to ensure axial focusing, the sum of the Thomas focusing and the spiral boundary focusing in eq.(4.1.1) must be greater than the defocusing effect from the first term (which is required to be negative to satisfy the condition of isochronism). In general, however, the spiral angle near the center of an AVF cyclotron approaches zero. The flutter amplitude also approaches zero at the center, since the effects of hills and valleys on the field cancel out within a radius that is comparable to(or less than) the gap width between the poles. We therefore have, at small radii,

$$B \approx \langle B \rangle, \qquad F \approx 0, \qquad \nu_z^2 = \gamma < 0 \qquad . \tag{4.1.3}$$

The beam would then experience an exponential growth in the z (axial) direction, as is indicated by eq. (2.5). This has disastrous consequence, because the dee(or the vacuum chamber) usually limit the available vertical height for the oscillation in any cyclotron.

To solve this problem, Richardson [RIC65] suggested that a magnetic cone (*i.e.*, a "field bump") be inserted at the center of a machine. This would cause the magnetic field away from the center to decrease monotonically until the bump field region is passed, *i.e.*, until the region where the field approaches the isochronous

field value. This results in a positive γ value and ν_z^2 to be positive. Therefore, axial focusing can thus be achieved. In the University of Manitoba cyclotron, this field bump approach is utilized; through the use of a pair of center plugs a bell-shaped field bump, of approximately 250 gauss at its peak, has been achieved. The bump field extends up to approximately 13 cm ($\sim 5''$) in radius.

Fig. 2.6 indicates that in the U of M cyclotron, the focusing effect for D^- ions from the field bump starts to become appreciable only at radii larger than 7 cm. These two figures clearly show that the values of ν_z for radii that are smaller than 7 cm, for D^- ions, are less than 0.1, values which are insufficient to provide an adequate focusing force. Investigation through computer simulated particle tracing showed that obtaining an adequate focusing force in this region is an absolutely necessity, because the subsequent motion of a beam is greatly dependent upon its motion in the earlier turns.

As we will later see, such a focusing force in the central region can be provided by the accelerating RF electric field. A precise controlling of the beam's early motion can then be achieved by properly designing the electrodes (dee-tips in the case of the U of M cyclotron), utilizing the results of the studies of the beam orbit dynamics.

The above considerations, therefore, led us to decide to carry out a design study of the new dee-tips for the U of M cyclotron. In view of the problem described above, one of the goals of that design study was to obtain sufficient axial focusing near the center of the cyclotron, thereby improving the beam quality of D^- ions. In choosing the central region dee geometry, we note that the magnetic field is about 1.95 tesla and that therefore the turn separation is exceedingly small. To prevent the injected

ions from hitting the mirror housing(which is at ground potential), the RF voltage has to be large in this region so that the ions can clear the structure during the first turn. The voltage has to be low enough to prevent sparking. For the N = 1 mode of acceleration, this means a 180° dee tip geometry. For N = 2, on the other hand, 90° dee tips are desired. As we could not find a eingle dee-tips structure which can be operated for both N = 1 and N = 2 mode, we decided to have two separate dee-tips, one for the H^- ion acceleration and the other for the D^- ion acceleration. The utilization of the separate dee tips would make it possible for the D^- ions to be accelerated in the second-harmonic mode, and consequently should lead to a significant improvement in the beam quality for D^- ions, as is described below.

The new dee-tips for D^- ions, as viewed from the top of the cyclotron, are depicted in fig. 4.1.

Based on the new central region and the dee structure, the electric field distribution in the U of M cyclotron was obtained from the successive over-relaxation method that was described above. Subsequently, we performed the beam orbit dynamics studies that are described in the following section.

4.2 Investigations based on the beam orbit dynamics studies

As was mentioned above, one important motivation for embarking upon a design study of the new dee-tips was to provide a sufficient axial focusing force for the first several turns of orbit in the cyclotron, for radii that are too small for the effect of magnetic field bump to become important. The design study, therefore, must also include beam orbit dynamics investigations. In such investigations, the motion of a beam in a specific design geometry is scrutinized to see whether that geometry yields

Fig. 4.1 The new N=2 central region of the University of Manitoba cyclotron, as viewed from the top of the cyclotron. 1a: South dee-tip, 1b: North dee-tip, 2: electrostatic mirror assembly, 4: hill.

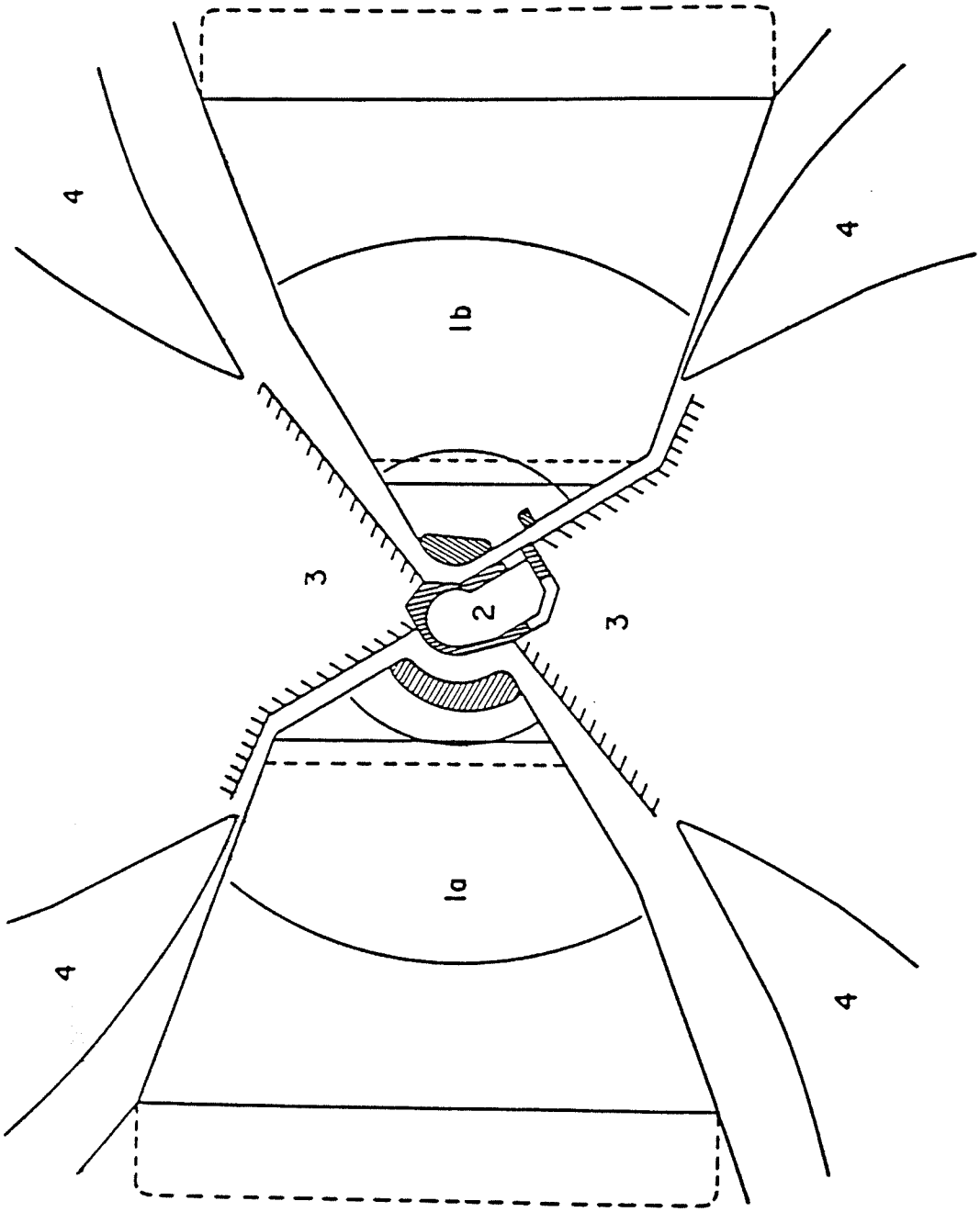
4
4
1b
3
2
3
1a
4
4

a satisfactory beam. Such studies, in fact, were carried out utilizing a successive approach in which a trial new geometry was first designed. Then the motion of a beam in this particular geometry was studied. Subsequently, the geometry was modified to obtain a beam whose motion was more satisfactory.

To facilitate this approach, a computer program, NUTRACK, was developed as a special version of the numerical orbit tracking program. NUTRACK is relativistically correct, utilizes double-precision, and has the capability to trace three-dimensional particle motions both forward and backward in time. The magnetic field mapping data (R20191.PRF) and the calculated electric potential data, are both read in as inputs for NUTRACK. Then, after utilizing additional input data (such as the particle specifications, the initial conditions, the oscillation frequency of the electric field, the dee voltage, *etc.*), the program starts integrating the following set of equations of motion:

$$\begin{aligned} \frac{d\vec{r}}{dt} &= \frac{\vec{p}}{m\gamma} \\ \frac{d\vec{p}}{dt} &= q(\vec{E}\cos\omega t + \frac{d\vec{r}}{dt} \times \vec{B}) \\ \frac{dW}{dt} &= \vec{F}\cdot\vec{v} = \frac{d\vec{p}}{dt}\cdot\frac{d\vec{r}}{dt} \end{aligned} \qquad (4.2.1)$$

To facilitate the computation, only the linear motions are investigated.

During the integration procedure, both the magnetic field and the electric field at the particle's position are calculated by employing the cubic spline approach. A fourth-order Runge-Kutta method is used to carry out the integration. The time is taken as the independent variable and a total of 2000 integration steps are taken per period of revolution of the particle. The output of the NUTRACK program consists of the instantaneous values of the particle's coordinates, momentum, energy, RF

phase, *etc.*. A thorough analysis of these parameters then provides all the necessary information about the motion of the beam of the charged particles.

The study of the beam orbit dynamics consists of (1) the analysis of the isochronism, (2) the investigation of the behavior of the beam orbit center, as well as of the radial and axial motions, and (3) the studies of other accelerator parameters such as the dee voltage, the injection conditions for the particles, *etc.*. The injection conditions include the starting RF phase for the reference particle, the injection angle at the mirror's center, the injection energy, and the position in space and time of the injection point. The simultaneous optimization of all of these parameters involves a thorough study of the radial and the axial motions in the central region.

4.2.1 The determination of the parameters for the accelerating electric field

The study of isochronism is very important for a cyclotron. This type of accelerator has the property that the orbital period of the beam is independent of the previous energy history of the ions. Therefore, phase oscillations do not occur, and the ions exhibit stability with respect to the RF phase. To ensure that particle synchronization is maintained through the acceleration process, there are two prerequisites: an optimized magnetic field distribution and accurate parameters for the associated accelerating electric field. The first requirement has been discussed in Chapter 2. The accelerating electric field parameters include the RF frequency, the dee voltage, the initial RF phase angle of particle, *etc.*.

If possible, a higher dee voltage is usually preferred. In this way, a larger energy gain per turn can be obtained; thus, a smaller number of turns and less

time are needed to achieve a given energy. The dee voltage of the accelerator basically depends on the available RF power from the supplying system. In the U of M cyclotron, the upgrading program increased the available RF power from 15 kW to 30 kW. It resulted in the increase in the available dee voltage to 40 kV. With this voltage, an energy gain per turn of as much as 120 keV can be attained. Consequently, the D^- particle needs only $200 - 250$ turns to attain an energy of 27 MeV.

One of the critical goals of our study was to find the optimum starting RF phase angle of the reference particle ϕ_o at the injection point; the reference particle should gain, on the average, the maximum possible energy per turn in reaching the desired energy. At the same time, the phase oscillation should be kept to a minimum at all radii.

For this purpose, a systematic search for ϕ_o was carried out by varying the initial RF phase from $\phi_0 = -270°$ by $\Delta\phi_o = \pm 10°$ with all the other initial parameters fixed. The resulting RF phases of chosen particles(while crossing the gap's middle line) as function of gap number is shown in fig. 4.2. From this figure we note that the phase angles of these particles gradually decrease due to the bump field in the central region of the cyclotron. By studying the phase delay we find that after three turns the particle with $\phi_o = -270°$ has gained the maximum energy, where its energy is 479 keV and the radius reached is 71 mm. Although the particle with $\phi_0 = -260°$ has a smaller phase excursion at the end of 3^{rd} turn $(-2°)$, a further investigation indicates that particles with initial RF phase angles of less than $-255°$ would hit the dee tip since their large phase excursion lead to a very small energy gain during the first gap crossing. We, therefore, choose $-270°$ as the initial phase

of the reference particle in our orbit dynamics study.

In principle, the choice of the RF frequency of the dee's electric field depends on the specific properties of the cyclotron magnetic field. From fig. 2.5 it can be seen that, in order to keep the phase excursion small, the RF frequency should be about 30.4 MHz.

To determine the optimum RF frequency more accurately, the particle trajectories were scanned for frequencies ranging from 30.400 to 30.418 MHz in steps of 0.003 MHz. The resulting energy gains per turn, as functions of the RF cycle number, are given in fig. 4.3. The energy gain per turn is $\Delta E = \Delta E_m \cos\phi$, where ΔE_m is the maximum possible energy gain per turn (160 keV for the U of M cyclotron), which depends only on the dee voltage and ϕ represents the average phase angle while the particle crosses the dee gaps. Hence the distribution given in fig. 4.3 is equivalent to the phase oscillation of these particles. From fig. 4.3, we note that in the central region where all the phases decrease in a similar way due to the bump field, their differences are negligible compared to the non-isochronism which is caused by the bulge field(See Chapter 2). In the middle region, fig. 2.5 indicates that the isochronism is very good, so that the energy gains per turn are kept stable within a range of ± 10 keV; the higher the frequency, the larger the energy gain per turn. In the outer region, where the radius is greater than 45 cm, the magnetic field falls off rapidly, and the phases of all of these particles increase. As the phase departs further and further from the optimum accelerating phase angle, the energy gain per turn drops accordingly, and the particles eventually enter the deceleration region. This limits the maximum energy available in the cyclotron. From fig. 4.3, it can be seen that the particles with higher RF frequency would enter the decel-

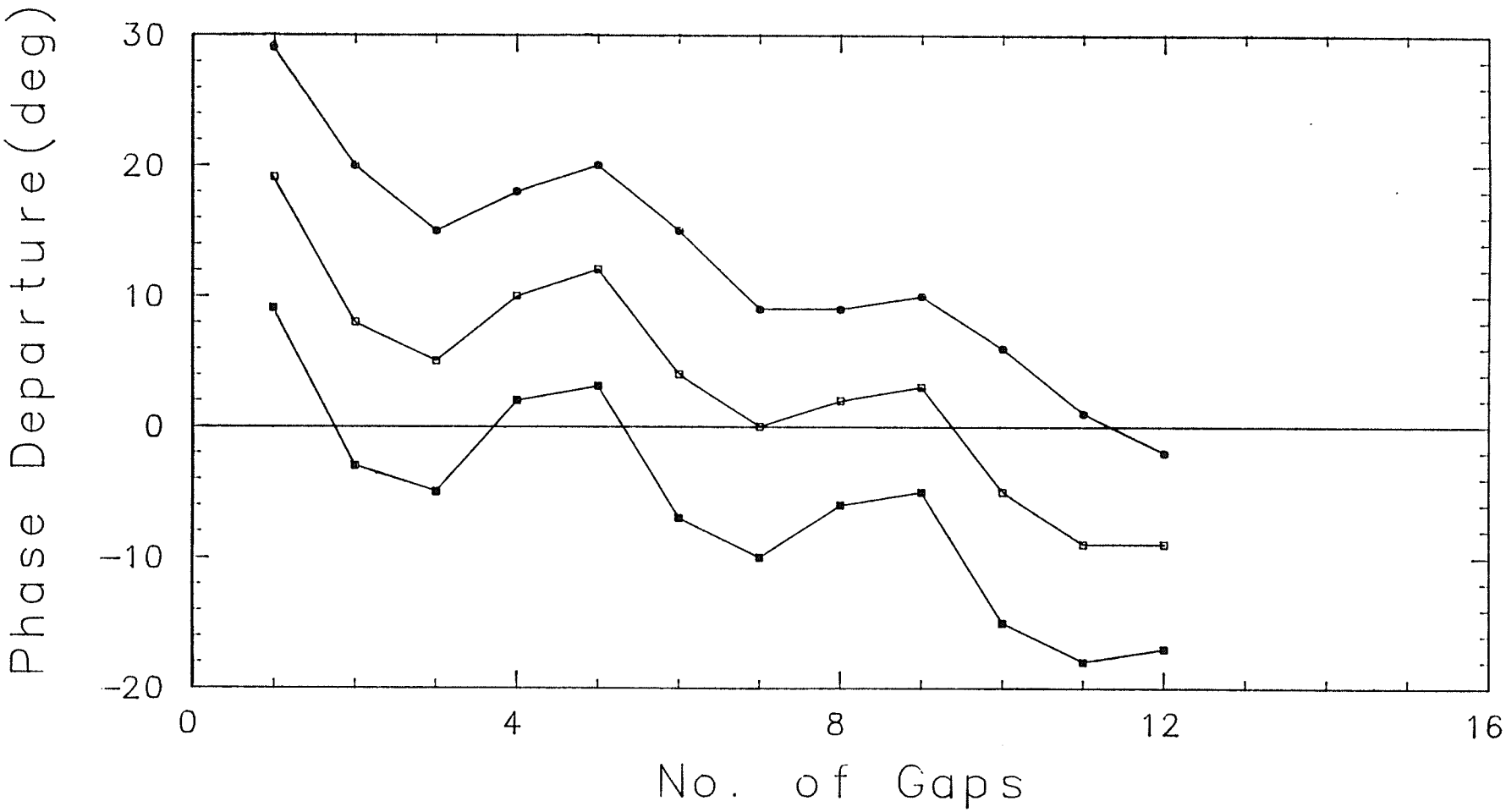

Fig. 4.2 The RF phase departure from the central phase when the three particles cross the central line of the first several accelerating gaps. The initial RF phase of the three particles are −260°(top), −270°(middle), −280°(bottom), respectively.

erating region earlier although the energy gain per turn is larger for most of the accelerating region. Maintaining a maximum energy per turn during acceleration usually leads to a better beam(in intensity, emittance, stability, etc) and therefore it is seen from this figure that we should choose this frequency if our need is for a D^- beam of 22 MeV(r = 46 cm) or less. On the other hand, for acceleration to highest possible energy, we should set the frequency to the lowest possible value(such as 30.402 MHz). Thus, the choice of the RF frequency depends on the desired energy for D^- beam from the cyclotron. Our calculation indicates that it is possible to obtain 27 MeV D^- ions from the University of Manitoba cyclotron, utilizing an RF frequency of 30.402 MHz, as is shown in fig. 4.4.

However, once the energy requirement is satisfied, a smaller RF frequency is preferred. In the following studies, we will use 30.408 MHz as the RF frequency of the reference particle. The available maximum energy is about 26 MeV which is attained when the particle has orbited through 226 turns.

With the three RF parameters chosen as described above, beam dynamic studies are then carried out to determine the beam properties in the longitudinal phase space. In this study, initial RF phases from $-257°$ to $-277°$ were examined. The results are as follows:

(1) the available maximum energy is E_m=26.3 MeV

(2) the maximum radius obtained is R_m=50.6 cm

(3) the required number of turns is N=226

(4) the energy spread, for an initial phase spread of 20°, is ΔE=110 keV, so that $\Delta E/E$=0.22%

Fig. 4.3 The energy gain/turn as a function of the average radius. The RF frequencies of the five representative particles are(from the lowest to the highest): 30.402, 30.405, 30.408, 30.410, 30.413 and 30.418 MHz, respectively.

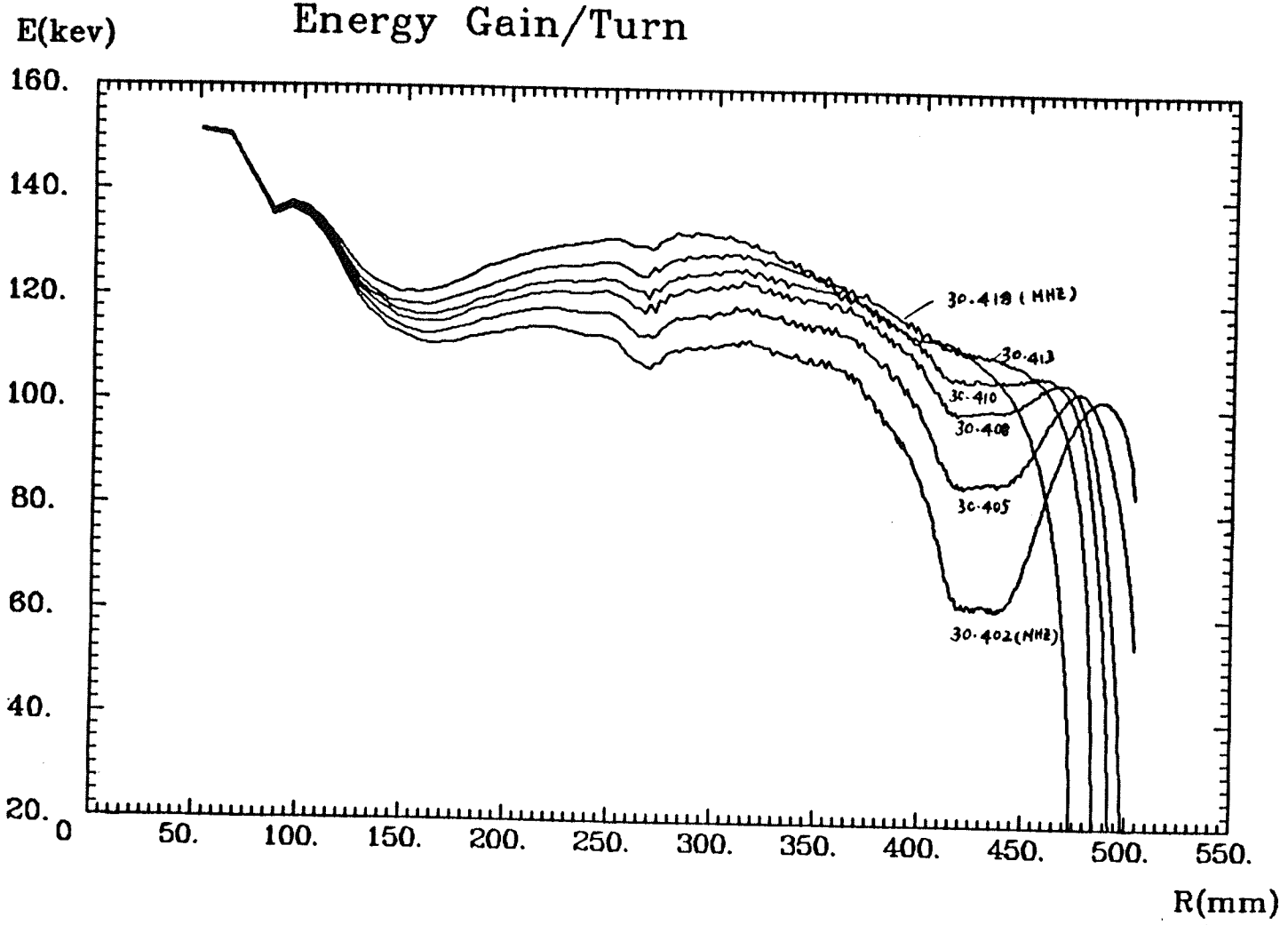
Energy Gain/Turn
E(kev)
160.
140.
120.
100.
80.
60.
40.
20.
0
50.
100.
150.
200.
250.
300.
350.
400.
450.
500.
550.
R(mm)
30.413 (MHz)
30.413
30.410
30.408
30.405
30.402(MHz)

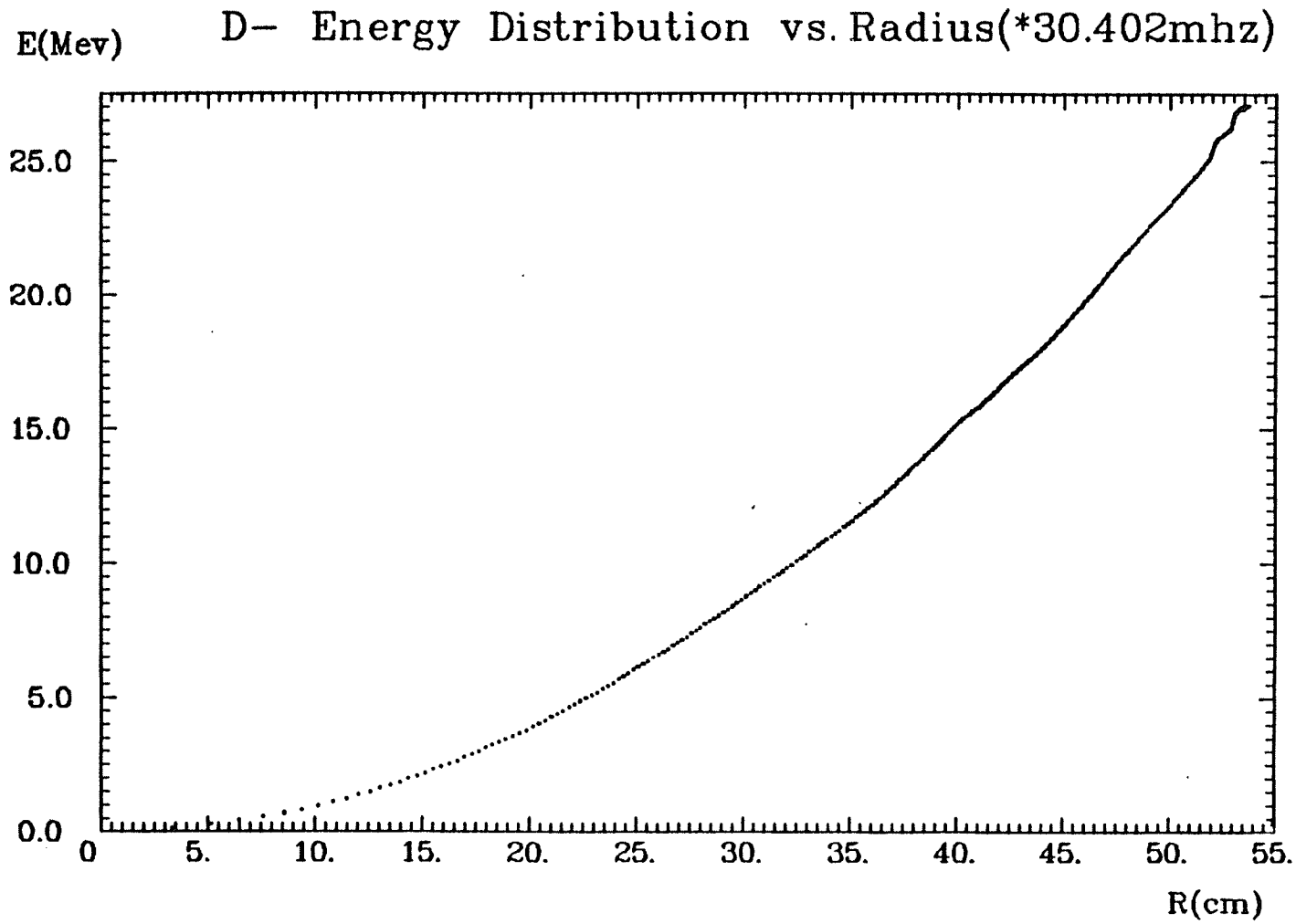

Fig. 4.4 The enegy gain of the particle with RF frequency 30.402 MHz as a function of radius.

4.2.2 The radial motion

In a cyclotron with a cylindrically symmetric magnetic field, a radially well behaved beam is a "well-centered" beam, whose center coincides with the center of the machine. Such a well-centered beam is highly desirable in a cyclotron, since then the coherent oscillations arising from the off-center motion can be minimized. Consequently, the motion in the outer region would then depend less upon the previous history of the beam and, hence, the beam extraction becomes much easier.

In a sector focused cyclotron, there is no cylindrical symmetry in the magnetic field and therefore the meaning of centering is less obvious. Nevertheless, one can define particle centering(for a given energy) in the sense of the average of the instantaneous center of curvature along the equilibrium orbit. The trajectories of actual particles depart from this equilibrium orbit in the course of their acceleration. The degree of the departure can be averaged over the one complete revolution and this quantity can be used as the measure of off-centering.

In order to study the radial motion of a beam, it is, therefore, appropriate to start by investigating the motion of the instantaneous center of the radius of curvature(we will call it "the orbit center"). Let us assume that $\vec{R}$ is the position vector of particle, $\vec{\rho}$ is the radius of curvature and $\vec{r}$ is the radial vector from the center of the cyclotron to the center of curvature of the orbit, as is described in Fig. 4.7. Then, from straightforward vector considerations, we obtain the relationship $\vec{R} = \vec{r} + \vec{\rho}$. Substituting $\vec{P} = q\vec{B} \times \vec{\rho}$ into the above equation, we subsequently obtain the position(X_c, Y_c) of the center of the particle's orbit in terms of the Cartesian

coordinates:

$$X_c = X - \frac{P_y}{qB_z}, \qquad Y_c = Y + \frac{P_x}{qB_z} \quad , \tag{4.2.2}$$

where (X, Y) and (P_x, P_y), respectively, are the position and the momentum of the particle at the time t. Note that both B_r and B_θ are zero here because we have confined the motion to the median plane (z=0).

For up to 50 orbits, the instantaneous motion of the center of the orbit of the reference particle for the D^- beam was obtained from eq. (4.2.2) and is given in fig. 4.5. The X and Y axes of this figure represent the directions along, and perpendicular to, the dee-gap, respectively. The origin denotes the center of the cyclotron. Each point on the figure indicates the instantaneous orbit center of the D^- beam. A "well-centered" beam is then the one whose reference particles' orbit center (averaged over one complete orbit turn) converges onto the cyclotron center. The figure shows that the overall center of the orbit is indeed relatively well-converged onto the origin.

It is reasonable to expect that the beam orbit centering is very sensitive to the injection angle of the particle. Figs 4.6 to 4.9 demonstrate the instantaneous motion of the center of four particles with the injection angles of 121°, 124°, 127°, and 130°, respectively. From these figures, it is obvious that 127° should be chosen as the injection angle of the reference particle.

It is then possible to fix the horizontal position of the mirror in such a way that the reference particle will pass through the mirror gap at the center of the gap.

In fig. 4.10, the trajectories of eighty D^- particles through up to fifteen turns are simultaneously depicted. The initial conditions of these particles at the injection

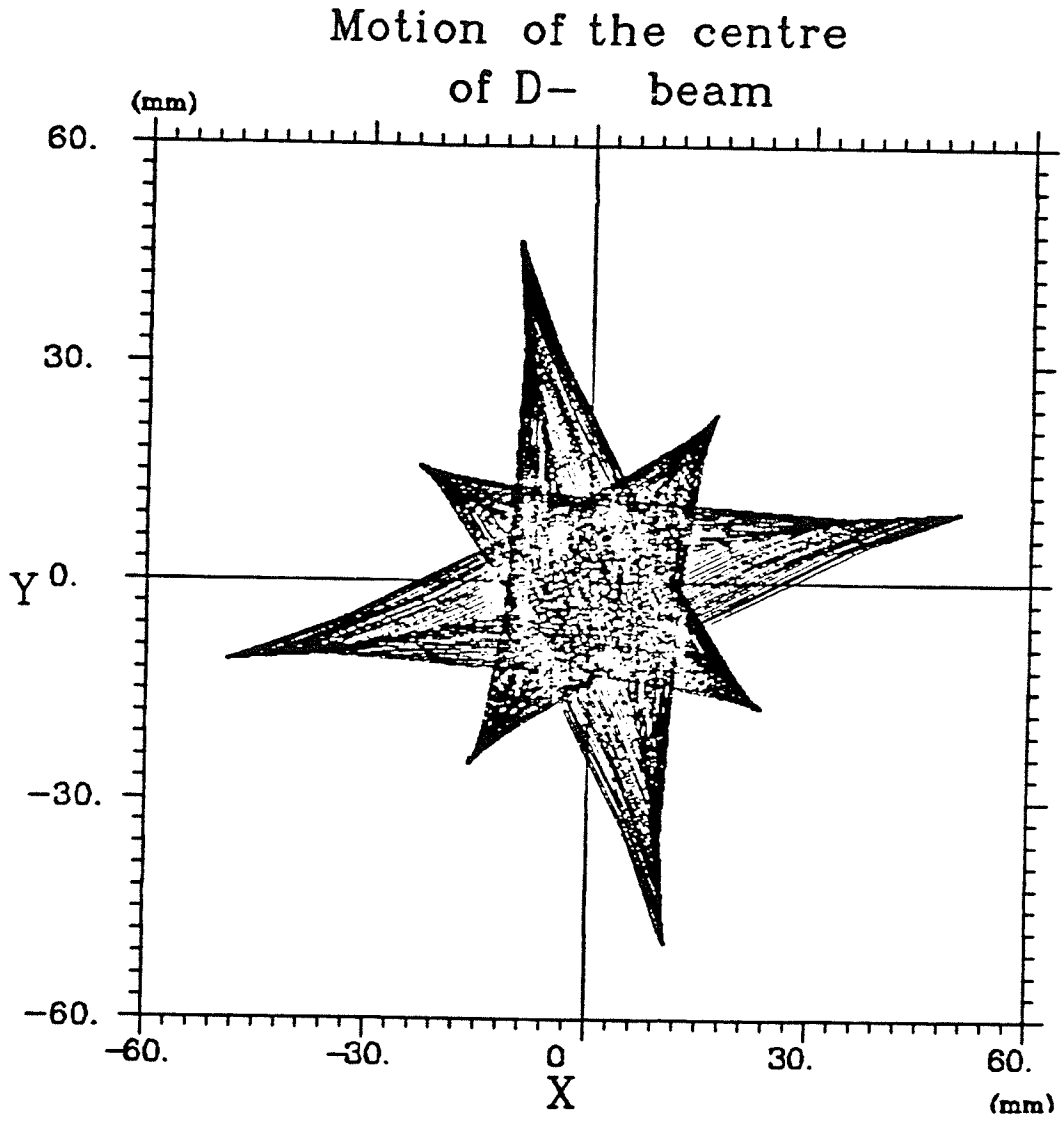

Fig. 4.5 The instantaneous motion of the center of the D^- beam in the newly designed central region of the University of Manitoba cyclotron. The horizontal and vertical axes denote directions along and perpendicular to the dee-gap, respectively. The origin of the graph represents the center of the cyclotron. This figure shows that the center of the beam converges well onto the origin of the graph.

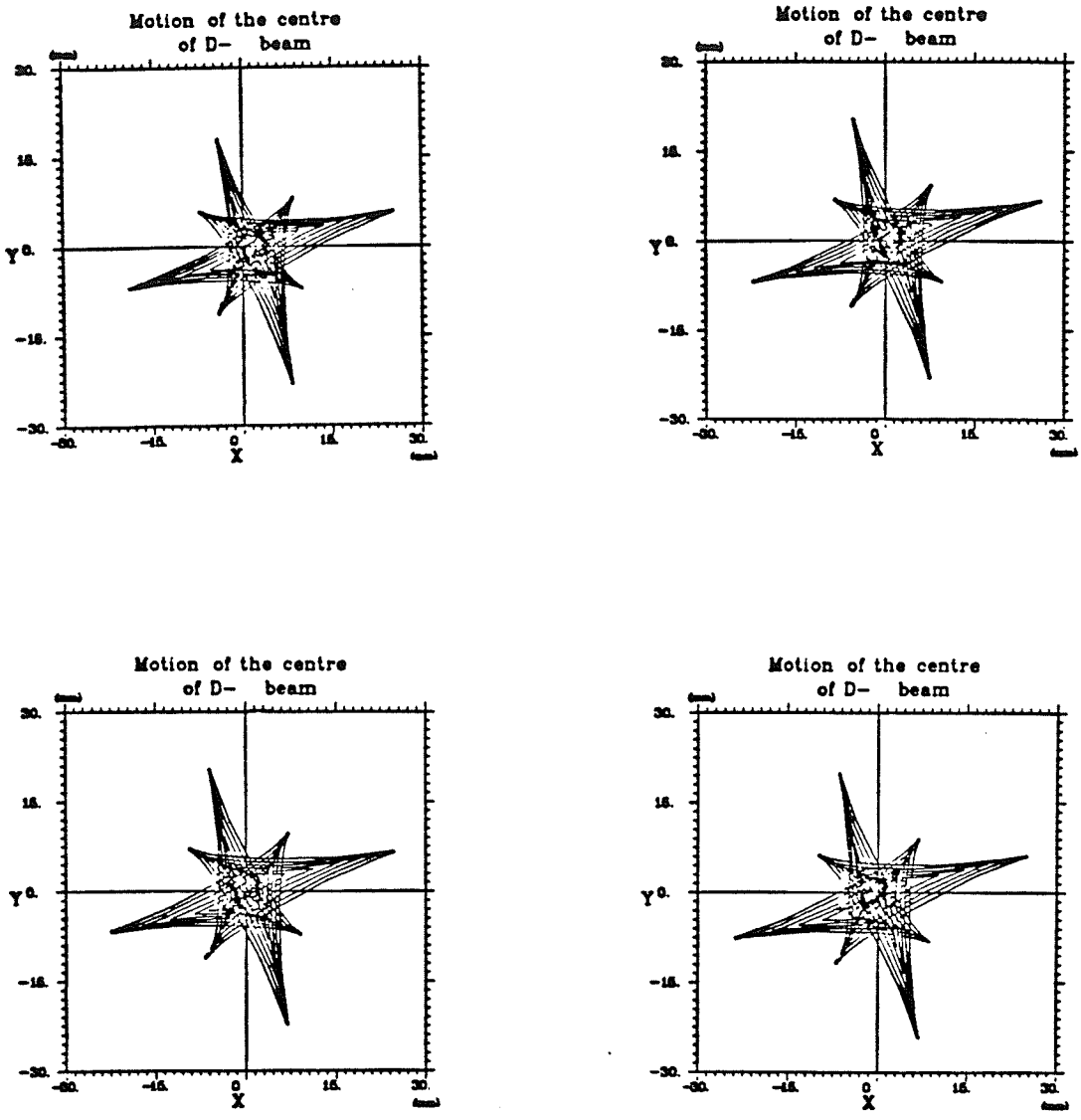

Figs. 4.6 – 4.9 The initial center motion of four selected particles. Their injection slope angles with the mirror are 121° (fig. 4.6, top left), 124° (fig. 4.7, top right), 127° (fig.4.8, bottom left), 130°(fig. 4.9, bottom right).

point were chosen from the $r - p_r$ phase space ellipse whose area is 120 mm mrad. The spreads in phase ($\pm 10°$) and energy (± 0.2 keV) were also taken into account in the calculation so that the diagram should closely resemble the real situation. Fig. 4.11 denotes the initial distribution of the centers of the eighty particles in X-Y plane. It can be seen that the distribution is assumed to be an ellipse.

Further theoretical analysis indicated that the radial spread of beam orbits is mainly caused by the effect of the accelerating gap crossing oscillation([BLO71]. Therefore, a more homogeneous electric field distribution would be helpful in improving the radial motion of the beam. In this study, we have tried to utilize an RF quasi-static field 1.1 kV less than $E_0 \cos \omega t$, *i.e.*, to use E=$E_0 \cos \omega t$ - 1.1 kV instead of E=$E_0 \cos \omega t$, this has reduced the shift of the center of the beam in the first 20 turns by about 30%.

4.2.3 The axial motion

As was mentioned earlier, a major problem that is associated with the axial motion of a beam in the central region of the cyclotron (especially for the U of M cyclotron) is the lack of axial focusing. In order to confine a beam to the vicinity of the median plane, an adequate axial focusing force is required. Such a focusing force not only prevents a beam from hitting the dee wall (or the vacuum chamber), but also restricts the beam to a linear motion region. This latter condition is very important, for otherwise higher-order effects will become dominant, thus invalidating the assumption of decoupled radial and axial motions. The axial geometry of the new central region of the U of M cyclotron was carefully optimized along these lines. The final geometry shows that the internal height of the dee is z=6 mm between the

Fig. 4.10 Fifty D^- particles' radial trajectories through up to fifteen orbit turns. The initial conditions of the particles were arbitrarily distributed; the phase space area was 120 mm mrad, the energy spread was ± 0.2 keV and the RF phase spread was $\pm 10°$. The six points on the figure in the central region denote the locations of the posts (See section 4.2.3).

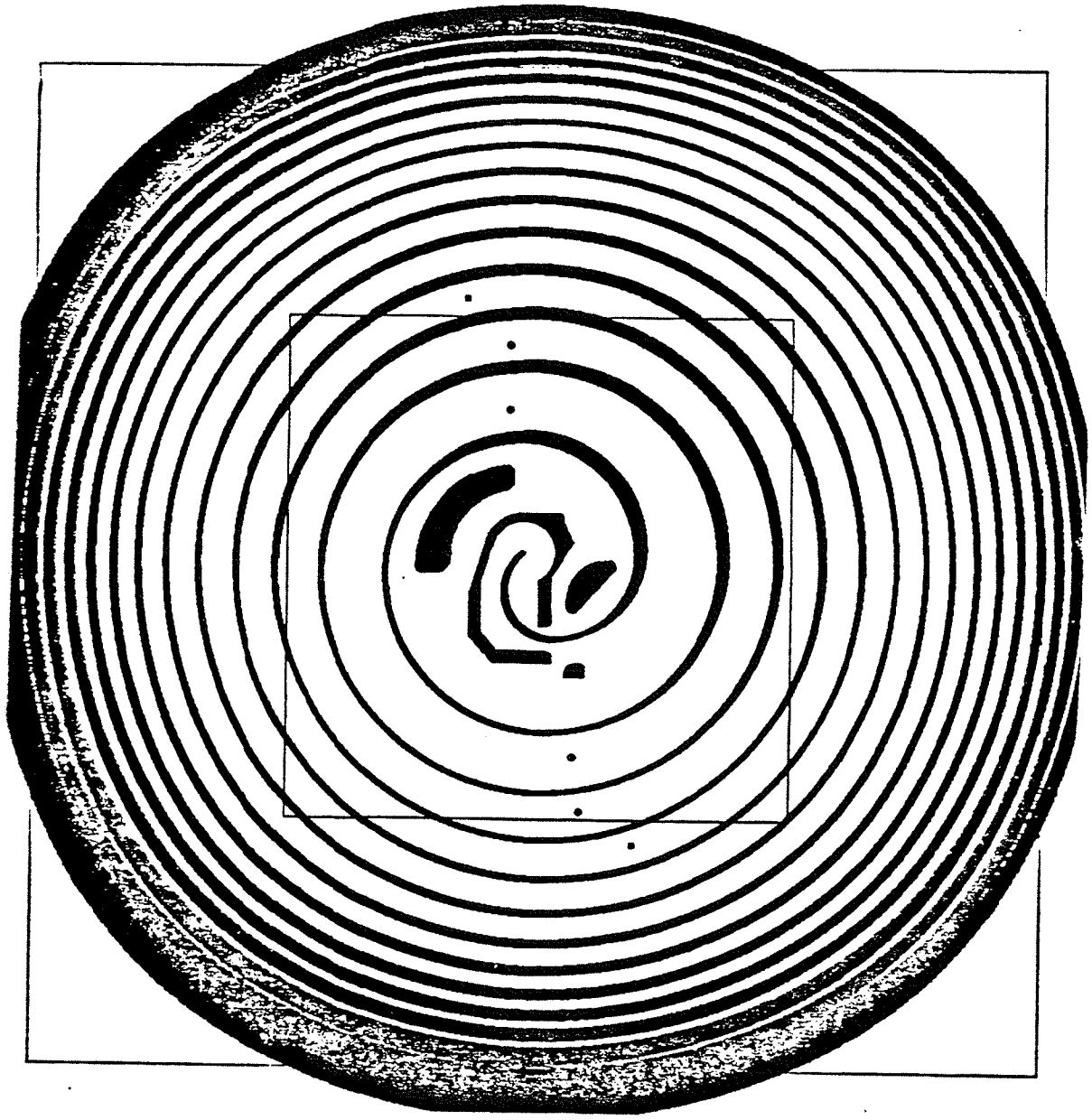

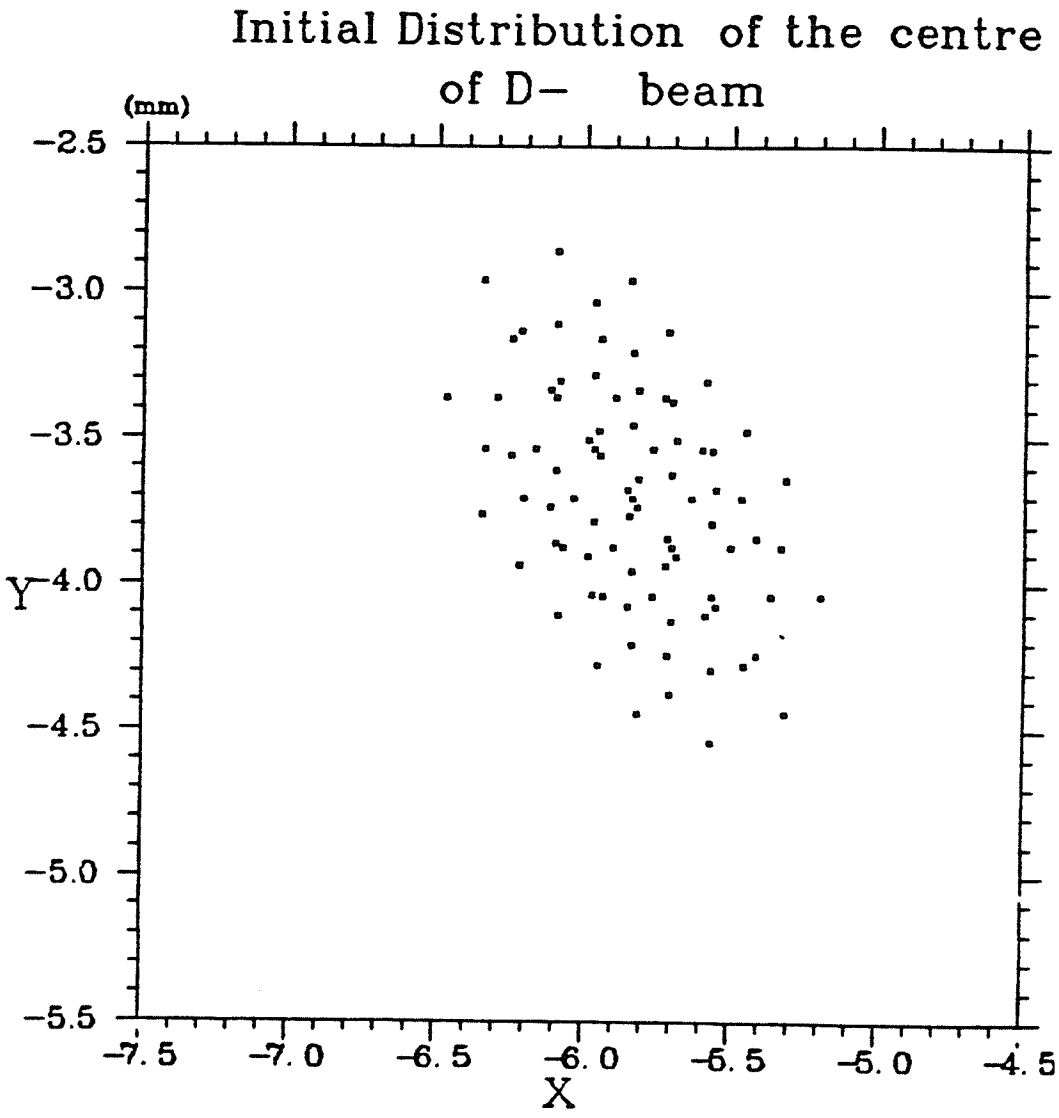

Fig. 4.11 The initial distribution of the center position for the beam described in fig.4.10.

first accelerating gap, and r=2.6 cm, then the internal dee height increases linearly with r till r=11 cm, where z is 2.2 cm.

To investigate the stability of beam in its axial motion, we studied two particle trajectories, off the median plane in the new central region of the U of M cyclotron, up through twenty five turns. The results are displayed in fig. 4.12. These trajectories were obtained by numerical integration of the particle's orbits. In fig. 4.12, the horizontal axis denotes the particle's orbit number and the vertical axis represents the displacement from the median plane of the cyclotron. The two particles shown in the figure are the orthogonal rays; they correspond to two linearly independent solutions of the second-order differential equation with the oscillation phase difference of 90° at the starting point. These two particles were chosen from the boundary in the beam phase space ellipse, whose area is 120 mm mrad, a value which corresponds to the actual emittance of the beam from the axial injection system. Fig. 4.12 indicates that the maximum amplitude of the oscillation is about 9 mm, a value that is unacceptably large. For such a large oscillation amplitude, most of the particles will hit the dee wall and will be lost.

The above problem was initially solved in the 1960's, by introducing an arrangement of grids along the edges of the dees([COX62]). In general, an accelerating gap (with a two-dimensional geometry) provides electric focusing on the entrance side and electric defocusing on the exit side. The net effect, to the first order, is a null focusing effect. A way of enhancing the electric focusing is to reduce (or eliminate) the defocusing force on the exit side. The enhanced electric focusing may be effective for an injected beam for up to 4 or 5 turns of orbit. The placement of mesh on the exit side will eliminate the defocusing force, thereby enhancing the rf electric

focusing considerably. This development, however, would result in a noticeable reduction in the beam transmission. But this adverse effect can be avoided when we simply replace the grid by a set of posts each of which is carefully placed between the successive turns so that the post will not intercept the beam. If we replace the grids by a set of posts, then most of the field lines will end at the posts (the field has no axial component at a post but only the horizontal component), thereby reducing the defocusing effect (see Fig. 4.13). By reducing the gap between the posts, we can reduce the defocusing effect of these second gaps almost completely. In the U of M cyclotron, therefore, a number of posts were placed along the leading edges of the two dee-tips. It should be noted that had we placed the posts on the leading sides of the ground shield, we would have further enhanced the focusing (see Fig. 4.1). Actually, placing posts on the ground shield turned out to be impractical from engineering point of view. It was, therefore, decided to place the posts along the entrance side of the dee rather than along the entrance of the ground shield.

The resulting axial motion of the D^- beam for up to tenth turn is depicted in Fig. 4.14. To obtain this figure, a total of twelve identical posts of 1.5 mm in diameter, were placed along the leading edges of the dee-tips (six for the South dee-tip and six for the North dee-tip). The posts cover up to five turns of orbit. The positions, the diameter, and the number of the posts were all carefully determined on the basis of detailed orbit studies so as to maximize the beam transmission. With the help of fig. 4.10, which provided a realistic picture of the radial trajectories of a number of particles, we can select precisely all the parameters for the posts. It is evident from Fig. 4.10 that while adjacent orbit turns would overlap after the eleventh turn, the turn spacings before the eighth turn are wide enough for the

Fig. 4.12 The axial motion of the two orthogonal D^- particles in the new N=2 central region of the University of Manitoba cyclotron. The horizontal and the vertical axes denote the turn number and the displacement from the median plane, respectively. No posts were placed. It is seen that the maximum oscillation amplitude is about 9 mm.

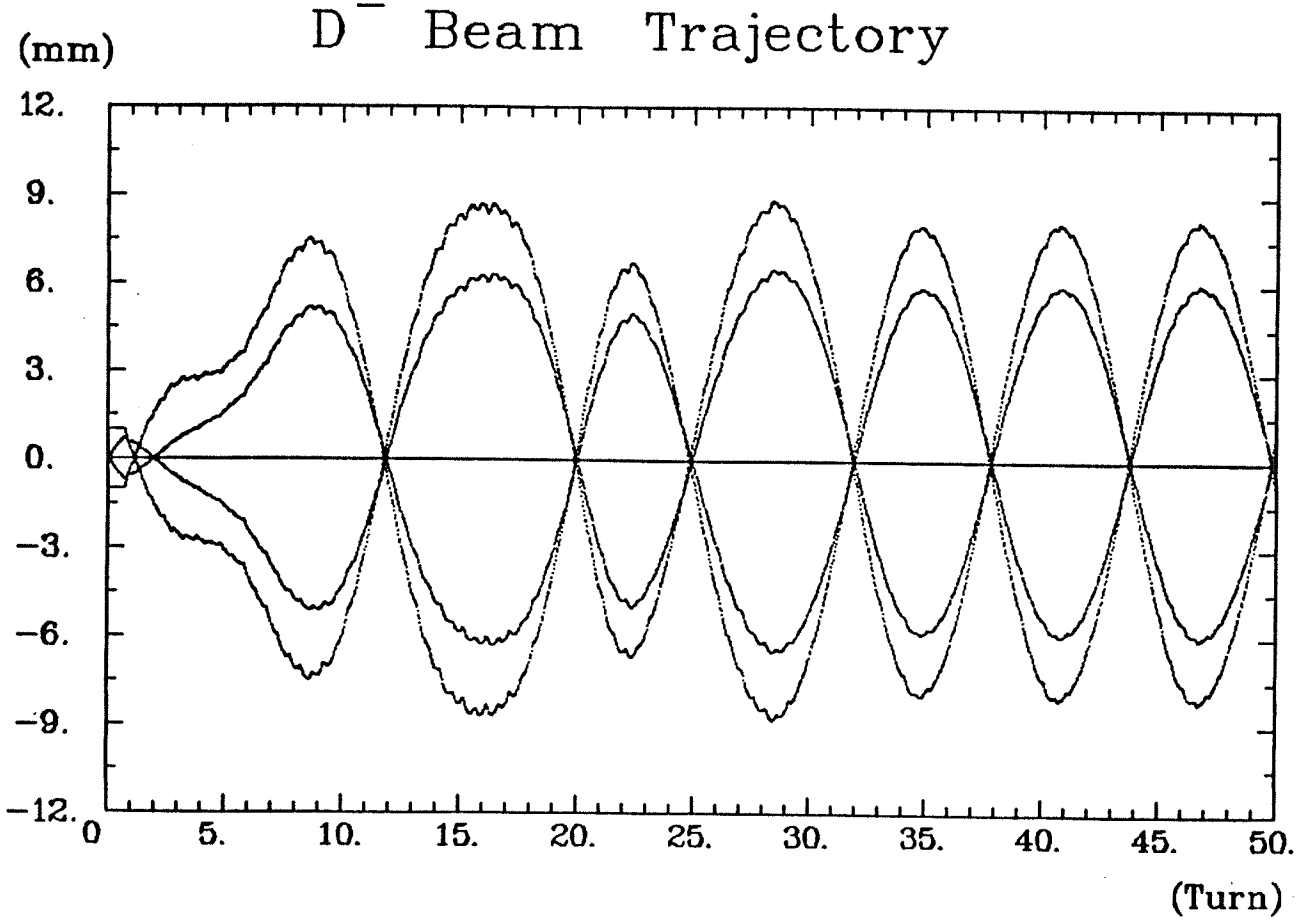
D⁻ Beam Trajectory
(mm)
12.
9.
6.
3.
0.
−3.
−6.
−9.
−12.
0
5.
10.
15.
20.
25.
30.
35.
40.
45.
50.
(Turn)

insertion of these posts without intercepting any beam. Fig. 4.14, when compared with Fig. 4.12, shows clearly the effects of these posts. The two particles' initial conditions are the same as those utilized in Fig. 4.12. It is seen from Fig. 4.14 that the trajectories are relatively well confined to the vicinity of the median plane; the maximum amplitude of the axial displacements is reduced to about 2 mm.

The effect of changing the injection energy were also investigated. Fig. 4.15 and fig. 4.16 show the axial motion of two sets of particles, with initial energies of 15 keV and 17 keV, respectively, and with all their other initial conditions being identical. It is seen that the amplitude of the axial motion of the set with the higher injection energy is much smaller, having been reduced to about half the amplitude of the set with the lower injection energy.

In actuality, the particles of the injected beam can differ in their initial energies, RF phases, displacements and divergences with respect to the median plane. We assume that for the D^- ion beam all of these parameters have a distribution which is centered around the parameters of the reference particle. The central region, whose effect is sensitive to the spreads in these particle parameters, will not accelerate some of the particles, and hence the acceptance of the cyclotron will be reduced. To increase this acceptance, and therefore to maximize the transmission of a beam throughout the central region, it is very desirable to have the central region less sensitive to these spreads in the particle parameters. Fig. 4.17 shows trajectories off the median plane for 80 particles. The initial conditions for these particles are selected in such a way that their trajectories form an area of 150 mm mrad in the $z - p_z$ phase space and that their energies and RF phase are (15$\pm$0.2) keV, and ($-270 \pm 5°$), respectively. Fig. 4.17 clearly reveals the insensitivity of the

(a)

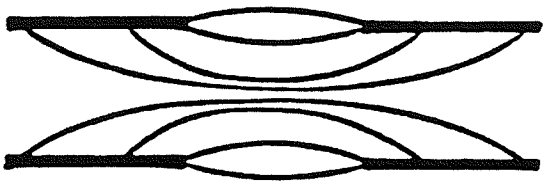

(b)

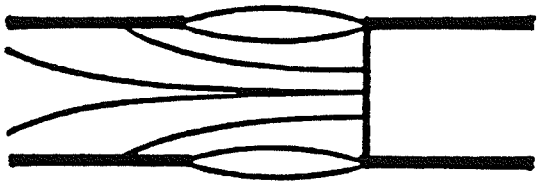

Fig. 4.13 The lines of the electric field (a) without and (b) with the post. These figures show that the presence of the post in the downstream side (on the right-hand side) removes some of the defocusing effects of the electric field lines.

Fig. 4.14 Two orthogonal particles' axial motion in the new N=2 central region of the University of Manitoba cyclotron. The horizontal and the vertical axes denote the turn number and the displacement from the median plane of the cyclotron, respectively. The Posts had already been placed. It is seen that the maximum amplitude is about 4 mm (see fig. 4.12 for comparison).

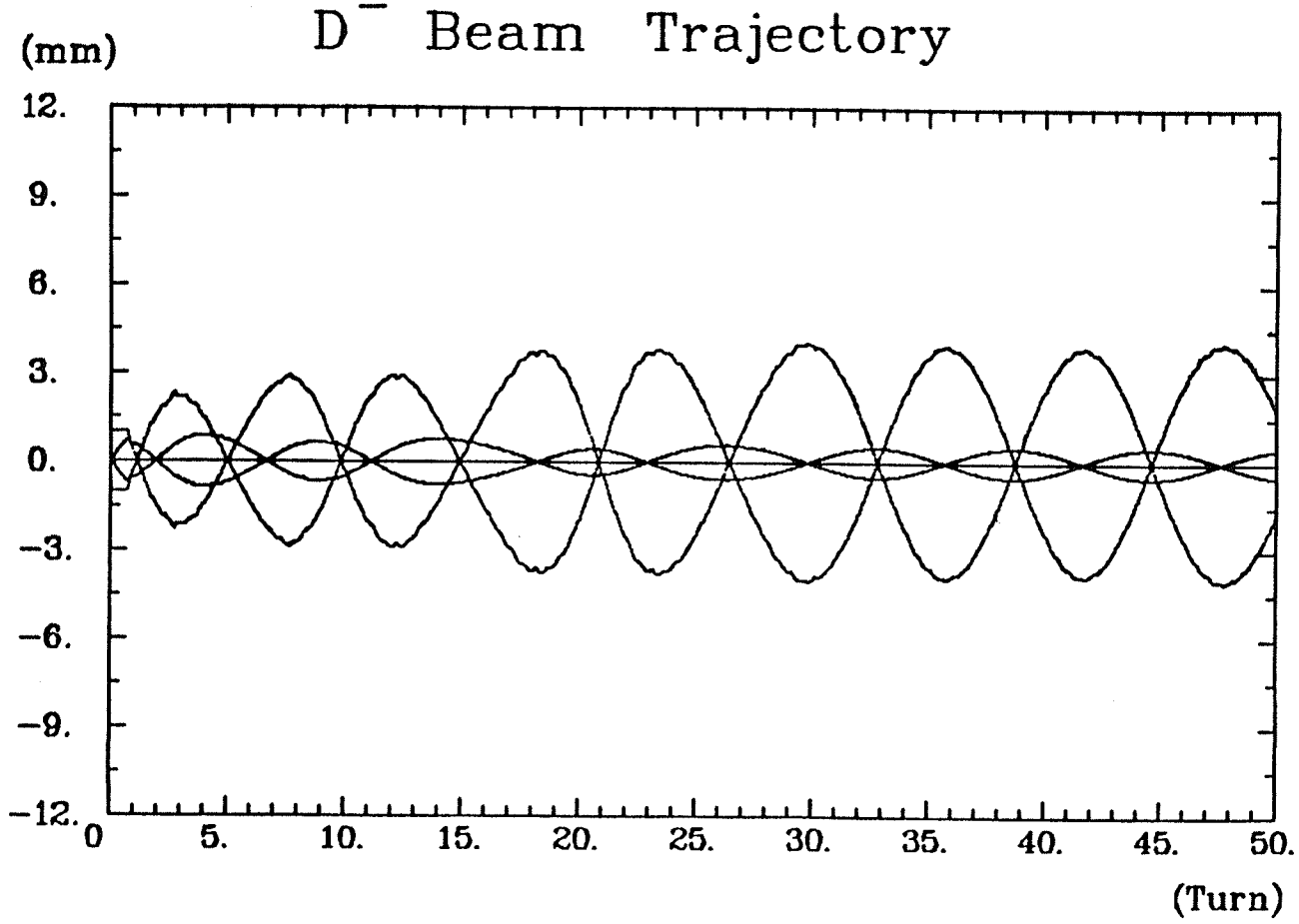
D⁻ Beam Trajectory
(mm)
12.
9.
6.
3.
0.
−3.
−6.
−9.
−12.
0
5.
10.
15.
20.
25.
30.
35.
40.
45.
50.
(Turn)

central region to these variations in the energies and the RF phases; the particle motions are extremely well confined to the median plane of the cyclotron, a valuable achievement.

Once the beam has progressed beyond six turns, the magnetic focusing that is due to the field bump progressively takes over the rf electric focusing. In that region the amplitude of the axial motion is gradually reduced as the degree of the magnetic focusing increases; this amplitude is inversely proportional to the square root of the average magnetic field along the radius and ν_z, as eq. (2.5) indicates. Therefore, the beam will hardly suffer from any further loss of axial focusing once the beam has cleared the dee-tips.

4.3 Conclusions

In the preceding sections, we have described in detail a major upgrading of the University of Manitoba cyclotron to improve the acceleration of D^- ions.

Based on the design study of the new central region, and on the optimized magnetic field, the systematic investigations of the beam orbit dynamics that are described in this chapter have been carried out. These studies have indicated the following major improvements in the performance of the cyclotron.

1. The maximum available energy of the D^- ion beam can be increased to 27 MeV.

Before the upgrade, the cyclotron was often unreliable as a source of D^- ion beams with energies above 17 MeV. The main problems were, (as discussed in Chapter 2), the poor isochronism at large radii and the dee voltage being too low. The 1984 upgrading project changed the cyclotron parameters completely as well

Figs. 4.15, 4.16 The axial motion of two sets of particles up through 10 orbit turns. The two sets have identical initial conditions except that the injection energy is 15 keV for the first set (fig. 4.15) and 17 keV for the second one (fig. 4.16).

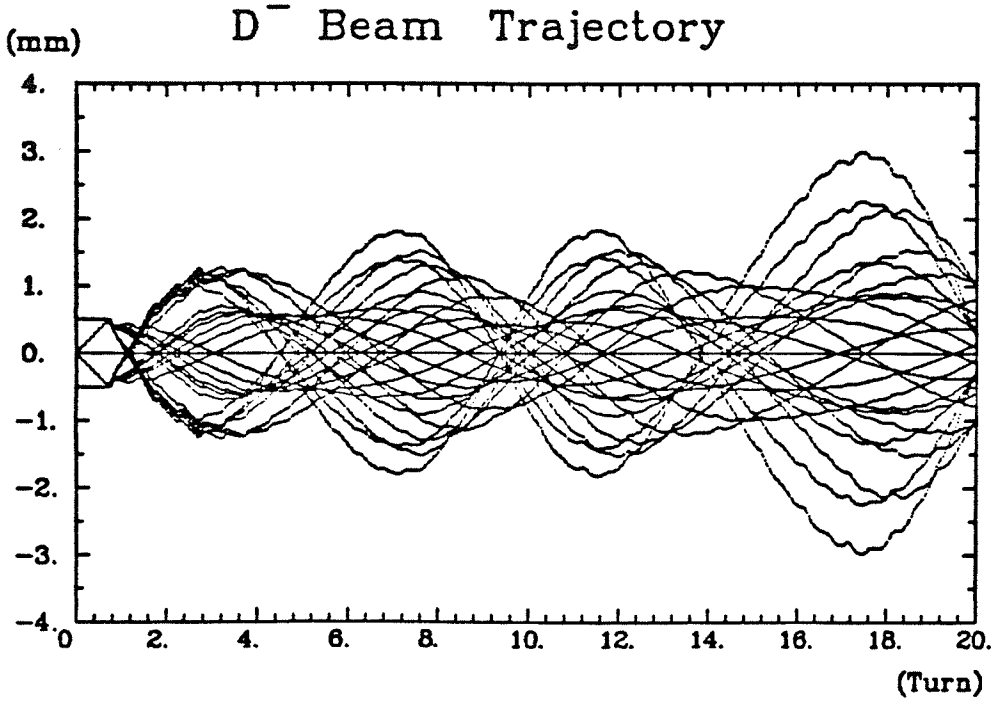
D⁻ Beam Trajectory
(mm)
4.
3.
2.
1.
0.
-1.
-2.
-3.
-4.
0
2.
4.
6.
8.
10.
12.
14.
16.
18.
20.
(Turn)

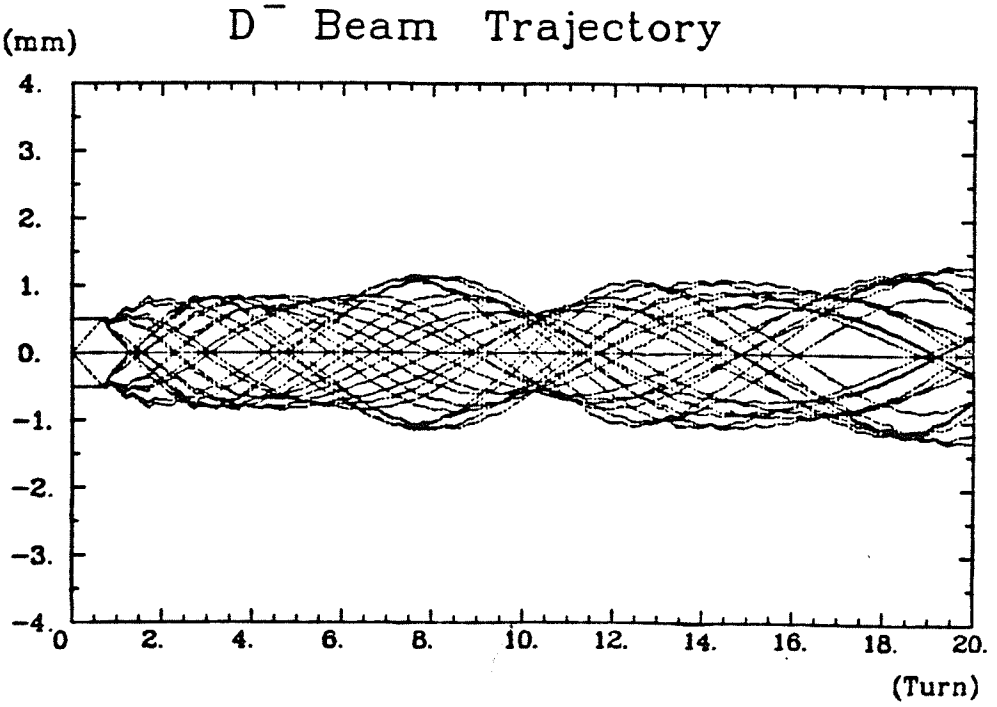
D⁻ Beam Trajectory
(mm)
4.
3.
2.
1.
0.
-1.
-2.
-3.
-4.
0
2.
4.
6.
8.
10.
12.
14.
16.
18.
20.
(Turn)

Fig. 4.17 The axial motion of eighty particles in the new N=2 central region of the University of Manitoba cyclotron. The horizontal and the vertical axes denote the turn number and the displacement from the median plane of the cyclotron, respectively. The Posts had already been placed. In this figure, all the possible spreads of the initial conditions were included. It is seen that the maximum oscillation amplitude is about 2 mm.

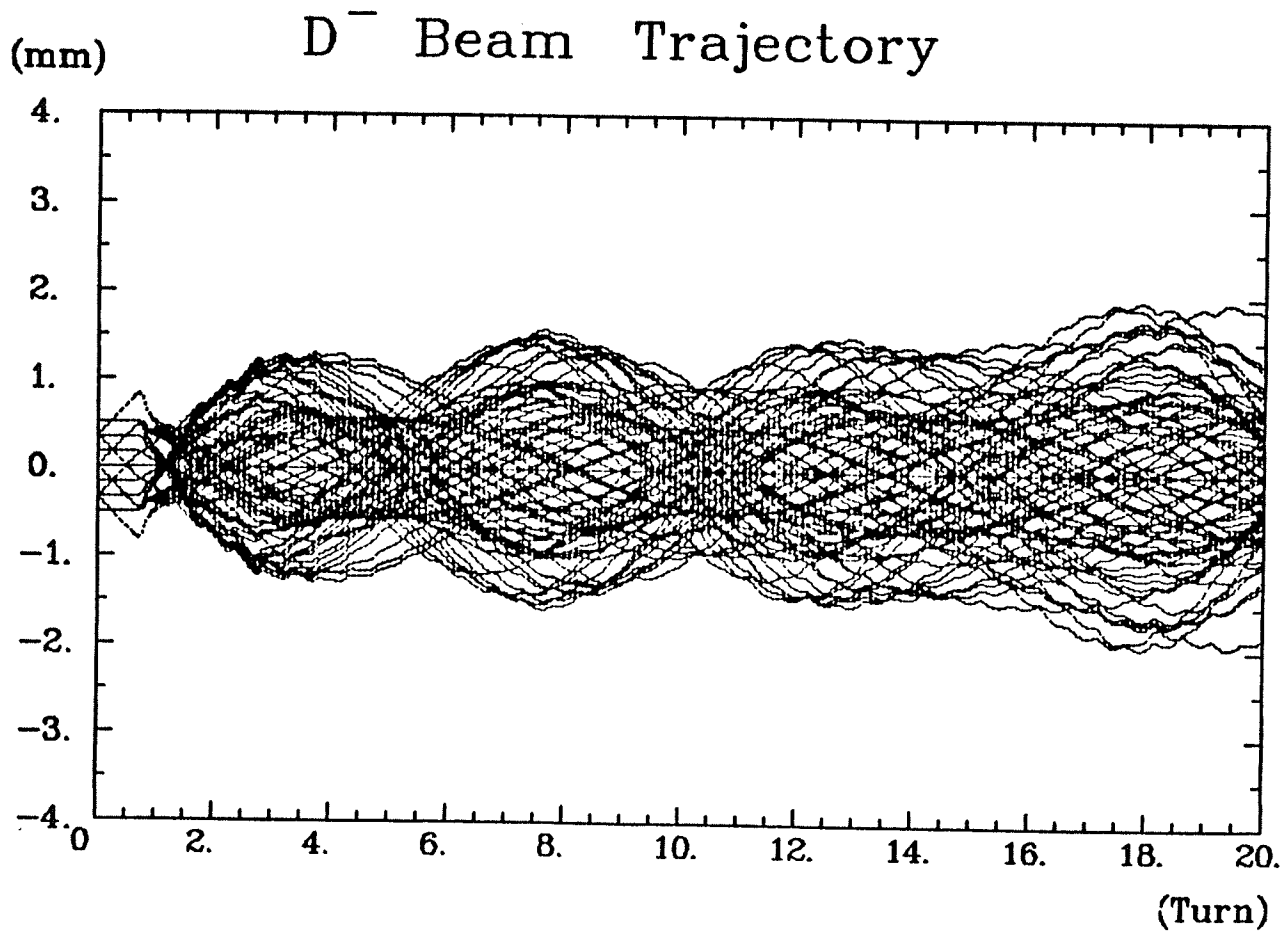
D⁻ Beam Trajectory
(mm)
4.
3.
2.
1.
0.
−1.
−2.
−3.
−4.
0
2.
4.
6.
8.
10.
12.
14.
16.
18.
20.
(Turn)

as significantly improved the magnetic field as described in Section 2.3. Thus, the rf changed from 14.24 MHz push-pull to 30.50 MHz push-push mode, the dee voltage was raised from 14.5 kV to 40 kV. The latter resulted in the increased energy gain per turn from 35 keV into 120 keV. Utilizing these new data, our beam tracing calculations predicts that the maximum attainable energy of D^- beam in the U of M cyclotron could now reach as high as 27 MeV.

2. The beam quality is predicted to improve significantly.

The author's calculations of the behavior of the D^- ion beam in transverse phase space have shown that with the newly designed central region and the optimized injection parameters, plus the insertion of the twelve posts, the beam has become very stablized in both its radial and axial motions. The betatron oscillation amplitude of the beam is predicted to be reduced to one half of its former value. Calculations indicate that for a 26 MeV D^- ion beam, an energy spread of only 0.5% is obtainable. Therefore, a D^- ion beam with higher intensity, better reproducibility, and smaller spot should now be attainable.

3. The beam transmission efficiency will be increased.

The significant improvement in the quality of D^- beam would necessarily also increase the transmission efficiency. Our estimate is that the overall transmission will be about 15%. With a 60 μA D^- beam from a duoplasmatron source, we therefore expect that a 9 μA deuteron beam will be extracted from the cyclotron. With the Ehlers source expected to be operational in the near future, we expect eventually to be able to extract a 20 μA deuteron beam with the energy ranging from 10 MeV to 26 MeV.

In making the above estimates, the axial injection system is assumed to be custom-made for the new dee-tips and central region. In reality, however, we will be initially using the old axial injection system with a re-adjusted injection optics system. This, however, will be only a temporary measure until the new axial injection system is completed.

4. The possibility of single-turn extraction

The single-turn extraction of a beam is often desirable in a cyclotron, since this is the best way to obtain an output beam with a very high energy resolution and a substantial current. As mentioned earlier, in the upgrading of the cyclotron, the dee voltage was raised from 14.5 kV into 40 kV. This, together with the simultaneous improvements in the isochronism and in the magnetic field distribution, has resulted in an increase in the energy gain per turn from 35 keV into 120 keV, thereby reducing the total number of turns required for the particle to reach a given energy. This reduction in the total turn number inside the cyclotron, will lead to a corresponding reduction in the beam phase excursion during the acceleration. Furthermore, the turn spacing should now become much larger than before. According to our tracing calculation, the turn spacing can reach values as large as 5 mm for a 25 MeV D^- beam. Therefore, this may lead to the possibility of quasi single-turn extraction. To achieve this goal, a system consisting of four remotely controlled radial slits was designed. The single-turn extraction will be possible only when the stripping foil is positioned precisely at the correct point. Such studies and calculations have been performed, utilizing the equilibrium theory and our orbit tracing program. This investigation will be described in the following chapter, Chapter 5.

Chapter 5

A Study of Positive Ion Beam Extraction

5.1 Introduction

The acceleration of negative ions in a cyclotron was first reported by Lofgren([LOF51]). The possibility of the premature stripping of the ions during the course of the acceleration, due to relatively large stripping cross section of air molecules, raised doubts as to the usefulness of H^- ions for the production of external beams of reasonable energy. However, a more detailed calculation of this cross section led to the suggestion that useful beams could be obtained up to 50 MeV of energy([VER63]). The possibility of producing external beams of different energies by stripping the electrons from the ions at various radii is clear([WRI57]). Slightly less obvious is the possibility of producing a variable energy beam along a single external beam line. This possibility was first suggested through the use of extracted neutral particles, and later through the use of extracted ions(PAU63], [RIC62]).

This method was applied to the Manitoba cyclotron early in 1966([BUR66]). Fig. 5.1 shows the schematic diagram of the extraction system in the Manitoba machine. As is shown in this figure, beams of various energies could be obtained by moving the stripping foil radially. Subsequently, these stripped particles are led to pass through the center of a bending magnet(a combination magnet) by moving the stripping foil azimuthally. The combination magnet can be adjusted to direct beams of any energy along the beam pipe axis.

The combination magnet was placed at the corner of the cyclotron vacuum chamber, 1.5 m away from the center of the cyclotron. It has a 20.4 cm diameter,

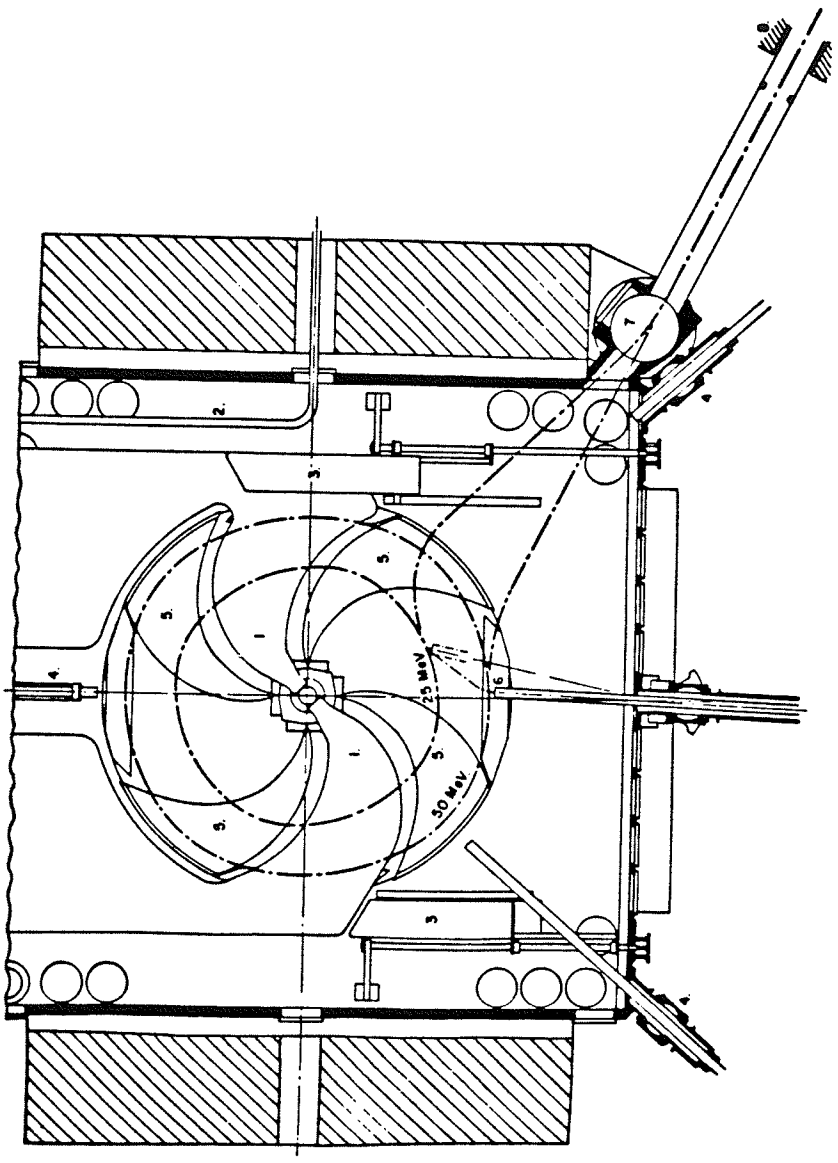

Fig. 5.1 The schematic diagram of the extraction system in the University of Manitoba cyclotron. In the figure, 1. Dees; 2. Coupling loop; 3. Trimming capacitors; 4. Beam probes; 5. Hills; 6. Stripping foil; 7. Combination magnet; 8. Quadrupole magnet.

a gap of 3.8 cm, and is of compact and economic design. Because it is close to the cyclotron magnet, the cyclotron magnet vertical yoke was used for its flux return path. This caused a slight inconvenience, as the cyclotron magnet detunes a little when the combination magnet current is changed. With the excitation current of the combination magnet turned off, there is already a field of 0.48 Wb/m^2. This is caused by flux leaking from the highly saturated vertical yoke. The field has to be increased to 0.83 Wb/m^2 for the minimum energy and decreased to -0.08 Wb/m^2 for the maximum energy. The maximum power consumption is about 1 kW.

To achieve the single-turn extraction of a positive ion beam, as was stated in the preceding chapter, both the radial and the azimuthal positions of the stripping foil must be adjusted precisely. Besides, after the University of Manitoba cyclotron underwent its extensive upgrade, the reshaping of the magnetic field resulted in a change in the extraction beam trajectory, and therefore the beam could no longer be extracted by placing the stripping foil according to the old data. It was therefore obviously desirable to carry out an appropriate beam extraction study. The stripped beam, in general, has to pass through the fringe magnetic field of the cyclotron. This beam is, therefore, expected to have been distorted to a varying degree (depending on its energy) by the time that it reaches the first focusing element, which is 2 to 3 meters away from the stripping foil. Thus, an extraction study will enable us to predict not only the positions of the foil as a function of the beam extraction energy, but also the beam trajectories and the relative parameters.

5.2 The calculation of the equilibrium orbits and of the extraction reference orbits

The starting point of the extraction study is the computation of the equilibrium orbits inside the cyclotron as a function of the energy of the accelerated H^- ions. The equilibrium orbits were computed by using the computer code MAPANL which was developed at the U of M Cyclotron Laboratory. The basic algorithm of MAPANL was introduced in the work of Gordon and Welton ([GOR59], [WEL59]) who developed methods to find the equilibrium orbit as a function of the energy. With the particle energy as an input, the program integrates the equations of motion over one magnetic field period(90°), using the azimuthal angle (θ) as the independent variable. Since the equilibrium orbit, by definition, is smoothly closed on itself, the initial values of r and p_r are the same as the final values of these variables along the equilibrium orbit. The determination of an equilibrium orbit then reduces to the determination of the initial values of r and p_r. Fig. 5.2 shows three equilibrium orbits that were obtained as the output of the program. They correspond to H^- ions with energies of 20, 35 and 50 MeV, respectively. The lower energy limit of 20 MeV is currently set by a limitation on the azimuthal swing of the stripper probe and by the uniform-field width of the combination magnet being only about 2 inches. For the same reasons, the maximum energy of the beam has been set to be 50 MeV.

The stripping foil is supposed to be placed at a position inside the cyclotron where it will intercept some of the equilibrium orbits. A computer code, EXTBEAM, was written by the author to trace the orbits of those intercepted H^- ions which are converted to H^+ ions at the point of interception. This code, EXTBEAM, by integrating the equations of motion, traces the particles all the way through the cyclotron field (including the fringe field) and through the field of the combination

magnet. The conditions for extraction are that the reference particle has to enter the combination magnet at 90° and that, on leaving the combination magnet, the particle trajectory has to be on-axis along the beam transport line. This is a successively iterative approach to find the optimum position (radial and angular) of the stripping foil. Table. 1 shows the extraction parameters (including the position of the stripping foil) for the three ion energies (20, 35 and 50 MeV, respectively) and Fig. 5.3 demonstrates the corresponding extraction reference trajectories.

Table 1. Extraction Parameters

Beam Energy (MeV)	20	35	50
Radius of The Stripping Foil (cm)	34.6	45.4	52.8
Azimuth of The Stripping Foil(deg.)	17.4	1.4	0.4
C.M.* Field Needed (kG)	-8.1	-2.1	2.3
Deflected Angle of The Beam at C.M. (deg.)	17.0	3.0	-3.4

C.M.* is an abbereviation for Combination Magnet

It is seen from the table 1. that the radial and azimuthal positions of the stripping foil have to be varied between 34.6 and 52.8 cm., and 17.4° and 0.4°, respectively, to accommodate particles with energies between 20 MeV and 50 MeV. It also should be noted that maximum excitation of the combination magnet as well as the maximum deflection are required for the lowest beam energy.

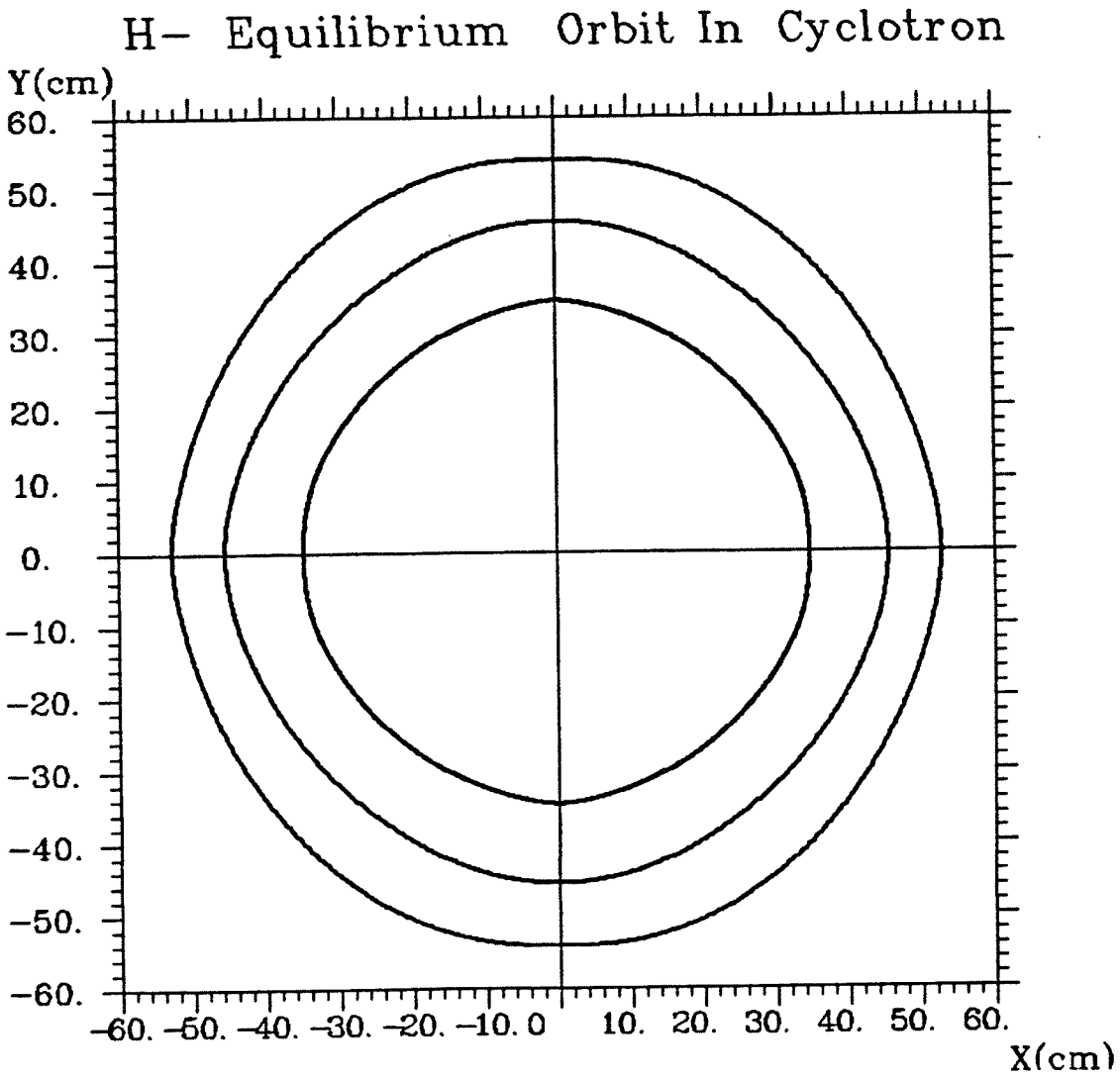

Fig. 5.2 H^- equilibrium orbits for three selected energies 20 MeV (the inner), 35 MeV (the middle) and 50 MeV (the outer). The origin of the figure corresponds to the geometrical center of the cyclotron.

For the initial runs to produce extracted beam with 50, 35 or 20 MeV, the location of the stripping foil and the combination magnet excitation current were selected based on our knowledge of the equilibrium orbits in the cyclotron and on our calculation of particle trajectories through the fringing field. After the experimental determination of the parameters for these beam energies, the computer code can then be used to compute parameter values for other beam energies to provide an interpolation table. Such a table would give the combination magnet power supply readings and the stripper locations necessary for the extraction of all energies between 20 and 50 MeV in a small energy interval.

5.3 A computer simulation of the extracted beam

To study the properties of the extracted beam, a simulative calculation has been carried out, based on the following assumptions. We assume that the beam at the point of stripping has a circular center spread of $r=\pm 1.5$ mm (See fig. 5.5), that the beam is centered at the cyclotron's geometrical center (*i.e.*, that the reference particle follows the equilibrium orbit) at the extraction radius and that a particle gains energy of 80 keV per turn near the extraction radius. The stripping foil is assumed to have a sufficiently wide radial width and zero thickness. A further assumption made was that the radial and axial motions can be decoupled. With this assumption, it was possible to study separately the radial motion and the axial motion.

For the study of the radial motion, a set of particles were selected having orbit centers (in the sense of an average over one complete turn) that were located as is shown in Fig. 5.4. The beam's center spread in the radial direction towards the

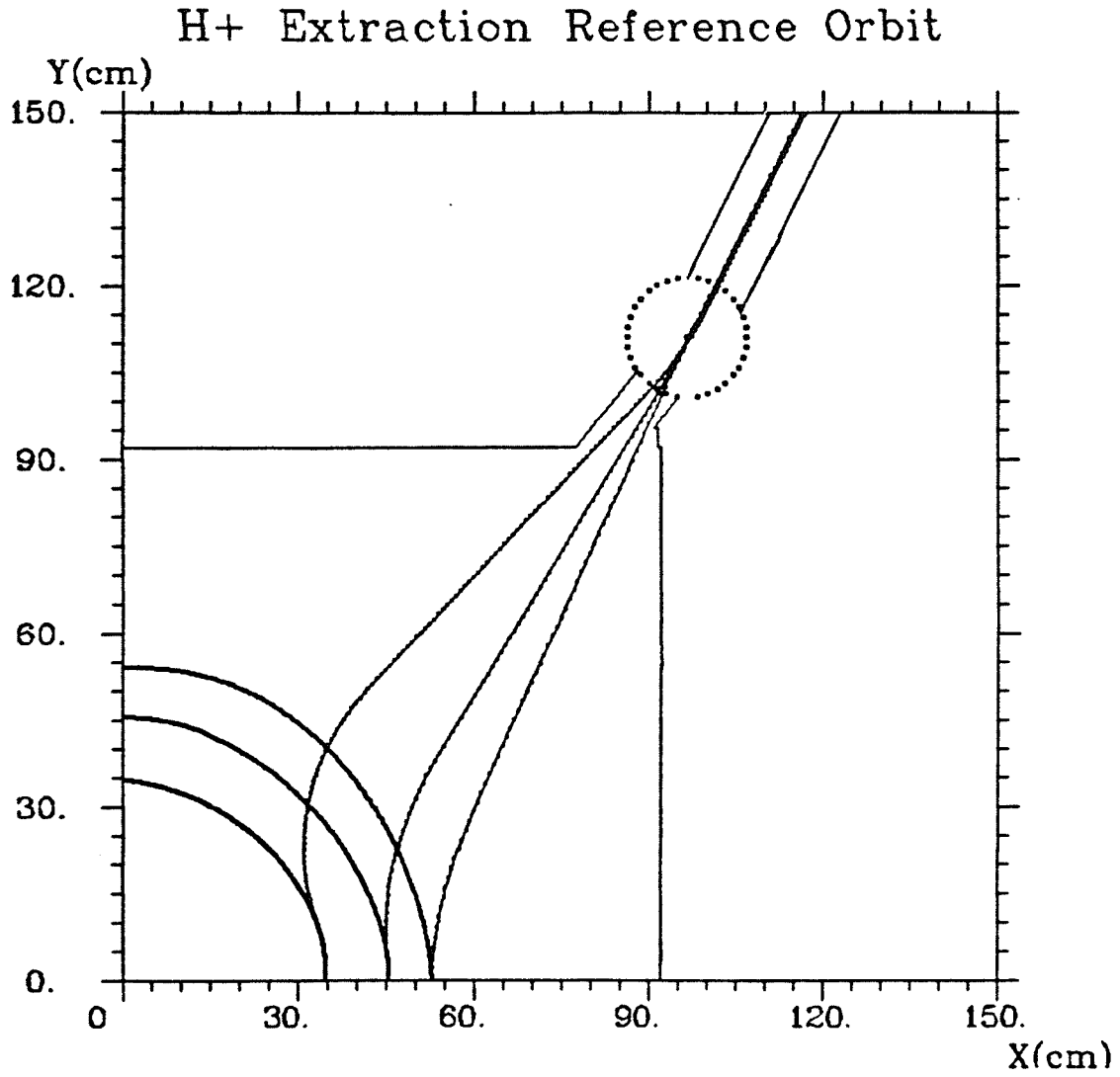

Fig. 5.3 H^+ extraction reference orbits for three selected energies: 20 MeV (upper), 35 MeV (middle) and 50 MeV (lower). The origin of the figure corresponds to the geometrical center of the cyclotron. The three curves in the lower left hand corner are the equilibrium orbits for the three selected energies 20, 35 and 50 MeV. The circle at the top represents the combination magnet.

stripping foil, induces an energy spread in the extracted beam; the center spread in the direction perpendicular to the above is responsible for the divergence of the extracted beam. In addition, the increment of 80 keV per turn in the beam energy, from the particle's acceleration, induces an additional spread in the energy and in the radial range. The results for the three selected extraction energies are shown in figs. 5.5, 5.6 and 5.7, respectively.

It is seen from the above figures that the radial beam width is as large as 23 mm for the 20 MeV H^+ beam at 160 cm downstream (about 30 cm further downstream from the location of the combination magnet). The radial beam width is reduced to 15 mm for 35 MeV beam, and to 11 mm for 50 MeV beam. The effective beam phase space area has been calculated with the program EXTBEAM for the three beam energies. These are as 23, 11 and 9 mm-mrad, respectively, at this location, as is shown in Figs. 5.8, 5.9 and 5.10. A direct experimental observation of the beam at this location has not been possible, but the results are inferred from the beam spot size further downstream (a fluorescent screen is placed after the beam is focused by a pair of magnetic lenses). The calculated and experimental results are in good agreement. The beam energy spread can also be deduced. The calculated values are 403, 508 and 595 keV respectively. These results compared favourably with our observed energy spread of 500 keV FWHH at 40 MeV.

The axial motion was also investigated. Fig. 5.11 shows the case of a 35 MeV beam. The vertical beam size is seen to be 17 mm. Our studies for the other two energies indicate that the size of the beam at the end point is approximately the same for all three energies. The corresponding vertical trace is demonstrated in fig. 5.12. This figure shows that the beam underwent a defocusing at r=30 cm from

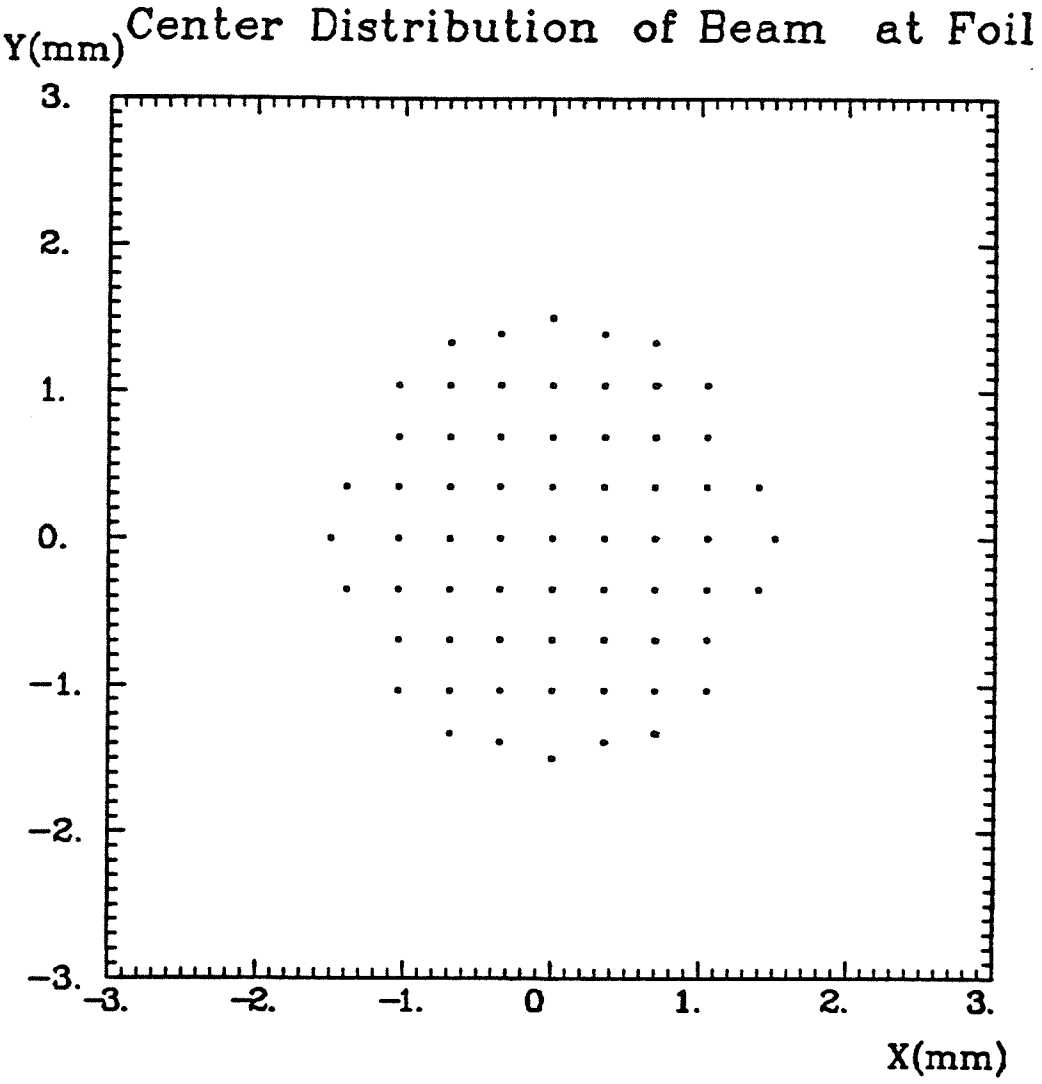

Fig. 5.4 The assumed center distribution of the beam at the stripping foil.

Figs. 5.5, 5.6, 5.7 The radial spreads of the beam along the extraction reference orbits for beam energy of 20, 35 and 50 MeV, respectively.

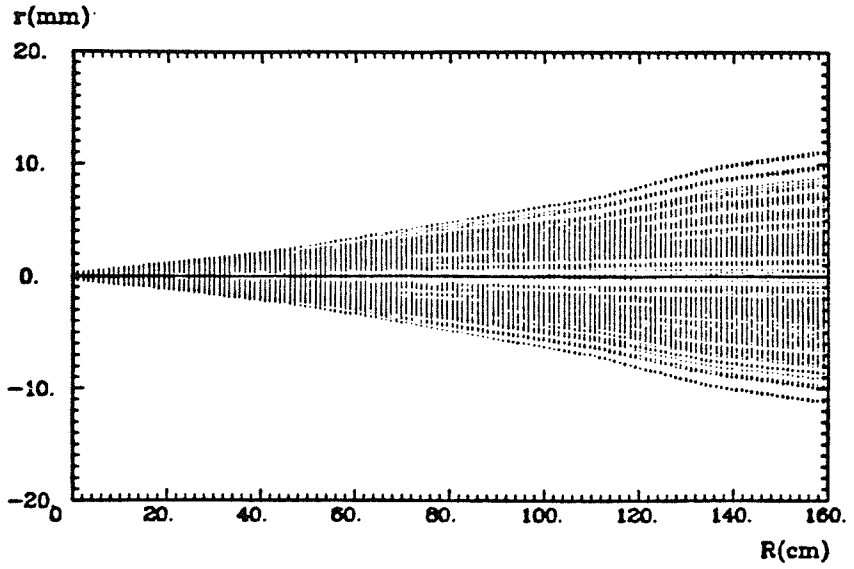
r(mm)
20.
10.
0.
−10.
−20.
0
20.
40.
60.
80.
100.
120.
140.
160.
R(cm)

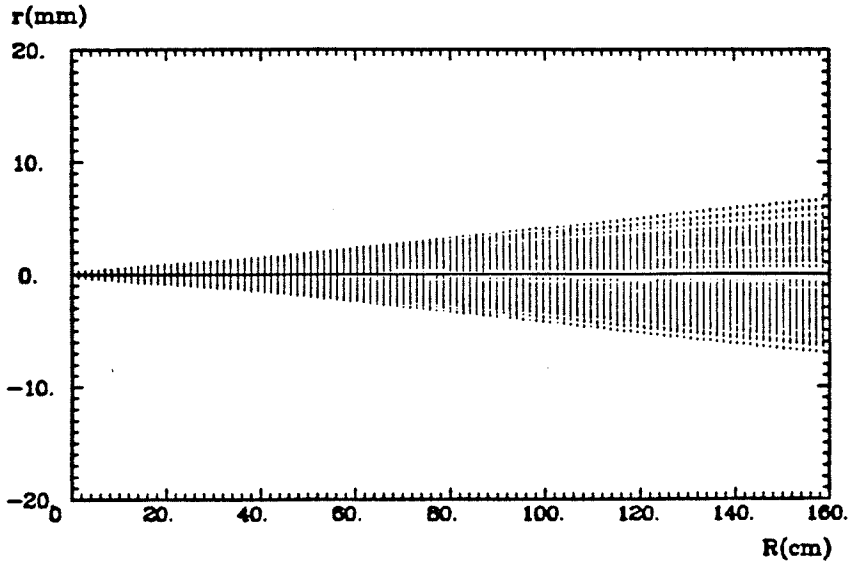
r(mm)
20.
10.
0.
−10.
−20.
0
20.
40.
60.
80.
100.
120.
140.
160.
R(cm)

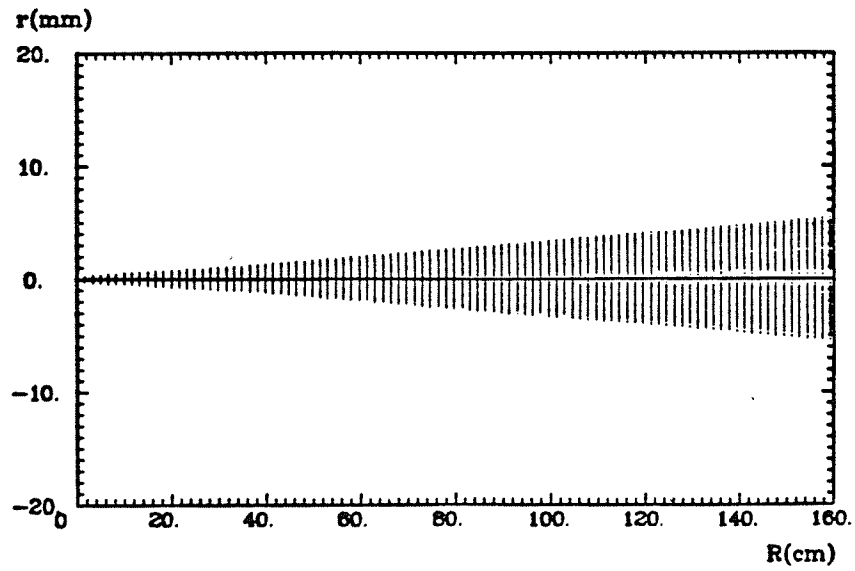
r(mm)
20.
10.
0.
−10.
−20.
0
20.
40.
60.
80.
100.
120.
140.
160.
R(cm)

the stripping point. This was caused by the effect of the fringing magnetic field. Further analysis and comparison of the calculational results for the three beams indicate that the defocusing effect depends primarily on the exit angle of beam when it is leaving the fringing field. The divergence is thus smallest for the 20 MeV beam with largest exit angle (See fig. 5.2), and the largest for the 50 MeV beam with the smallest exit angle. Even so, this divergence is acceptable. In the radial direction, on the other hand, the effect of the fringing magnetic field on the beam is always focusing.

Figs. 5.8, 5.9, 5.10 The radial phase distribution of the extracted beam at a position 20 cm downstream from the combination magnet.

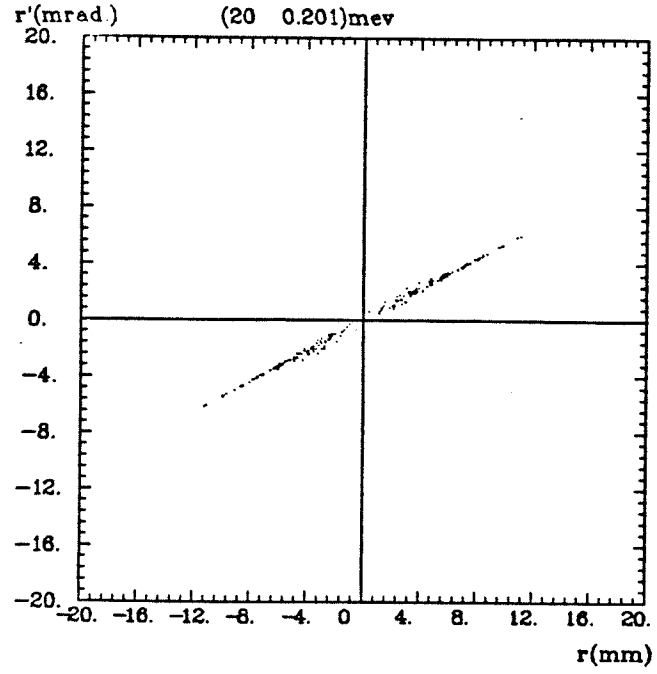
r'(mrad.)
(20 0.201)mev
20.
16.
12.
8.
4.
0.
-4.
-8.
-12.
-16.
-20.
-20. -16. -12. -8. -4. 0 4. 8. 12. 16. 20.
r(mm)

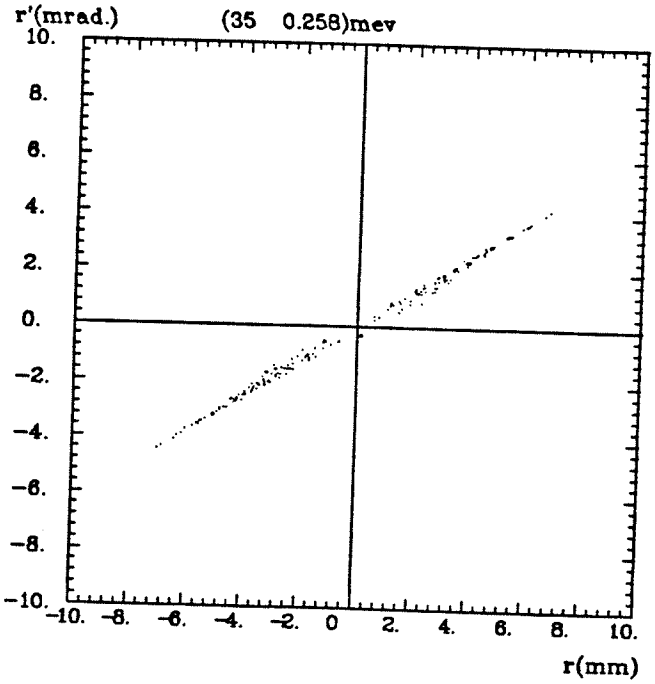
r'(mrad.)
(35 0.258)mev
10.
8.
6.
4.
2.
0.
-2.
-4.
-6.
-8.
-10.
-10. -8. -6. -4. -2. 0 2. 4. 6. 8. 10.
r(mm)

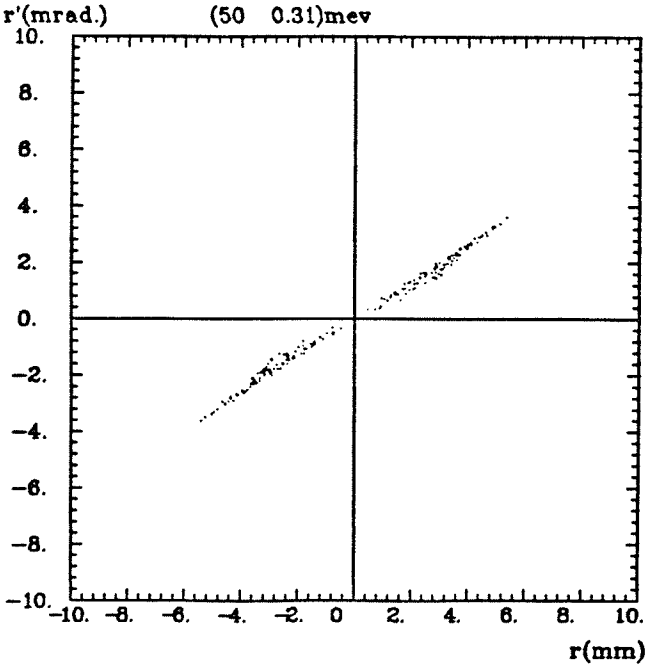
r'(mrad.)
(50 0.31)mev
10.
8.
6.
4.
2.
0.
-2.
-4.
-6.
-8.
-10.
-10. -8. -6. -4. -2. 0 2. 4. 6. 8. 10.
r(mm)

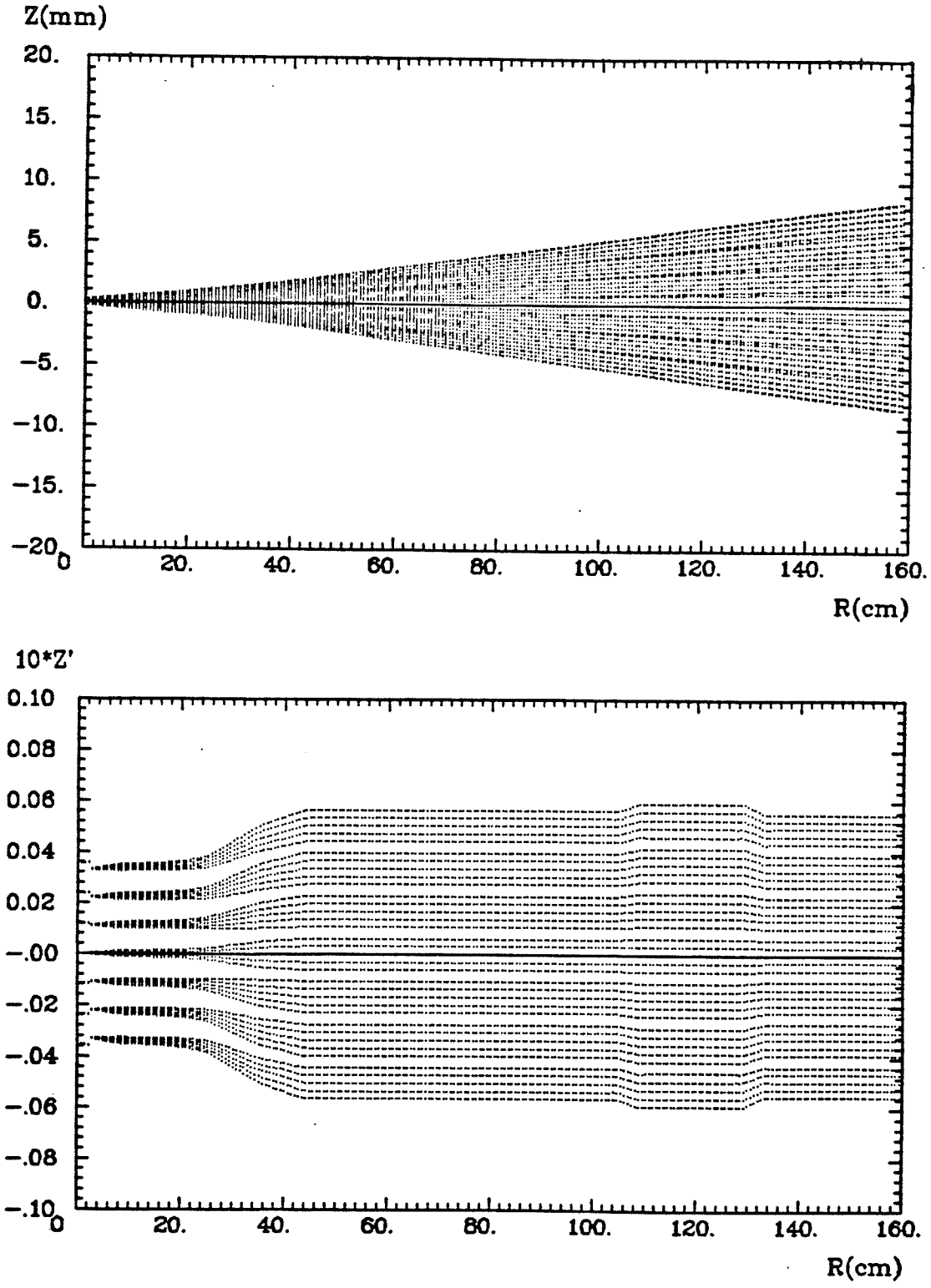

Figs. 5.11, 5.12 The vertical spread (fig.5.11) and the axial slope revolution of the 35 MeV H^- ion beam along the reference orbit starting from the stripping foil.

Part II

A Design Study

of

Beam Extraction

from the Princeton University Cyclotron

Chapter 6

Historical Background

The Princeton University cyclotron was completed in 1969. It is a constant-orbit, multi-particle, variable energy machine. A close copy of the Michigan State University's old K=50 cyclotron*, it has a three-sector, pseudo spiral-ridge magnetic field configuration. The choice of the cyclotron control setting parameters (*e.g.*, RF, dee voltage, profile coil currents, *etc.*) was such that the saturation in the cyclotron magnetic field is small enough to accelerate a range of ions in a fixed-orbit acceleration mode [POL69]. The accelerating system consists of two 134° dees, which can be operated in either push-pull or push-push modes over the frequency range of approximately 14 to 23.5 MHz, allowing for the acceleration of particles in almost any harmonic mode. The maximum energies for typical particles are: 48 MeV protons, 29 MeV deuterons, 58 MeV alpha particles, 85 MeV $^{3}He^{++}$ ions, and 75 MeV $^{12}C^{4+}$ ions. A complete listing of the energy ranges for the various particles that can be accelerated in the Princeton University cyclotron is given in Fig. 6.1.

The magnetic field of the Princeton University Cyclotron is a close replica of the old M.S.U. K=50 cyclotron field. The mapping of MSU's magnetic field was carried out in the early 1960's [BER66]. This mapping utilized a Hall probe to measure the magnetic field on the polar grids of points with one inch radial spacing at four degree azimuthal intervals. Data for seven different excitations of the main magnet and for four different excitations of the eight pairs of the concentric trim coils were Fourier analyzed. The resulting data for the trim coil excitations and

---

* K is defined as $E_{max}=Kq^2/A$, where E_{max} is the maximum energy in MeV, q is the charge number (q=1 for proton), A is the mass number(A=1 for a proton)

Fig. 6.1 The energy vs. the orbital frequency diagram for the acceleration of various particles in the Princeton University AVF Cyclotron. The gap band in the figure indicates that the frequency is outside the range of the RF tuning.

PRINCETON AVF CYCLOTRON

ENERGY vs. TUNING RANGE

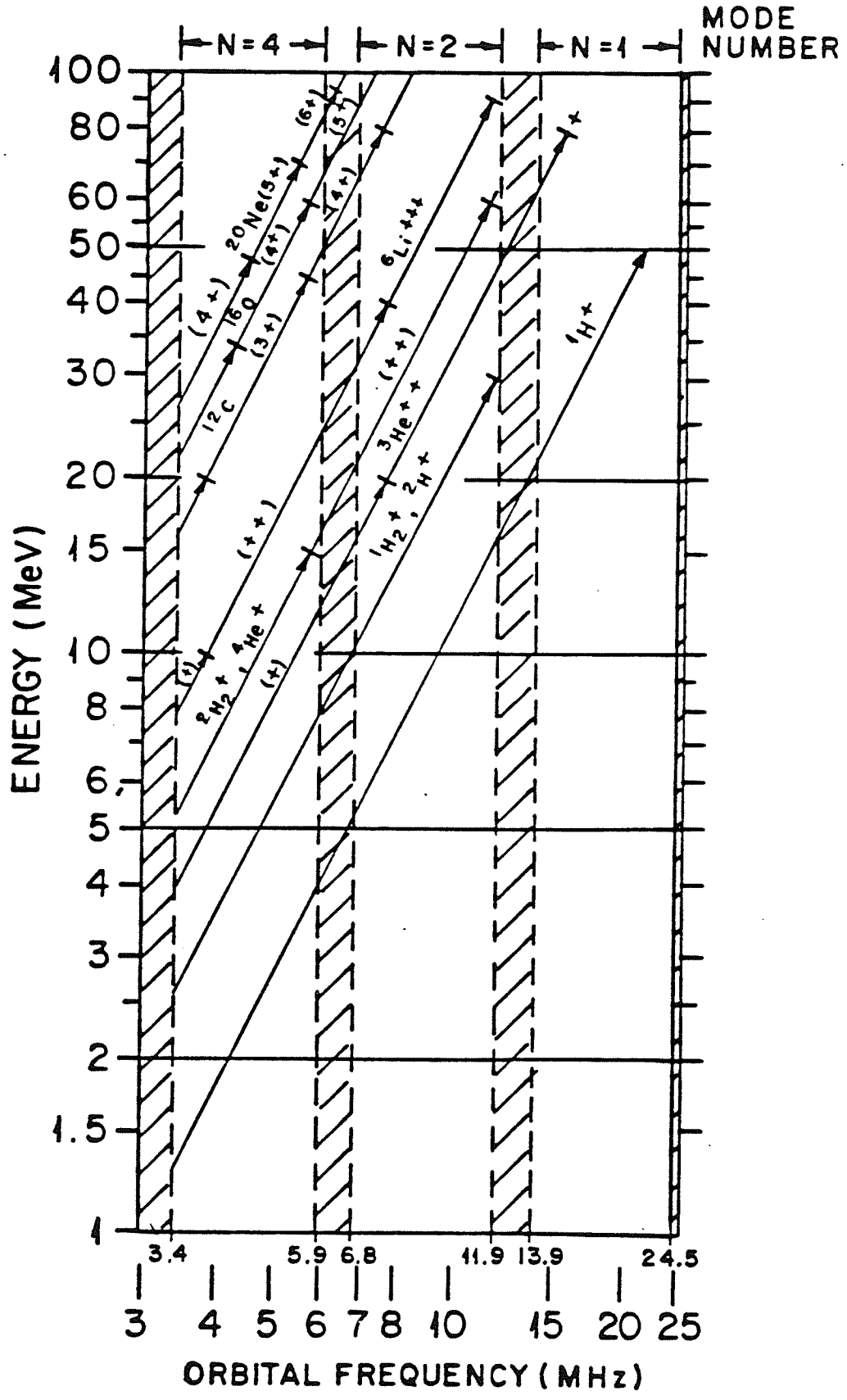

for the first three flutter components of the main magnet fields, as well as for the average magnetic field, were then punched onto cards.

The SETOP program, a computer code which was developed at MSU, reads these magnetic fields to determine the precise optimum control setting parameters of the cyclotron ([BER66], [BER68]). With the particle's specification and its maximum desired energy as input parameters, the SETOP program interpolates (by using a double three-point Lagrangian method) the measured magnetic field values in order to calculate the optimum field distribution. In the region where there is an axially (or radially) defocusing force the field is subsequently adjusted at the expense of abandoning isochronism so that the resulting field always gives adequate focusing forces in both the axial and radial directions. The basic methods of calculating ν, ν_r, and ν_z (as defined in section 2.1) are nearly the same as those in MAPANL, an equilibrium orbit code which was described in chapter 2, and therefore I will not go into further detail here.

The frequency range of the Princeton cyclotron is 13.4 to 24.5 MHz. The electrostatic deflector is mechanically similar to the M.S.U. design inside the vacuum chamber. The septum tip is quickly replaceable. The oil-filled high voltage bushing at the end of a coaxial cable accepts 100 kV from a Cockroft-Walton supply above the shielding.

Unlike the University of Manitoba cyclotron, the Princeton cyclotron accelerates positive ions, and the extraction of the beam is performed utilizing the precessional extraction method. There are two notable features about the precessional extraction method for a variable energy machine like the Princeton cyclotron.

1. The beam trajectory in the cyclotron remains constant, both for different particles and for the same particle with different maximum energy. This is ensured by adjusting design parameters to satisfy the following scaling laws([DAH73])

$$\frac{T}{qV} = constant, \qquad \frac{Mv}{qB\rho} = constant, \tag{6.1}$$

where T is the kinetic energy, q the charge, V the dee voltage, M the mass, v the velocity, B the magnetic field, ρ the trajectory (radius) of a beam. These two equations can be combined to yield

$$\frac{(M/q)V}{B^2\rho^2} = constant, \tag{6.2.}$$

or,

$$\frac{vB\rho}{V} = constant. \tag{6.3.}$$

These equations indicate that to form a constant orbit the ratio between (M/q) and (M_0/q_0) should be the same.

2. Single-turn extraction can be achieved and therefore a beam with high energy resolution and of substantial intensity is expected.

The single-turn extraction of a beam can be achieved only when the beam phase width is so narrow that the beam bunches of succeeding turns do not overlap with the preceding turns. To achieve this purpose, two radial slits were placed, one at the 18^{th} orbit turn and another at the 28^{th} orbit turn, in order to restrict the beam phase width. Two sets of first harmonic coils were installed at r=5 inches and r=26 inches, respectively, the radii where the beam crosses ν_r=1. The role of these coils will be explained in chapter 8.

In the Princeton cyclotron, with careful attention to centering and phase selection, the 35 MeV proton beam was extracted with 94% efficiency and an energy spread of 0.08% FWHM(before magnetic analysis) as early as 1969. Beam currents were deliberately held down below 2 μA during the early operation ([POL69]).

Motivated by the demands of nuclear physics experiments, beams of a wider variety, with substantial improvements in intensity and in energy resolution, are required in this laboratory. In addition, this cyclotron began operation in 1968 and is now showing signs of age. Therefore a proposal for extensive modifications to the existing system has been submitted and is under consideration.

The Princeton cyclotron was primarily designed to provide high energy resolution for light ion beams. Inherent in the design is a radial beam spread as a function of rf phase, producing high energy resolution by the use of slits defining the radial size (and thus the rf phase width) of the beam at two internal points. For the N=1 acceleration mode, this approach works to restrict the rf phase, but the energy resolution is presently limited to about 1/800 by rf ripple and by the instabilities in the other power supplies. For the N=2 mode of acceleration, used for ^{4}He beam and low energy proton and ^{3}He beams, the phase-dependent radial spread is much larger, restricting beam intensity substantially if the phase selection slits are used. Therefore, one objective of the upgrade program is improvements in the power supply ripple and stability, and changes in the orbit dynamics in the N=2 mode, to produce an energy resolution of at least 1/2000, and possibly as good as 1/10000, for as large an energy range as possible.

The spread in the rf phase results in a large radial beam spread. Hence, the extraction process selects a limited range of rf phase, even when the internal phase

selection slits are removed. As a result, the extracted beams from the machine have relatively low intensity, particularly in the N=2 mode. This problem is increased by a relatively low power dissipation limit on the extraction septum. Therefore, an additional objective of the accelerator upgrade program is the development of a design to permit the extraction of a large fraction of the internal beam in the N=2 mode. This is needed to satisfy the high-intensity, low energy resolution requirements of many experiments.

Starting in 1986, a design study has been carried out by Dr. M. Yoon (now at the Argonne National Laboratory) in consultation with Professor S. Oh of the University of Manitoba. They have developed a design for a new central region of the accelerator which should greatly reduce the phase dependent radial beam spread. The proposed new design incorporates, among other things, a higher dee voltage for better turn separation and reduced space charge effects. This design, coupled with a new design study of the extraction system as well as some improvements to power supply systems, is expected to enhance beam intensity by about a factor of four for moderate resolution beams and enables single turn extraction to be accomplished for most of the energy range in the N=2 mode, providing the excellent energy resolution and brightness needed for high resolution experiments.

The initial beam orbit dynamics study by Dr. Yoon and Professor Oh was limited to the central region of the Princeton cyclotron. The author of this thesis extended the study to cover the full energy range of the machine and carried out a design investigation of the beam extraction system. This work is described in the following part of this dissertation.

Chapter 7

The Upgraded Beam Orbit Dynamics Program

7.1 Introduction

Analytical treatments of most of the physical phenomena which occur in an AVF cyclotron have been available through the work of Smith and Garren ([SMI59]), Hagedoorn and Verster ([HAG62]), and especially Gordon ([GOR83]). These analytical results are very useful in revealing how the various orbit properties depend on the specific parameters of the magnetic field. However, when highly accurate results are required on a routine basis, then a computer code becomes indispensable. At present, nearly all the practical designs of accelerators with AVF focusing anywhere in the world are carried out using complicated analytical calculations that are accompanied , inevitably, by numerical solutions for the particle orbits.

In the Princeton cyclotron, the beam orbit dynamics study was performed mainly utilizing the computer program PRINWHEEL. This program is a modified version of the computer code TRIWHEEL, which was initially developed at TRIUMF for a design study of the cyclotron's central region. The program is a beam tracing code; it first reads rf electric and magnetic field data, then uses the Runge-Kutta method to integrate Lorentz's equations with any step size. The old version of the program was non-relativistic and written in single precision. Some trouble developed when we studied the isochronous property of the cyclotron with this program; cumulative errors from the large-range tracing calculations were so serious that it was not possible to get reasonable results. Therefore, most of the code, and especially those parts which are relevant to the integration calculation

of the beam and to the isochronism study, have been changed from single precision into double precision. Also, in the modified version, PRINWHEEL, the fields of the two sets of harmonic coils used for the precessional extraction of the beam (see Chapter 8), have been included. This is accomplished by approximating the effect of the coils as a constant magnetic field, over a certain radial width and azimuthal range, and then combining this data with the main magnetic field data set.

To make it possible to extend the beam orbit dynamics study over the full energy range and to carry out a systematic investigation of the beam extraction from the Princeton cyclotron, the PRINWHEEL program has been further changed by the author further to include two other very important modifications:

1. Employing an impulse approximation method to replace the original relaxation method of calculating the accelerating electric field at large radii.

2. The code is expanded to include non-linear effect in the axial motion. The expansion is aimed at studying the beam extraction where the non-linear effect(through the coupling resonance, the geometrical resonance etc.) is very important. The non-linear effect in the code can be switched on(or off) as desired. These two code modifications will now be described in sections 7.2 and 7.3, respectively.

7.2 The impulse code

In the program PRINWHEEL, the electric potential distribution is obtained in a quasi-static approximation, employing the successive overrelaxation method to solve numerically the three-dimensional Laplace equation. The mathematical basis and computational details have been given in chapter 3. This method, when utilizing a fine size step, has an excellent computational accuracy. However, it

requires excessive computer memory and takes too much CPU time. To cover the full energy range of the cyclotron (up to r=32 inches), as a temporary treatment, the electric potential calculation was initially performed with a mesh of dimension of (512,512,15) and with a step size of 4 mm, representing a near full-capacity use of our computer memory. But, even this calculation was still too coarse to be reliable; when we tried to perform a beam orbit dynamic study based on this data set, it gave incorrect results.

Therefore, we utilized instead an impulse approximation method to replace the calculations of the accelerating electric field. The principle used was the following. We assumed that the electric field is concentrated in the accelerating gap and its effect on the circulating beam can be represented by an abrupt change of particle energy at each gap and then remains constant between the gaps. This assumption can be expressed as

$$\Delta E = qV \cos \omega t \quad . \tag{7.2.1}$$

The corresponding change in momentum, δP, of the particle in consequence of the energy change can be calculated. The relation between δP and δE ($\Delta E = \delta E$) can be derived from Fig. 7.1. There P denotes the momentum of the particle before crossing the gap and δP represents the increment in momentum after crossing the gap, which is assumed to be perpendicular to the central line of the gap. Also, E_o is the rest energy of the particle, E_k is its kinetic energy and c is the velocity of light. Including relativistic effects, we have

$$|P|^2 = \frac{E_k(E_k + 2E_o)}{c^2} \tag{7.2.2}$$

$$|P+\delta P|^2 = \frac{(E_k+\delta E+2E_\circ)(E_k+\delta E)}{c^2} \tag{7.2.3}$$

From eqs (7.2.2) and (7.2.3), we get

$$(P+\delta P)^2 - P^2 = \frac{\delta E(\delta E+2E_k+2E_\circ)}{c^2} \tag{7.2.4}$$

Let us define

$$F(\delta E, E_k, E_\circ) = \frac{\delta E(\delta E+2E_k+2E_\circ)}{c^2} \tag{7.2.5}$$

Then, we obtain the quadratic equation:

$$(\delta P)^2 + 2P\delta P\cos\alpha - F = 0 \quad , \tag{7.2.6}$$

where α is the angle between P and δP, as shown in Fig. 7.1; which usually is of small magnitude.

From eq (7.2.6), we can get

$$\delta P = \sqrt{P^2\cos^2\alpha + F(\delta E, E_k, E_\circ)} - P\cos\alpha \tag{7.2.7}$$

It should be noted that eq. (7.2.7) is exact. Furthermore, all the quantities on right hand side of eq. (7.2.7) can be easily obtained from the tracing calculation.

After we derive the magnitude δP, the dynamical expressions describing the particle while it is crossing the accelerating gap can be approximately written as

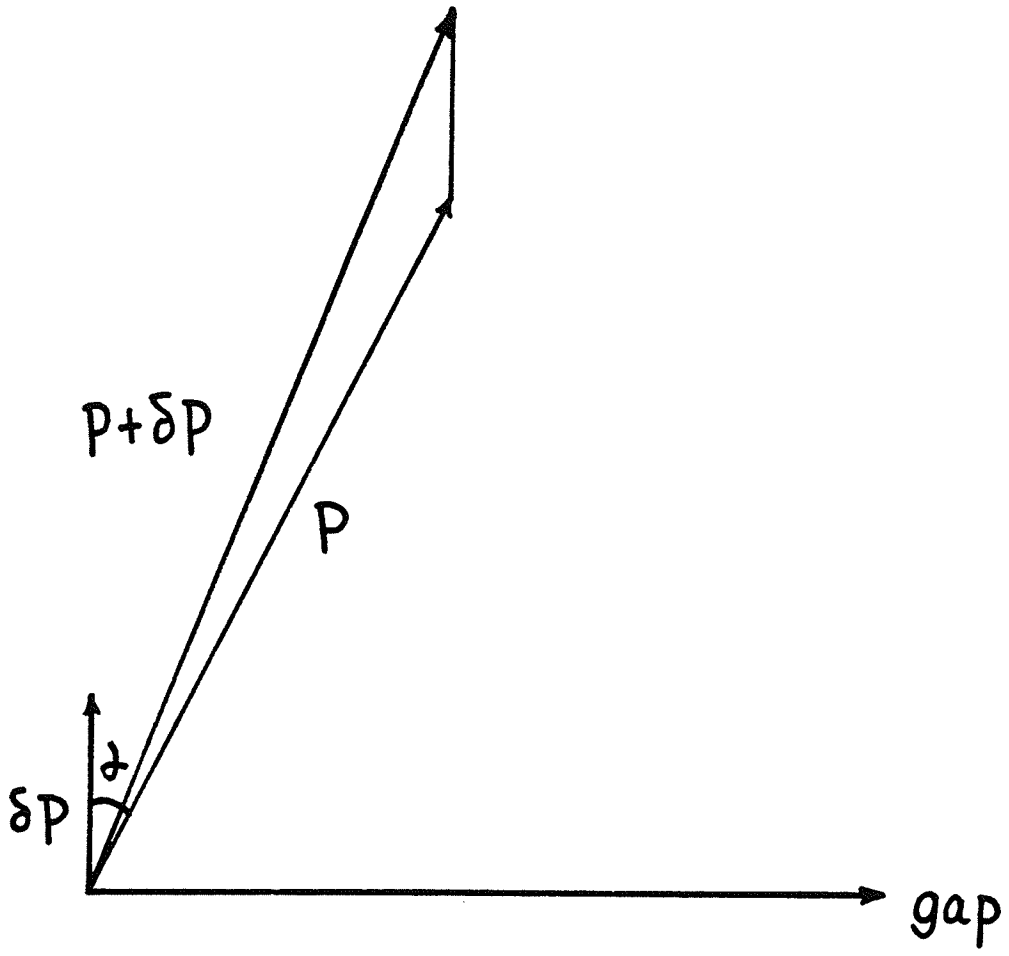

Fig. 7.1 The schematic diagram of the paprticle's momentum change at the accelerating gap

follows:

$$\begin{aligned} E_a &= E_b + \delta E, \qquad \delta E = qV\cos\omega t \\ P_{xa} &= P_{xb} + \delta P_x, \qquad \delta P_x = |\delta P|\cos\beta \\ P_{ya} &= P_{yb} + \delta P_y, \qquad \delta P_y = |\delta P|\sin\beta \\ P_{za} &= P_{zb} + \delta P_z, \qquad \delta P_z = 0 \quad . \end{aligned} \tag{7.2.8}$$

Here, the subscripts b and a denote, respectively, "before" and "after" crossing the gap, β is the angle between the X-axis and the line perpendicular to the central line of the gap, and all the other quantities have the same definitions as above.

In deriving eq.(7.2.8), the vertical component of the electrical field has been neglected. This approximation is justified since the effect of this component is quite small once the particle reaches 20 or more turns of orbit inside the cyclotron. We have also made the additional assumption that the vertical motion has no effect on the gap-crossing process except indirectly through the values of x, y, P_x, P_y and t.

In order to keep the advantage of the previous version of computer code, PRINWHEEL, we do not utilize the new impulse computer code within the range where the relaxation data set with a step size of 2 mm can cover ($r \leq 0.25$ m), and even outside this region, we still use the Runge-Kutta method to integrate Maxwell's equations except that the electric field components are set to zero. This approach enables us to describe very accurately the betatron oscillation of particles in transverse phase space, as well as their phase shifts and energy spread properties in longitudinal phase space.

The cross checking of the results of the study based on the impulse code against well established methods was carried out in two different ways. In one method, the result based on the former was compared with the results that are obtained when

the electric field is computed entirely from the relaxation method with a fine step size. In another check, the results from the impulse code were compared with the measurements of beam properties that were obtained after setting the cyclotron parameters to be identical with those of the input data. We found that in both cases the agreement was excellent.

7.3 The nonlinear code used in the beam extraction study

As mentioned in chapter 6, the magnetic field distribution in the median plane in the Princeton cyclotron was obtained by using the independent program "SETOP" (a cyclotron magnetic field optimization code that was developed at Michigan State University). Once the magnetic field in the median plane, B(r, θ), is known, the field off median plane (i.e. for $z \neq 0$) can be calculated by using a series expansion method. The results can then be expressed by the following equations:

$$\begin{aligned} B_z(z) &\approx B_z(0) \\ B_r(z) &\approx z\left(\frac{\partial B_r}{\partial z}\right)_{z=0} = z\left(\frac{\partial B_z}{\partial r}\right)_{z=0} \\ B_\theta(z) &\approx z\left(\frac{\partial B_\theta}{\partial z}\right)_{z=0} = \frac{z}{r}\left(\frac{\partial B_z}{\partial \theta}\right)_{z=0} \end{aligned} \quad , \tag{7.3.1}$$

where we used $\nabla \times \vec{B} = 0$.

In the previous version of the computer program PRINWHEEL, the first-order expressions (7.3.1) were employed to obtain those magnetic field components which are needed to carry out the integration of Maxwell's equations. However, when it came to the investigation of the beam's extraction, the first order expressions are found to be insufficient.

Fig. 7.2 shows the magnetic field distribution along the radius from the cyclotron center to the entrance of the electrostatic deflector, where "D" represents the location of the electrostatic deflector which is used for the beam extraction. It can be seen from this figure that the main magnetic field falls off rapidly in the extraction region; therefore, nonlinear effects can be expected to be very strong there. Fig. 7.3 exhibits several resonant lines in the extraction region; in that figure the horizontal axis denotes the radial focusing frequency and the vertical axis represents the axial focusing frequency, as defined in Chapter 2. Curve C in Figure 7.3 represents the evolution of a particle's trajectory in the ν_z vs ν_r plane. The particle starts from the bottom end of the curve C, and then moves up along this curve. Those resonant lines with which the curve C intersects would affect the motion of the particle before extraction. The names, defining expressions of these resonances, and the radial positions where they occur, are as follows.

1. Integer: $\nu_r=1$, at r≈4.11 inches and r≈27.44 inches,

2. Coupling : $\nu_r - 2\nu_z=0$, at r≈27.94 inches.

3. Half integer : $\nu_r = \frac{1}{2}$ at r≈27.98 inches,

4. Difference : $\nu_r - \nu_z=0$, at r≈28.98 inches.

Among these resonances, the second is a nonlinear resonance, while all others are linear. The study of the nonlinear coupling resonance $\nu_r - 2\nu_z = 0$ is very important. As is well known, it is the effect of this resonance on the extracted beam that limits the available maximum energy in all synchrocyclotrons and most cyclotrons. Even in those cyclotrons where the beam can pass this resonance, some special treatment has to be preceded after careful beam dynamics studies. As the

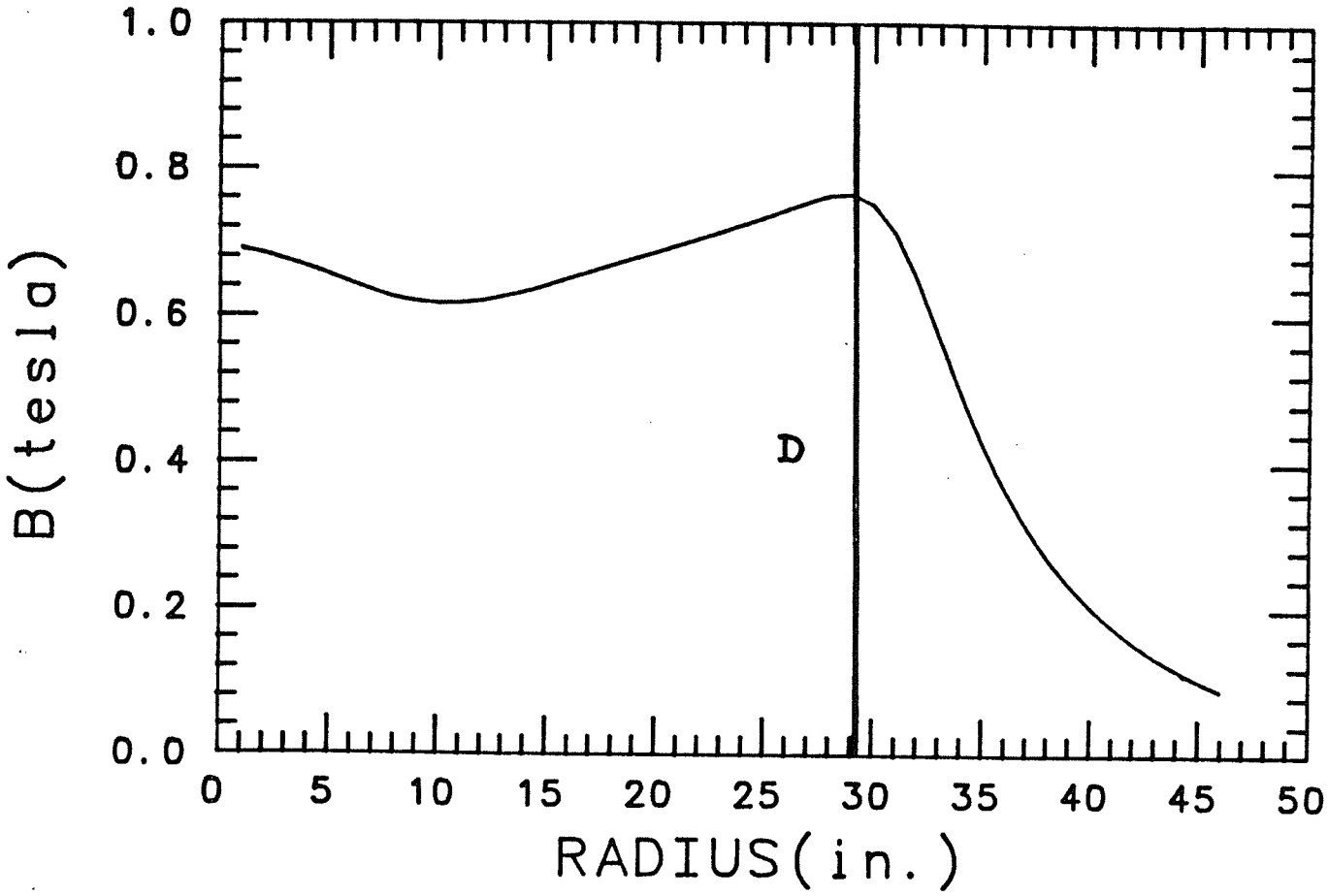

Fig. 7.2 The magnetic field distribution along the radius to the entrance to the electrostatic deflector, where D represents the radial location of the deflector.

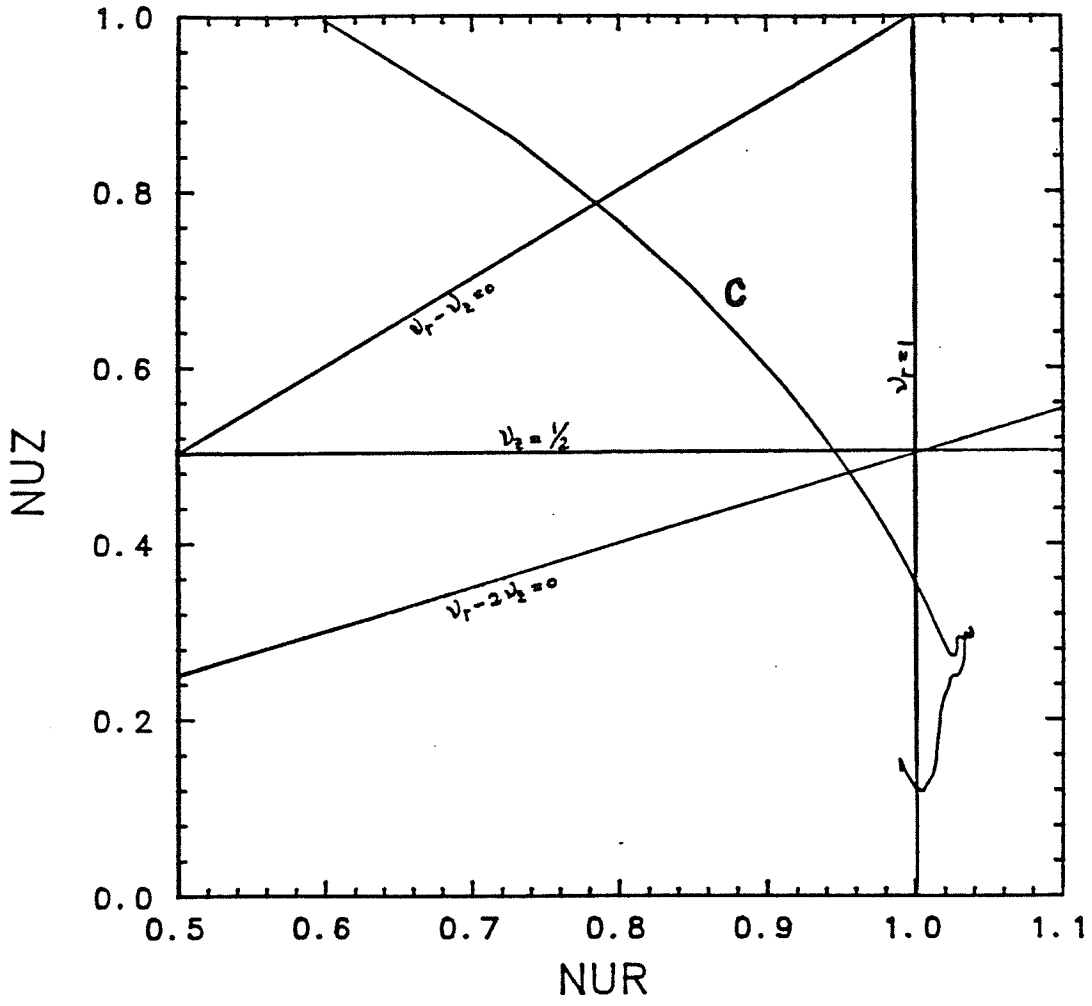

Fig. 7.3 The contours of several resonance lines in the extraction region. The horizontal axis denotes the radial focusing frequency and the vertical axis represents the axial focusing frequency, their definitions are the same as that described in chapter 2. The curve C provides the evolution of a particle in the ν_z vs. ν_r plane. The particle starts from the bottom of curve C, then moves up along it.

resonance is caused by a nonlinear property of the magnetic field, an extended calculation of all the magnetic field components to include higher order terms is required.

In studying the nonlinear motion, the author of this dissertation utilized the following formulae for the components of the main magnetic field off the median plane ($z \neq 0$).

$$\begin{aligned} B_z &= [B(r,\theta) - (z^2/2)B'(r,\theta) + (z^4/24)B''(r,\theta)] \\ B_r &= z\frac{\delta}{\delta r}[C(r,\theta,z)] \\ B_\theta &= \frac{z}{r}\frac{\delta}{\delta\theta}[C(r,\theta,z)] \quad , \end{aligned} \tag{7.3.2}$$

where,

$$\begin{aligned} C(r,\theta,z) &= B(r,\theta) - (z^2/6)B'(r,\theta) \\ B'(r,\theta) &= LB(r,\theta) \\ B''(r,\theta) &= LB'(r,\theta) \quad , \end{aligned} \tag{7.3.3}$$

Here L represents a two-dimensional Laplace operator, which we express in terms of the radius r and azimuthal angle θ. Thus, B_z has terms of order z^2 and z^4 off the median plane, while B_r and B_θ have a z^3 term in addition to the usual linear one.

These magnetic field components can be derived from a vector potential since they satisfy the condition: div B=0. As a result, the equations of motion can be derived from a Hamiltonian, and the results of the calculations therefore satisfy Liouville's Theorem (in four dimensions).

The nonlinear code requires as input a table of the median plane field $B(r,\theta)$, which is derived from the computed field data. For the nonlinear orbit code, corresponding tables for $B'(r,\theta)$ and $B''(r,\theta)$ are also required, and these are obtained

by utilizing twice a two-dimensional interpolation code on the $B'(r,\theta)$. All these data are calculated and stored in advance. Since B' and B'' involve, respectively, second and fourth derivatives of the median plane field, these derivative functions (especially B'') will always exhibit much more noise than the original field data. However, this noise usually looks more troublesome than it actually is, since the process of orbit integration acts like an averaging process in filtering out the high frequency components of the noise.

Chapter 8

Beam Dynamic Study for Upgrading Beam Extraction

8.1 Introduction

A major concern regarding the beam extraction system for cyclic accelerators is obtaining a large enough turn separation at the extraction radius. This separation must be sufficient to permit the placement of a septum, or a septum magnet, at that location in order to extract the circulating beam out of the machine. In classical cyclotrons, very high dee voltages are used, and the turn separation at the extraction radius is, therefore, rather large (1 cm). In these cyclotrons the beam is extracted by means of an electrostatic field which is applied between a septum and a high voltage electrode. With a cooled septum, large external beam currents can be obtained.

In synchrocyclotrons and isochronous cyclotrons, the dee voltage is rather small and hence the orbit separation can be as small as a fraction of a millimeter. In such cases an electrostatic deflector system alone may not be adequate. However, there are several methods to enlarge the orbit separation. First, using the regenerative method, radial oscillations can be excited in such a way that a large increase in the oscillation amplitude per revolution is obtained ([VER59]). Alternatively, the precession of the orbit center can be used to get sufficient orbit separation ([AMSPH]). With the regenerative method, large increases in the radial oscillation amplitudes are introduced, the phase of the oscillations remaining constant. With the orbit precession method, a fixed amplitude and a rapidly increasing phase is used. Both mechanisms give similar results if they are applied at the right places.

One of the main concerns in the design of a beam extraction system for a

Fig. 8.1 A schematic diagram of the beam extraction system in the Princeton University cyclotron. 1. south dee; 2. north dee; 3. outer first harmonic coil (one of the three-coil set); 4. inner first harmonic coil (one of the three-coil set); 5. initial orbit; 6. ion source; 7. pole tip sector; 8. final orbit; 9. elecreostatic deflector electrode; 10. magnetic deflector; 12. septum; 13. extracted beam

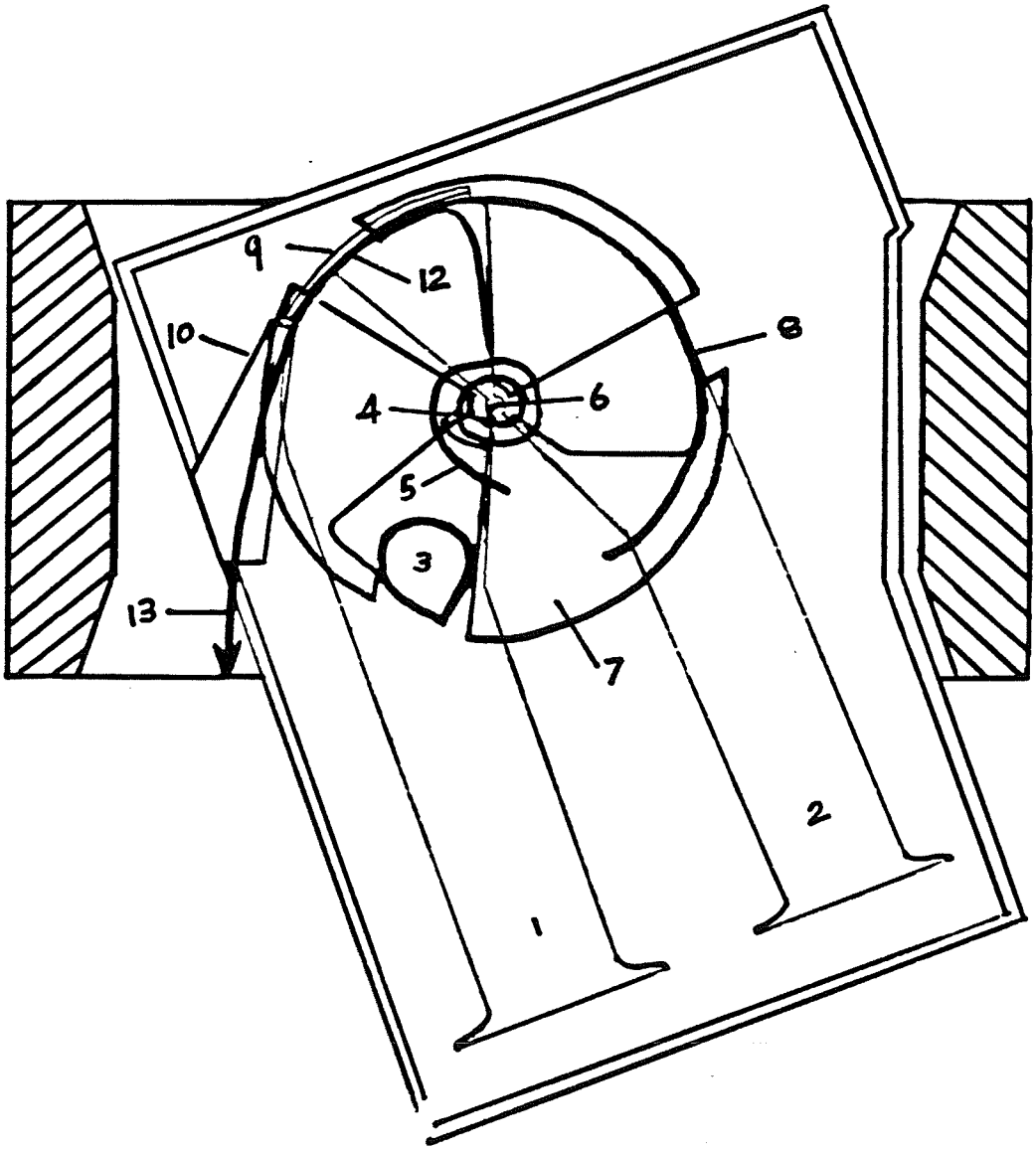
9
12
10
8
4
6
5
3
13
7
2
1

cyclotron is the beam loss on the septum. The loss generates heat that, when white hot, will induce thermionic emission of electrons from the septum and subsequent breakdown. Warping from thermal expansion is another matter of concern. Thus, the beam loss can be the factor that limits the maximum beam current available from a cyclotron. In other words, the extraction efficiency can be the critical limiting factor for an intense beam extraction. To maximize the intensity of the extraction beam, one usually relies on a design with a higher allowable heat dissipation and effective cooling, thinnest possible septum based on a low thermal expansion with high temperature melting point, wider turn separation and, of course, a better beam optics through the septum channel.

In the Princeton cyclotron, the extraction of the beam is achieved by means of precessional resonance. Fig. 8.1 provides a schematic diagram of the extraction system. Here, two sets of first harmonic coils (abbreviated as FH) are installed, in proximity to the ν_r=1 resonance, at r=5 inches and r=26 inches, respectively. Initially, the inner set of FH coils centers the beam orbits so that their centers coincide with the geometric center of the cyclotron. Then, the outer FH coils cause an eccentric oscillation of the beam orbit to occur near the entrance to the electrostatic deflector, so that an increased beam orbit separation can be obtained. Afterwards, the electrostatic deflector, and subsequently the magnetic channel, bend the beam out into the beam transport line.

The efficiency and quality of the extracted beam depend, to a great extent, on the precise design and the fine adjustment of the extraction system. The parameters that need to be optimized include the amplitudes and azimuthal angles of the two sets of the FH fields, as well as the location, geometry and field strength of the elec-

trostatic deflector and of the subsequent magnetic channel. Previous operational experiences and theoretical analyses have shown that the main limiting factor, in obtaining high currents from the old extraction system, is the power that is dissipated in the extraction region as a result of inadequate turn definition and control. In addition, visual examination on a used electrostatic deflector plate shows that a large fraction of the beam is lost inside the electrostatic channel. Therefore, a systematic computer design study of the extraction system is not only necessary for coupling with the newly designed central region, which is a part of the current upgrade proposal, but might also be helpful in improving the existing accelerator system, utilizing the present central region.

8.2 The optimization of the First Harmonic fields

8.2.1 The precessional resonance

We shall soon describe the more realistic numerical orbit tracing study of the beam extraction. First, however, let us consider a more theoretical approach. This approach will help us to thoroughly understand the principle of resonance extraction and will assist us in determining the optimized parameters for the extraction system.

In an arbitrary magnetic field, the basic equation of motion for a particle is:

$$m\vec{a} = q(\vec{V} \times \vec{B}) \quad , \tag{8.2.1}$$

with m: the mass of the particle; $\vec{a}$: the acceleration of the particle; q: the charge of the particle; $\vec{V}$: the velocity of the particle; and $\vec{B}$: magnetic field.

Obviously, the solution for the orbit depends on the magnetic field distribution. The symmetry of the magnetic sector structure of the Princeton AVF cyclotron

suggests that in the median plane(z = 0) we should take the form of the magnetic field to be:

$$B_z(r,\theta,0) = B_o(r)(1 + f\cos 3\theta) \tag{8.2.2}$$

where f is the flutter field component and B_0 is the average of the field over all azimuthal angles. An accurate contour map of the magnetic field in the Princeton cyclotron is shown in Fig. 8.2.1.

The centered closed orbits must have the same symmetry as B_z; therefore, we choose for the radius r(θ) of an orbit in the median plane can be written:

$$r(\theta) = r_o(1 + \sum_i g_i \cos(3i\theta + \delta_i)) \qquad (i = 1,2,3\cdots) \tag{8.2.3}$$

where $r(\theta)$ is a solution to the equations of motion that is valid only in the median plane of the Princeton cyclotron . Here g_i represent fluctuations in the orbit radius, and the main features of the solutions are as follows.

(1) $g_1 \gg g_j$, where j=2,3,$\cdots$, and

(2) $g_1 \cong f/9$

The above equations indicate that the main fluctuations in the orbit radius coincide with the angular fluctuations in the field strength. For the Princeton cyclotron, we have $f \cong 35\%$, and therefore, $g \cong 4\%$. The average radius of the largest orbit is about 30 inches; at this radius, the amount of the radial fluctuation can be derived and is found to be

$$(r_{max} - r_{min})_{<r>=30''} \cong 2.4''$$

Therefore, we can consider the actual closed orbit of the AVF cyclotron as a com-

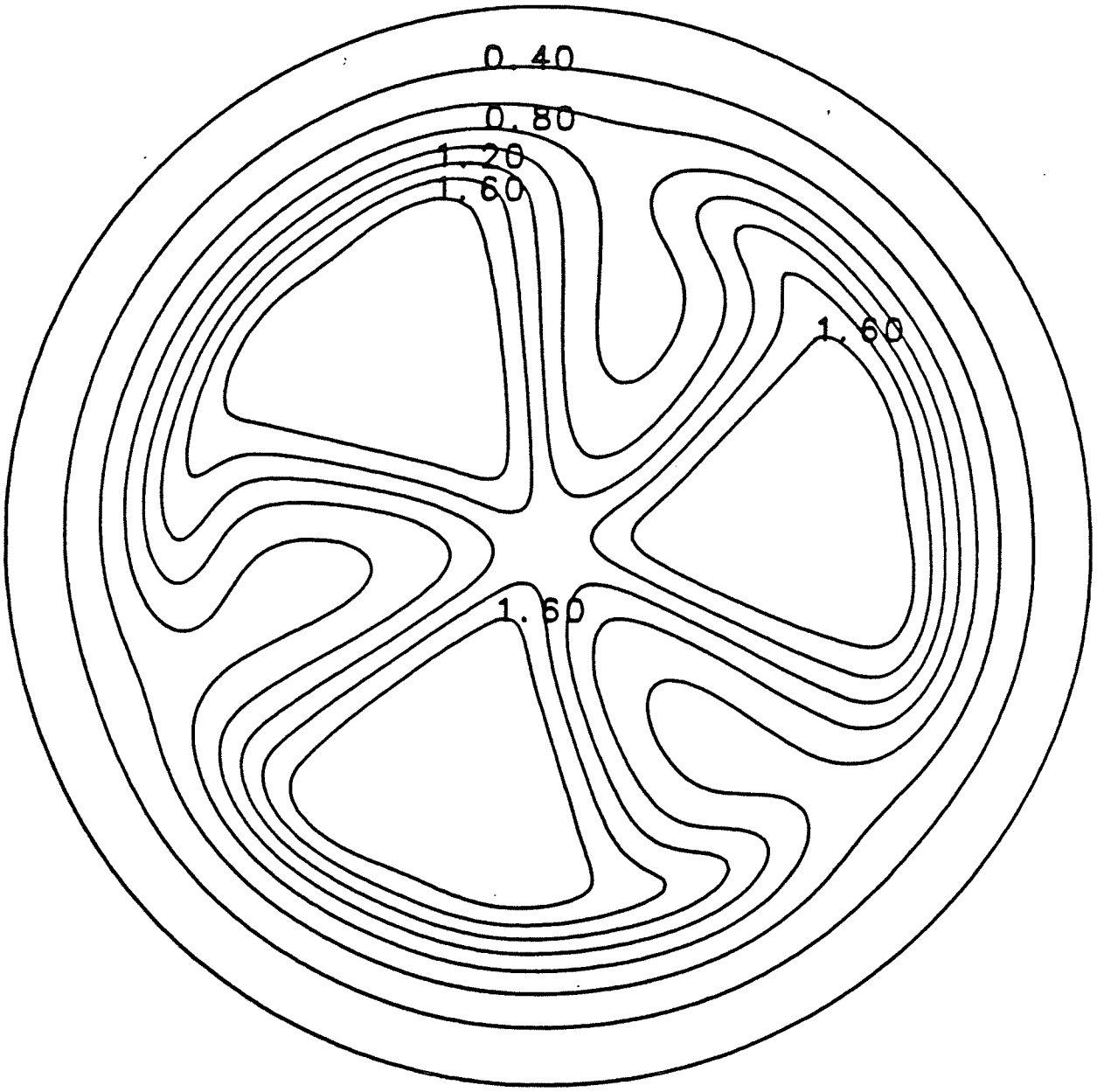

Fig. 8.2.1 The magnetic field contour map for a 20 MeV deuteron beam in the Princeton University AVF cyclotron.

bination of a circular closed orbit, which arises from the average magnetic field B_o, and of a small radial modulation to the former which is due to the third harmonic components of the magnetic field.

In an axially symmetric magnetic field, we may simplify the problem by linearizing the equation of motion (8.2.1). We then derive the expression for the linear oscillation about the closed circular orbit in the median plane to be:

$$y = A_y \cos(\nu_y \theta + \alpha_y) \tag{8.2.4}$$

Here, y may represent either a radial oscillation or an axial oscillation; $\theta = \omega_o t$, with ω_o the angular frequency of the particle; A, the amplitude of oscillation and α, the initial phase angle, are determined by the initial conditions for the particle; ν is the oscillation frequency. For the radial motion, we have

$$\nu_r^2 = \frac{\omega_r^2}{\omega_o^2} = 1 + k \quad ,$$

while for the axial motion,

$$\nu_z^2 = \frac{\omega_z^2}{\omega_o^2} = -k \quad ,$$

where,

$$k = \frac{r}{B}\frac{dB}{dr}$$

As the Princeton cyclotron is very close to a radial ridge cyclotron when r is not large, and the linear additivity of the solutions of the linear equation of motion, we

can take the following form,

$$R(\theta) = r_o(1 + \sum_i g_i \cos 3i\theta) + A\cos\nu_r\theta \quad , \tag{8.2.5}$$

as the linear approximation to the solution R(θ) for the radial motion in an AVF cyclotron. On the right hand of eq. (8.2.5) the first two terms, multiplied by r_o, represent the closed orbit for a fixed energy; the second term represents periodical oscillations around the closed orbit. But here the ν_r should be taken as the average oscillation frequency value, over all azimuthal angles. Fig. 8.2.2 demonstrates the radial trajectories of a reference particle for its first 20 orbital turns in the Princeton cyclotron.

From eq. (8.2.5) we note that if the betatron oscillation frequency ν_r is not an integer(for example, let ν_r=1+ε, where $\varepsilon \ll 1$), then R(θ) will not close upon itself but will " precess". The number of turns in a complete precession cycle is given by

$$N_r = \frac{1}{|\nu_r - 1|} = \frac{1}{|\varepsilon|} \tag{8.2.6}$$

The maximum radius change per turn due to this precession, Δr_p, is given by:

$$\Delta r_p = 2\pi A \sin(\nu_r - 1) \approx 2\pi A(\nu_r - 1) \tag{8.2.7}$$

If there is some perturbation of the magnetic field, the closed circular orbit r_o would be deformed. For simplicity, let us assume that field perturbations are of the form $b_z(\theta)$, being a function only of the azimuthal angle in the median plane.

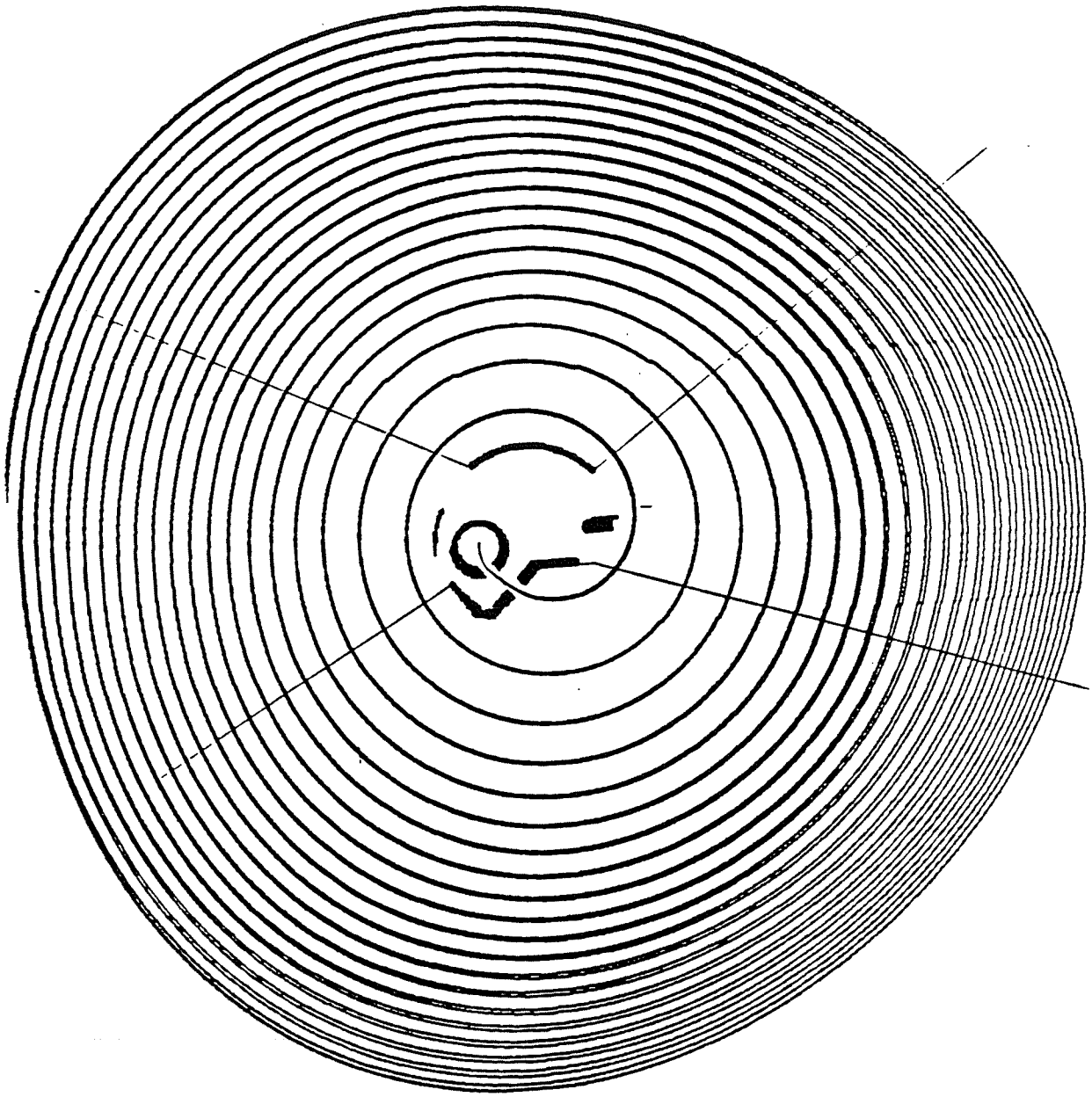

Fig. 8.2.2 The radial trajectory of the proton beam in the Princeton University cyclotron.

Expanding $b_z(\theta)$ in a Fourier series, we have

$$b_z(\theta) = \sum_{n=0}^{\infty} b_n \cos(n\theta + \beta_n) \tag{8.2.8}$$

Substituting eq. (8.2.8) into the equation of motion (8.2.1), we can derive a solution for the deformation of the orbit as follows:

$$x_d = \sum_{n=0}^{\infty} D_n \cos(n\theta + \beta_n) \quad , \tag{8.2.9}$$

Neglecting the higher order terms, D_n has the form:

$$D_n = r_o \frac{b_n}{B_o}[(\frac{1}{n^2 - \nu_r^2}) + (\frac{1}{(n^2 - (3)^2}))] \tag{8.2.10}$$

From eq. (8.2.10) we note that if among the Fourier components of the field perturbation there is a component for which the order n has a value that is approximately equal either to ν_r or to 3, then the deformation associated with that component will be very large, that is, resonance occurs. In the design of an accelerator, such a resonance usually has a very destructive effect on the beam, and hence many efforts are made usually to avoid the occurrence of this resonance phenomenon. However, the resonance method that is employed in the Princeton cyclotron depends on this phenomenon to achieve centering of the beam orbit, and then to obtain a large turn spacing in the extraction region.

8.2.2 Centering of beam orbits

A well centered beam is desirable in a cyclotron so that during most of the acceleration process the beam can be kept in the linear region of the r- p_r phase

space([BLO71]). The resonance extraction method requires a well-centered beam at the beginning so that the amplitude of the coherent oscillation over the trajectory prior to the beam extraction is negligible in amplitude compared to the amplitude of the orbit displacement that is due to the resonance. However, as is explained in section 8.2.1, precessional oscillation also occurs in a cyclotron. This precession causes the successive beam orbit centers to spread out extensively in space. Fig. 8.2.3 shows motion of the instantaneous center of the orbit of a 20 MeV deuteron ion during the first 75 orbital turns, and Fig. 8.2.4 depicts the precessional motion of the orbit center, by tracing the same particle from the ion source out to the extraction region. The origins of the two plots correspond to the geometrical center of the machine. It can be seen from Fig. 8.2.4 that the amplitude of precession is about 7 mm and remains constant over most of the acceleration region; this amplitude mainly depends on the initial conditions of the particle.

The reason that the beam center spreads out again during the final few orbits in Fig 8.2.4 can be understood by a more complete analysis, including the effects of the acceleration. In the smooth acceleration approximation, utilizing the WKB method ([JXU83]), the amplitude A of the betatron oscillation can be expressed as

$$A = A_i \frac{1}{\sqrt{\nu_r B}} \quad , \tag{8.2.11}$$

where, A_i represents that part of the amplitude which is completely determined by the initial conditions. When a particle reaches the extraction region, the cyclotron magnetic field drops off quickly, as does the value of ν_r, and consequently the amplitude is significantly increased. Fig. 8.2.5 shows the distribution of ν_r along the average radius of the Princeton cyclotron. We note that the curve crosses

Fig. 8.2.3 The instantaneous position of the orbit center (center of curvature) up to 75 turns for a 20 MeV deuteron. The horizontal and vertical axes denote along and perpendicular to the the dee gap, respectively. The origin of the figure represents the cyclotron center.

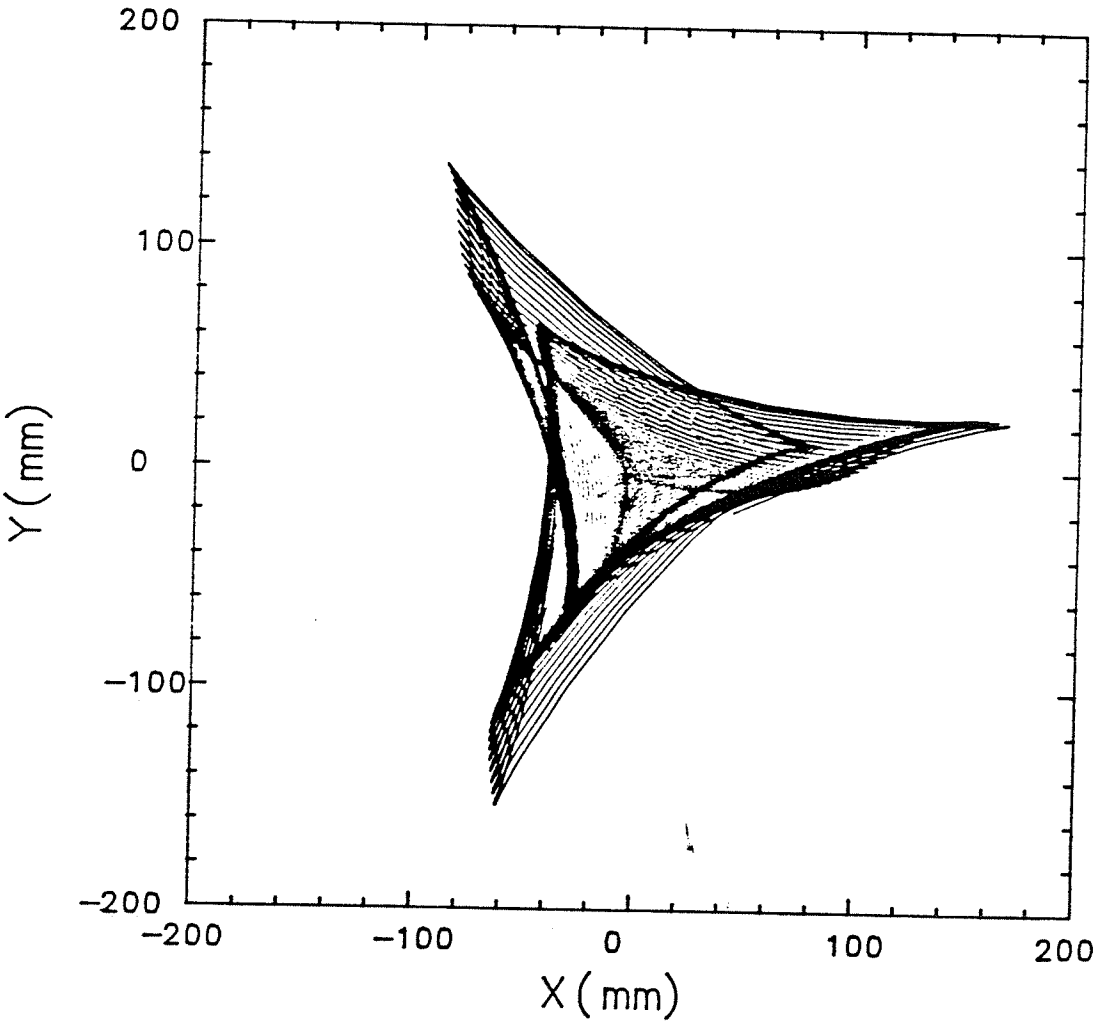
200
100
0
−100
−200
−200
−100
0
100
200
Y (mm)
X (mm)

Fig. 8.2.4 The precessional motion of the 20 MeV deuteron beam's orbit center from the ion source until the extraction region. Each point in this figure represents the position of the center as averaged over one complete orbit turn. This figure shows that the precessional amplitude is approximately 7 mm.

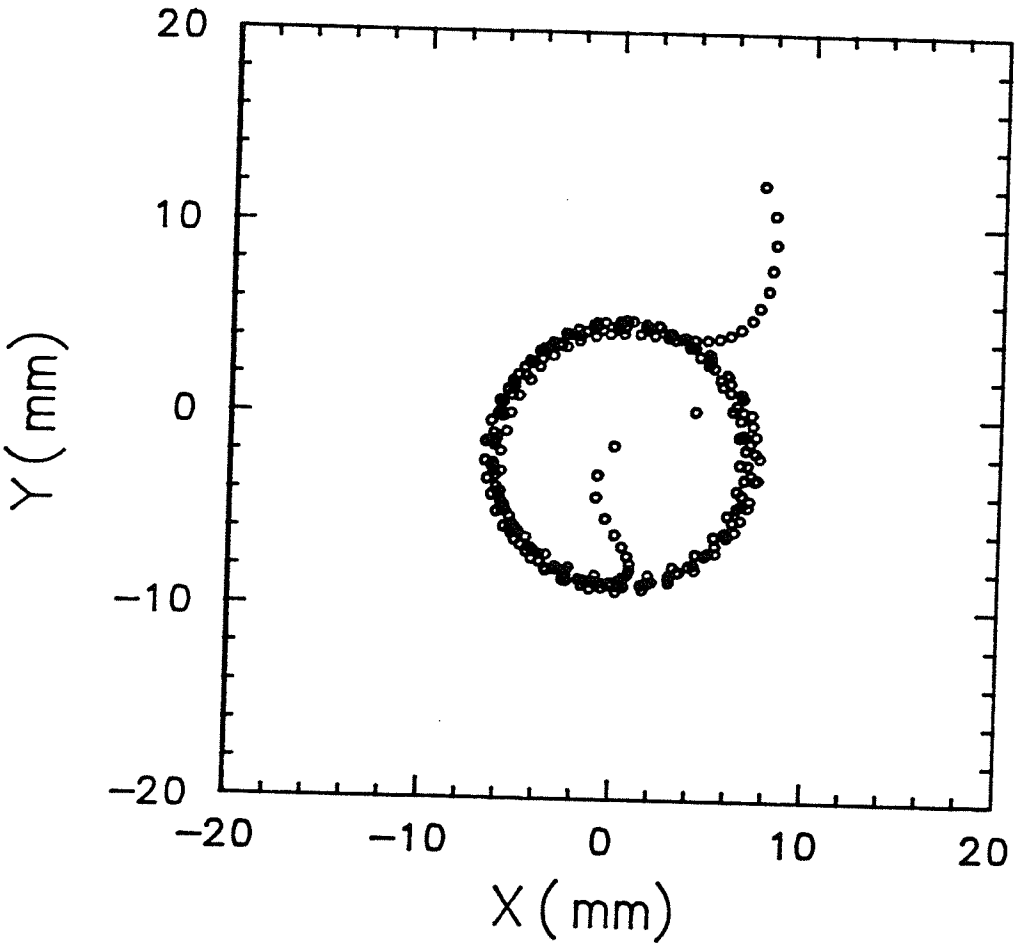
20
10
0
−10
−20
Y (mm)
−20
−10
0
10
20
X (mm)

the $\nu_r = 1$ line at two points, corresponding to r=4 inches and r=27.4 inches, respectively. Except for the central region and the extraction region, where the value of ν_r changes greatly and is below unity, the value of ν_r remains nearly constant in most regions and is about 1.03-1.04. According to eq. (8.2.6), the number of turns needed for the particle to complete a precessional oscillation is about 30. This is in agreement with the result of our detailed computation.

To achieve the centering of the beam, an effect that opposes the effects of the precessional oscillation must be introduced. An introduction for the first harmonic field component will do this job. By comparing eqs (8.2.4) and (8.2.8), we see that by choosing the order n of the perturbing field to be approximately equal to ν_r(it should be n=1 for the Princeton cyclotron), the deformation of the beam orbit will have nearly the same form as the precessional oscillation and its amplitude will be

$$D_1 = r_o \frac{b_1}{B_o}\left(\frac{1}{1-\nu_r^2}\right) \quad , \tag{8.2.12}$$

where b_1 is the amplitude of the first-harmonic field, B_o and r_o are average magnetic field and radius respectively. If we place the first harmonic field in the region where the value of ν_r is just above 1 so that $1 - \nu_r^2 < 0$, and choose properly the value of the FH amplitude b_1 and of its azimuthal angle, then it is possible to roughly cancel the effect of the precessional motion.

Figs. 8.2.6 and 8.2.7 show the movement of the orbit centers when a first harmonic field component was introduced to the cases for Figs. 8.2.3 and 8.2.4. The amplitude and the azimuthal position of the first harmonic coils have been optimized and their optimal values are found to be $b_1 = 27$ gauss and $\phi_i = 65°$ with reference to our coordinate system. By comparing the two sets of figures, we

can see that after the addition of the first harmonic field the orbit centering has improved significantly over most of the acceleration range, except in the extraction region.

Our studies indicate that the optimized values for the amplitude b_1 and the azimuthal angle ϕ_1 of the first harmonic field depend strongly on the species of the beam; for example, the optimized values are $b_1 = 18$ gauss and $\phi_1 = 56°$, respectively, for a 12 MeV proton beam. This dependence on the beam species can be explained on the basis of eqs (8.2.4) and (8.2.12); the reference particles for the different ion have different injection conditions, and, most importantly, the different ions require different magnetic fields to achieve identical trajectories in the Princeton cyclotron.

8.2.3 The enhancement of the orbit space

An ideal centered orbit is, by definition, the centered stable equilibrium orbit. In such a case, the successive separations of orbits of the beam depend on the energy gain per turn. This separation Δr_e can be expressed as

$$\Delta r_e \approx \frac{r_o}{2}\left(\frac{1}{\nu_r^2}\frac{\Delta E}{E}\right) \tag{8.2.13}$$

Here r_o is the radius of the equilibrium orbit, ν_r is the frequency of radial oscillations, ΔE is the energy gain per orbit turn, and E is the energy of the particle. For 20 MeV deuteron ions in the Princeton cyclotron, $\Delta E = 35.56$ keV, $r_o = 29$ inch; let us also take $\nu_r \approx 1$. Substituting these values into eq. (8.2.13), we obtain a turn separation of about 0.7 mm. It is important to emphasize that an actual beam always has a radial width, due to its initial RF phase spread which causes an energy dispersion

Fig. 8.2.5 The averaged radial focusing frequency distribution along the radius. The straight line in the figure represents the $\nu_r = 1$ resonance. It can be seen that the resonance happens at r $\approx$ 4 inches and r $\approx$ 27 inches. Except for the central region and for the extraction region, where the value of ν_r is below unity and changes greatly, the value of ν_r is nearly a constant over most of the acceleration regions.

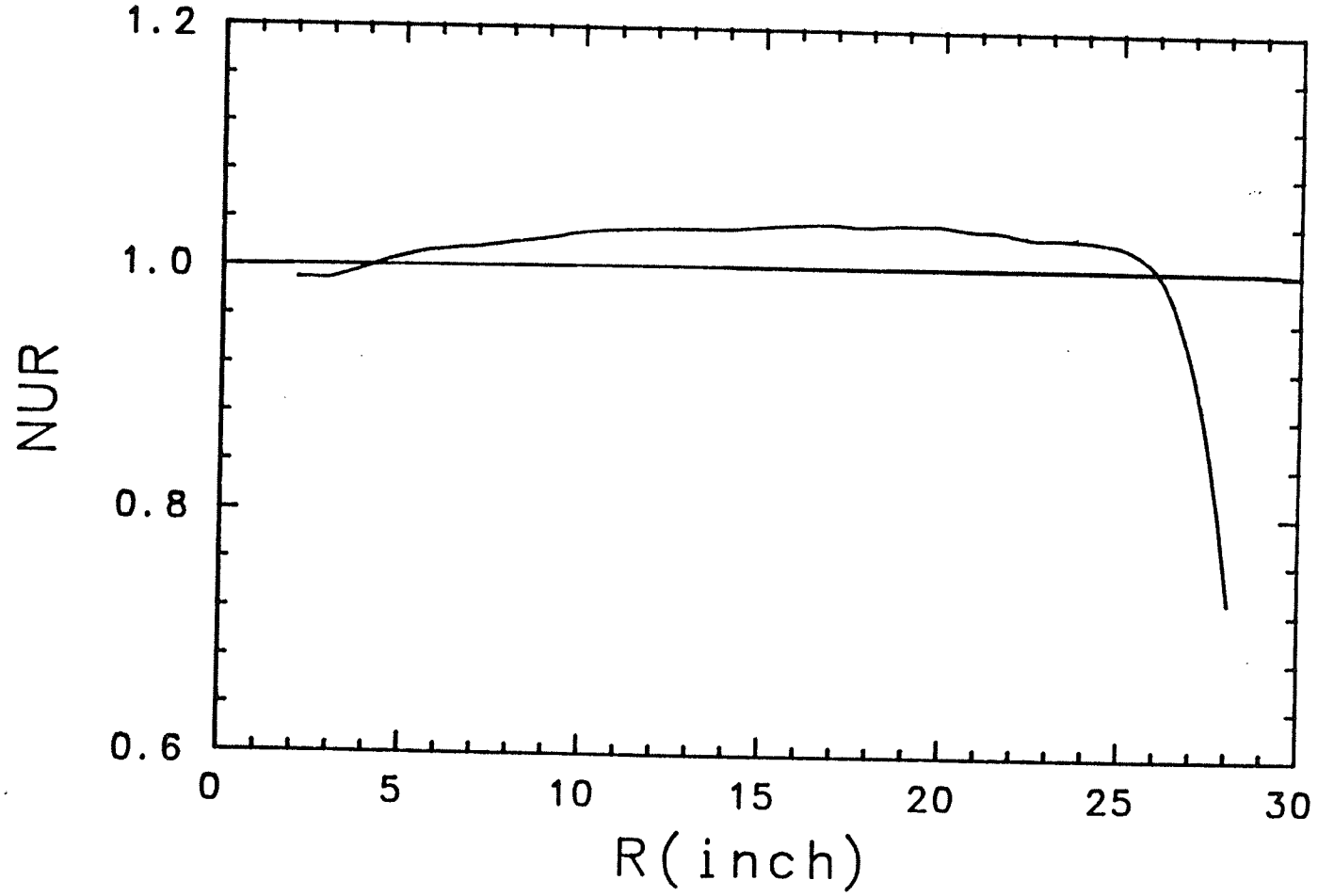
1.2
1.0
0.8
0.6
NUR
0
5
10
15
20
25
30
R(inch)

Fig. 8.2.6 The instantaneous position of the orbit center (center of curvature) for the first 75 turns for a 20 MeV deuteron after the installation of the inner first harmonic field (of $B_i = 27$ gauss and $\Phi_i = 65°$). By comparing this with Fig. 8.2.3, it can be seen that the overall center now converges to the origin.

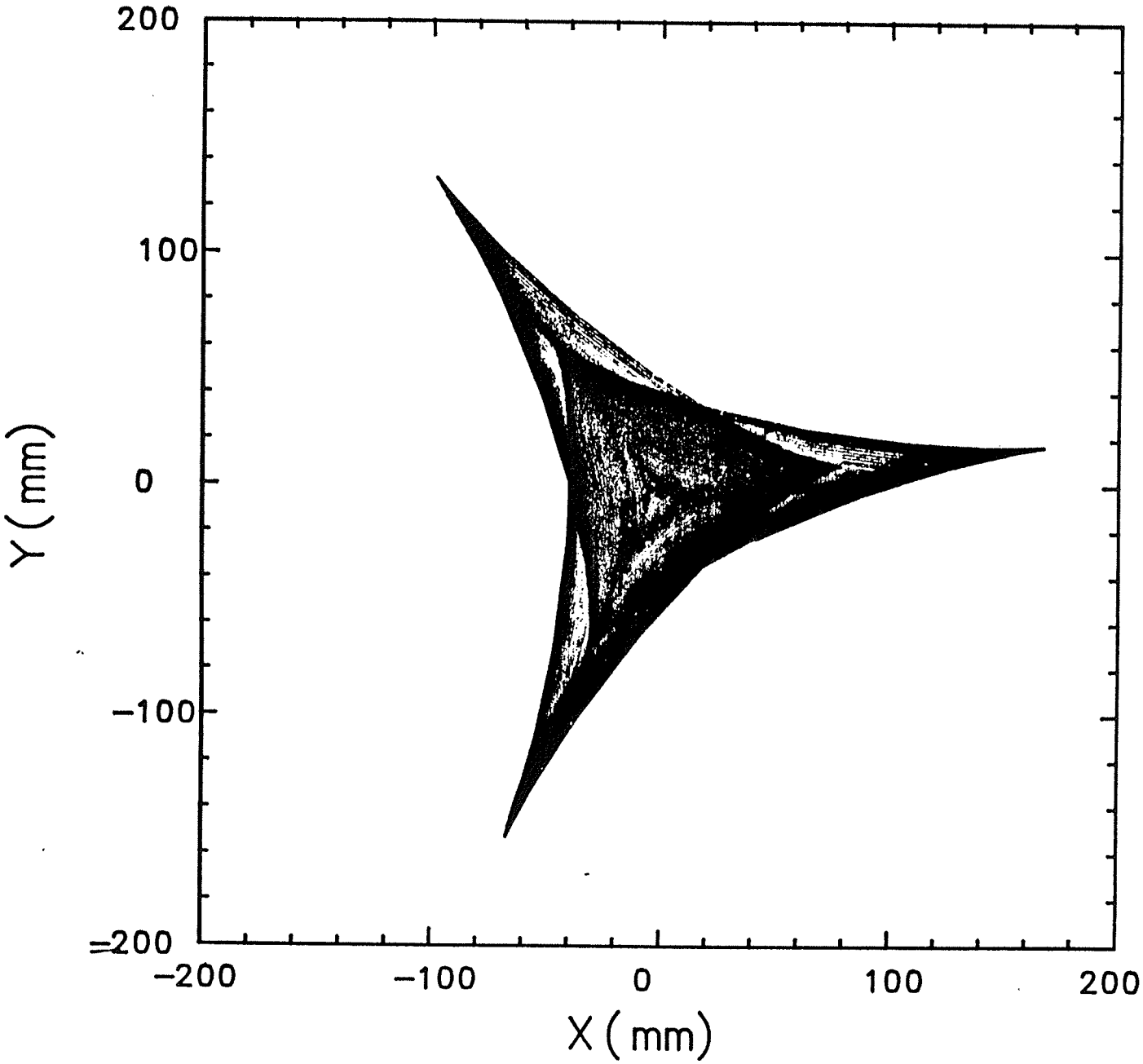
200
100
0
−100
−200
Y (mm)
−200
−100
0
100
200
X (mm)

in the beam, and also due to the betatron oscillations about the equilibrium orbit. As a result, the beam bunches in successive orbits may actually overlap before the extraction. In such a case, it is not possible to attain a single-turn extraction of the beam.

One option for solving the above problem of overlapping successive orbits is to utilize the first harmonic perturbing field, but in a different way. From Fig. 8.2.5, it can be noted that the value of ν_r is 1 at r = 26 inches, and that it then continually drops off for increasing larger radii. Apparently, the installation of the outer FH field coils at $r \approx 27$ inches (where $\nu_r < 1$) would cause a steady increase in the radial displacement. According to eqs. (8.2.8) and (8.2.9), this displacement has the form

$$x_d = r_o \frac{b_1}{B_o} \frac{1}{1-\nu_r^2} \cos(\theta + \beta) \quad . \tag{8.2.14}$$

As the frequency ν_r continues to fall even more rapidly, the displacement is converted to an oscillation amplitude and the orbit then precesses with rapidly increasing angular speed. With a proper choice of the azimuthal angle, this precessional motion will reinforce the radius gain per turn, and thereby yield an exceptionally large Δr_p at the position of the electrostatic extraction channel.

The resultant maximum turn separation Δr can now be expressed as the sum of two terms,

$$\Delta r = \Delta r_e + \Delta r_p \quad , \tag{8.2.15}$$

where Δr_e and Δr_p are given by eqs. (8.2.13) and (8.2.7).

Figs. 8.2.8 and 8.2.9 demonstrate the precessional motion of the orbit center

for 12 MeV proton ions with and without the installation of the outer FH field, of 1 gauss, at $r \approx 26$ inches. The comparison between these two figures clearly shows that switching on the outer FH field induces a large off-center motion while the beam passes through the ν_r=1 resonance. This causes a significant increase in the turn separation Δr at the entrance to the electrostatic deflector, as is shown in Figs 8.2.10 and 8.2.11. In these two figures the X-axis represents the orbital radius which passes the entrance to the electrostatic deflector and Y-axis denotes the separation between two succesive orbits.

It is obvious that the magnitude of the orbit displacement is proportional to the field strength and that the direction of this displacement is directly correlated with the azimuthal angle of the field. Figs. 8.2.12 and 8.2.13 demonstrate another set of relative beam outputs, using a 2 gauss outer FH field instead of the 1 gauss FH field that was used previously. By comparing these two figures with Figs. 8.2.9 and 8.2.11, we can see that this larger FH field induces a larger precessional motion, and results in a large turn separation for extraction, than did the 1 gauss field. However, this larger radial amplitude would cause a large axial oscillation through the nonlinear coupling resonance, as will be described in Section 8.3.2, which follows. Therefore, based on a compromize between the two conflictting requirements, an extraction system using the smallest possible radial oscillation amplitude that is just about strong enough for 100% extraction is to be preferred.

Fig. 8.2.7 The precessional motion of the 20 MeV deuteron beam's orbit center from the ion source until the extraction region after the inner first harmonic field of $B_i = 27$ gauss and $\Phi_i = 65°$ was installed. Each point in this figure represents the position of the center as averaged over one complete orbit turn. This figure shows that the precessional amplitude is less than one mm.

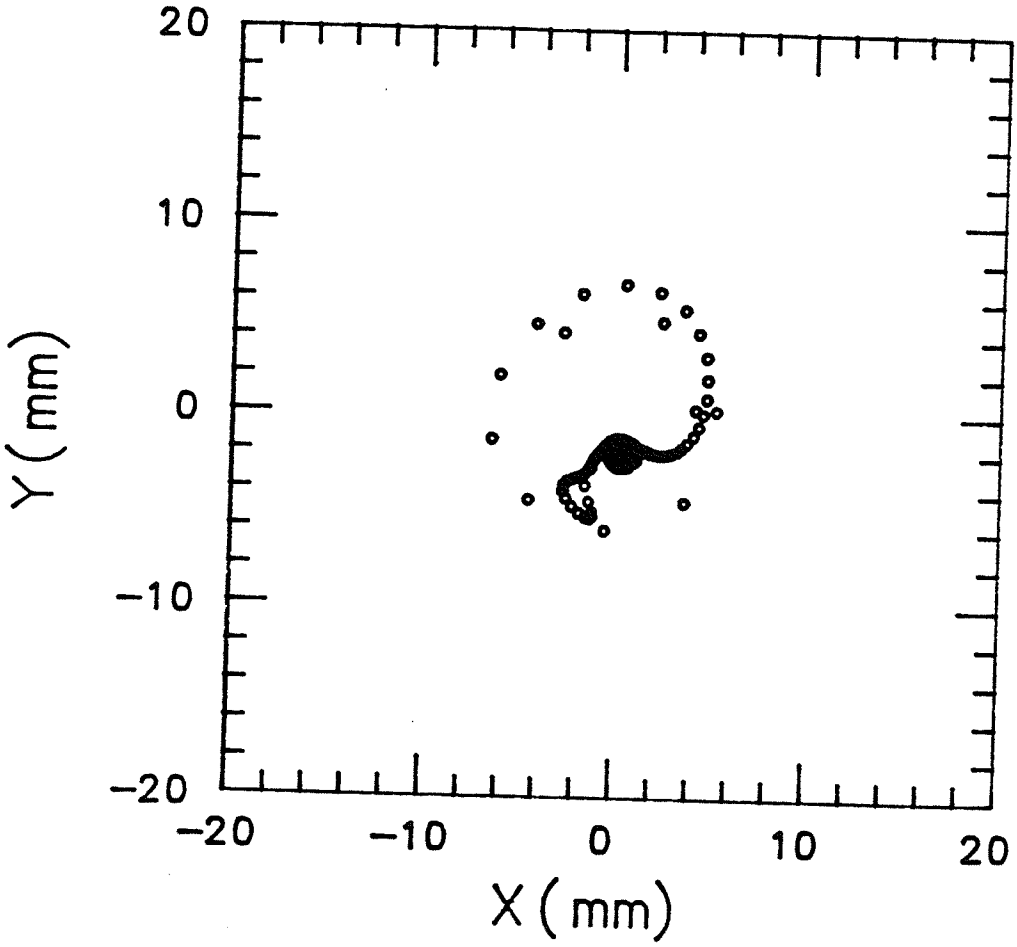
20
10
0
−10
−20
Y (mm)
−20
−10
0
10
20
X (mm)

Fig. 8.2.8 (the first following) The precessional motion of the 12 MeV proton beam's orbit center from ion source until the extraction region with the inner first harmonic field of $B_i = 18$ gauss and $\Phi_i = 56°$ and without any outer first harmonic field installed. The figure shows that the precessional amplitude is less than two mm.

Fig. 8.2.9 (the second following) The precessional motion of the 12 MeV proton beam's orbit center from ion source until the extraction region with both the inner first harmonic field of $B_i = 18$ gauss and $\Phi_i = 56°$ and an outer first harmonic field of $B_O = 1$ gauss and $\Phi_o = 60°$ installed. The figure shows that the average center converges firstly, then due to the effect of the outer FH, they spread out again so that an incresing turn space can be obtained at the entrance to the electrostatic deflector.

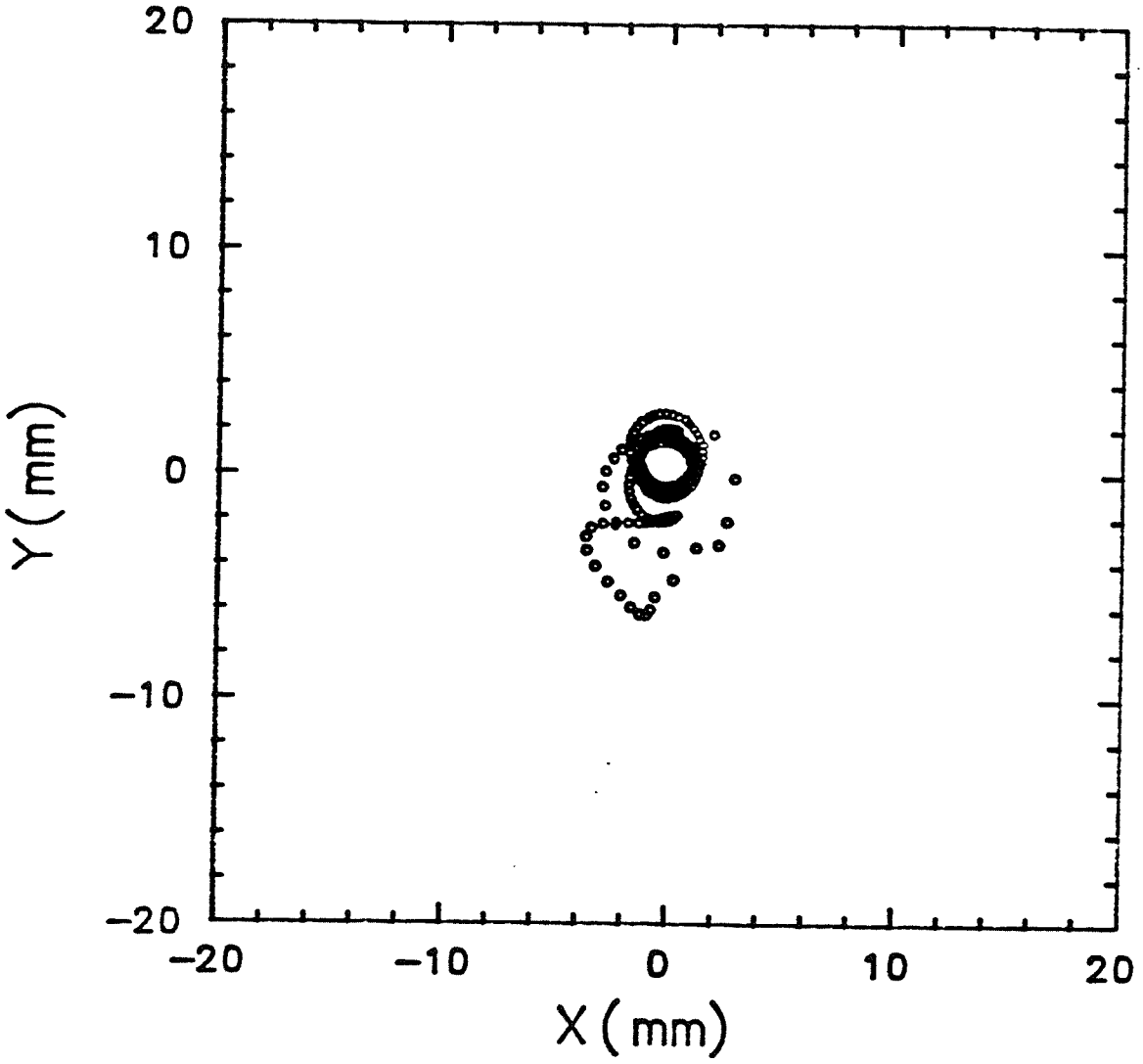
20
10
0
−10
−20
Y (mm)
−20
−10
0
10
20
X (mm)

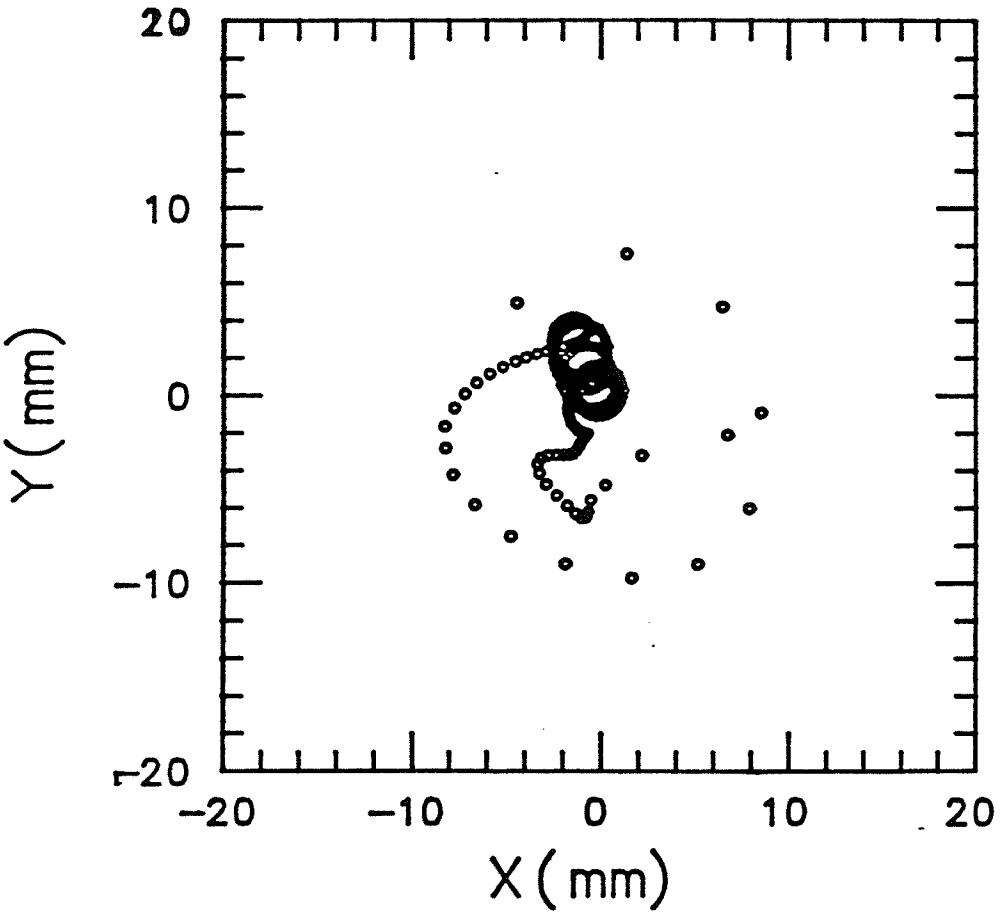
20
10
0
−10
−20
−20
−10
0
10
20
Y (mm)
X (mm)

Fig. 8.2.10 (the first following) The turn separation distribution for the 12 MeV proton beam before outer FH field was installed. The horizontal axis denotes the radius to the entrance to the electrostatic deflector and the vertical axis represents the difference of successive orbit radius, that is $\Delta r = r_{n+1} - r_n$. The figure shows it is nearly a constant (about 1.5 mm).

Fig. 8.2.11 (the second following) The turn separation distribution for 12 MeV proton beam after an outer FH field of $B_o = 1$ gauss and $\Phi_o = 120°$ was installed at r = 27 inches. Comparing with fig. 8.2.10 it is seen that due to the effect of the outer FH field, the turn space increases gradually. After one loop it reaches up to 8 mm at the entrance to the electrostatic deflector.

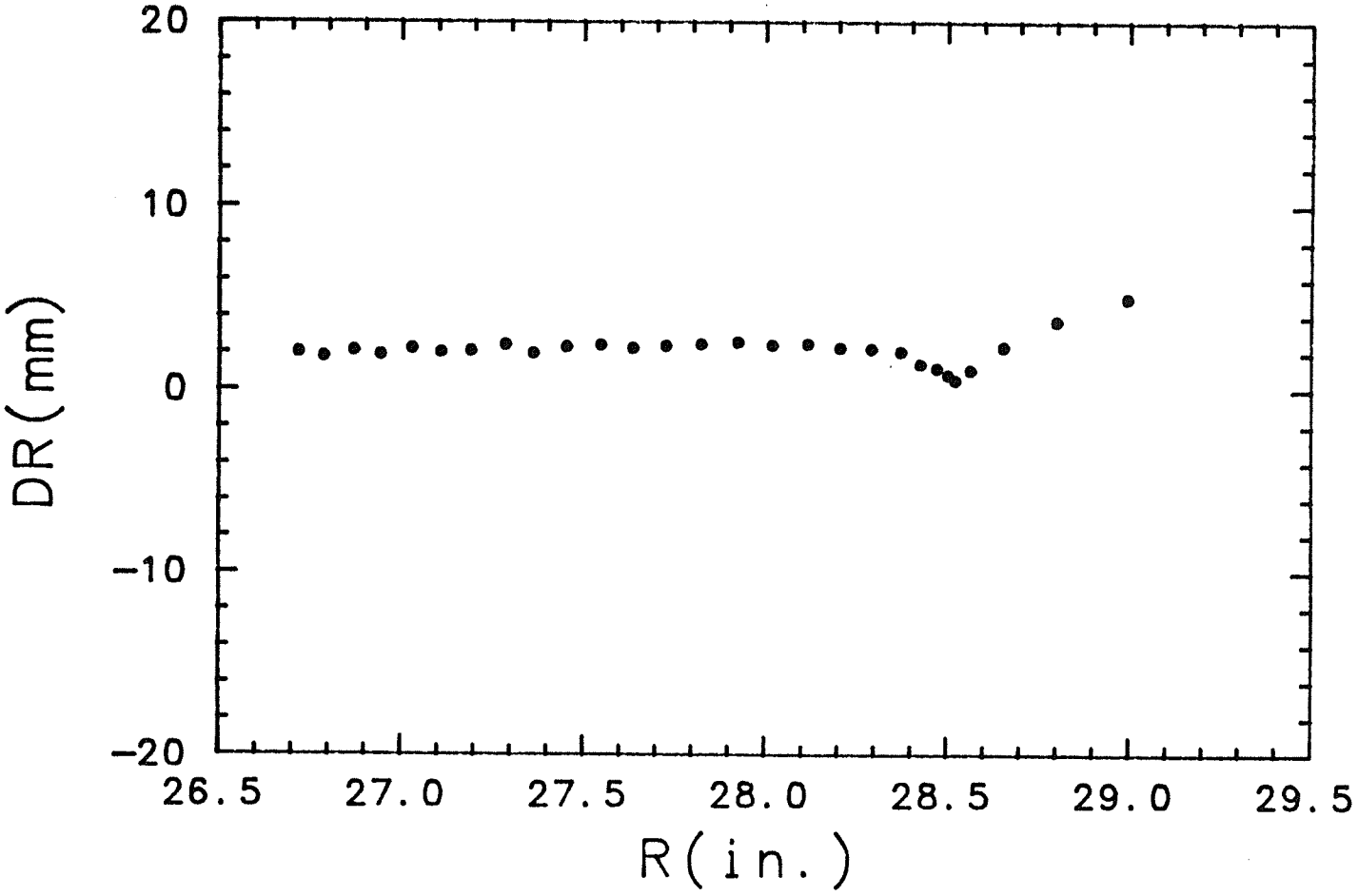
20
10
0
−10
−20
DR(mm)
26.5
27.0
27.5
28.0
28.5
29.0
29.5
R(in.)

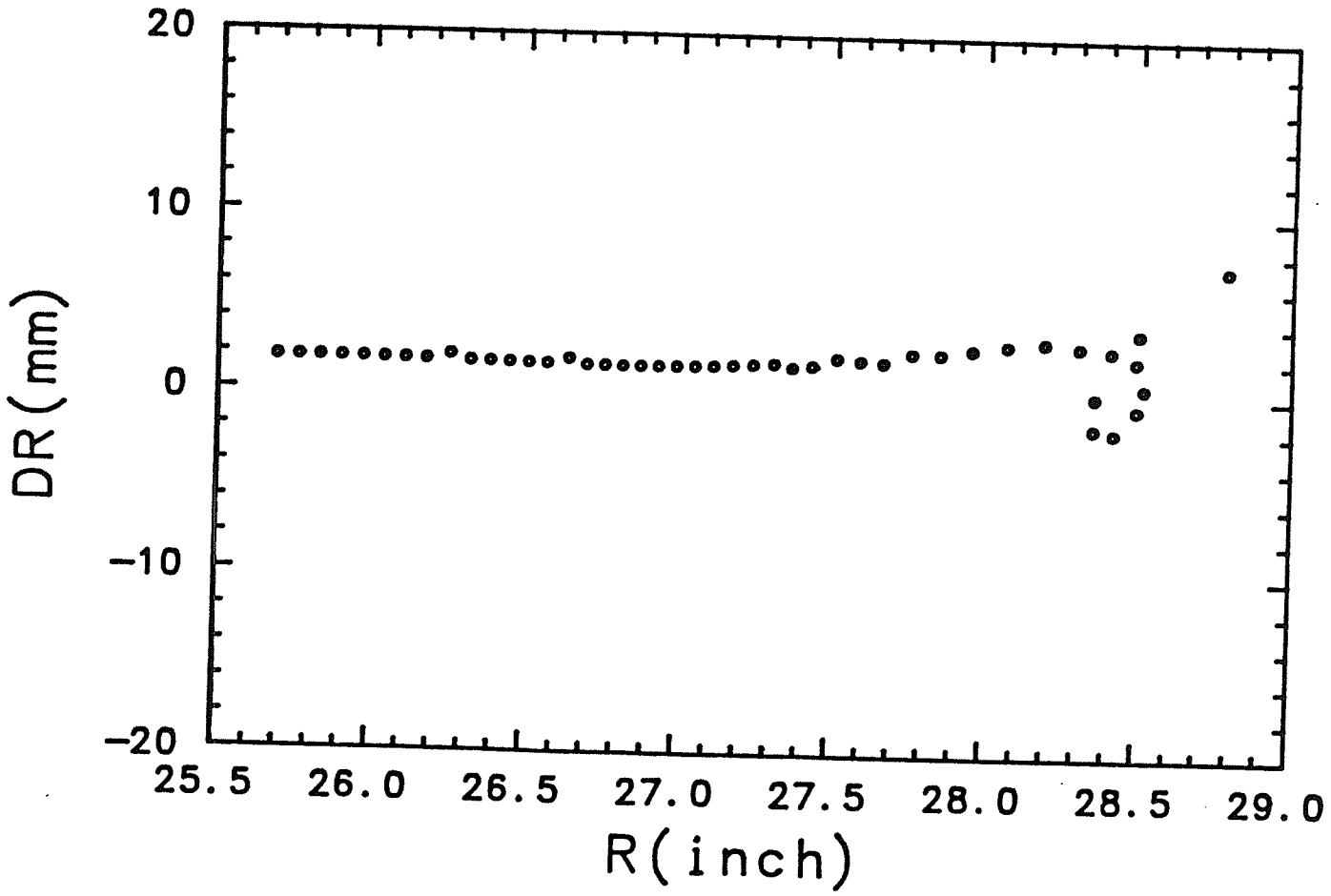
20
10
0
−10
−20
DR(mm)
25.5
26.0
26.5
27.0
27.5
28.0
28.5
29.0
R(inch)

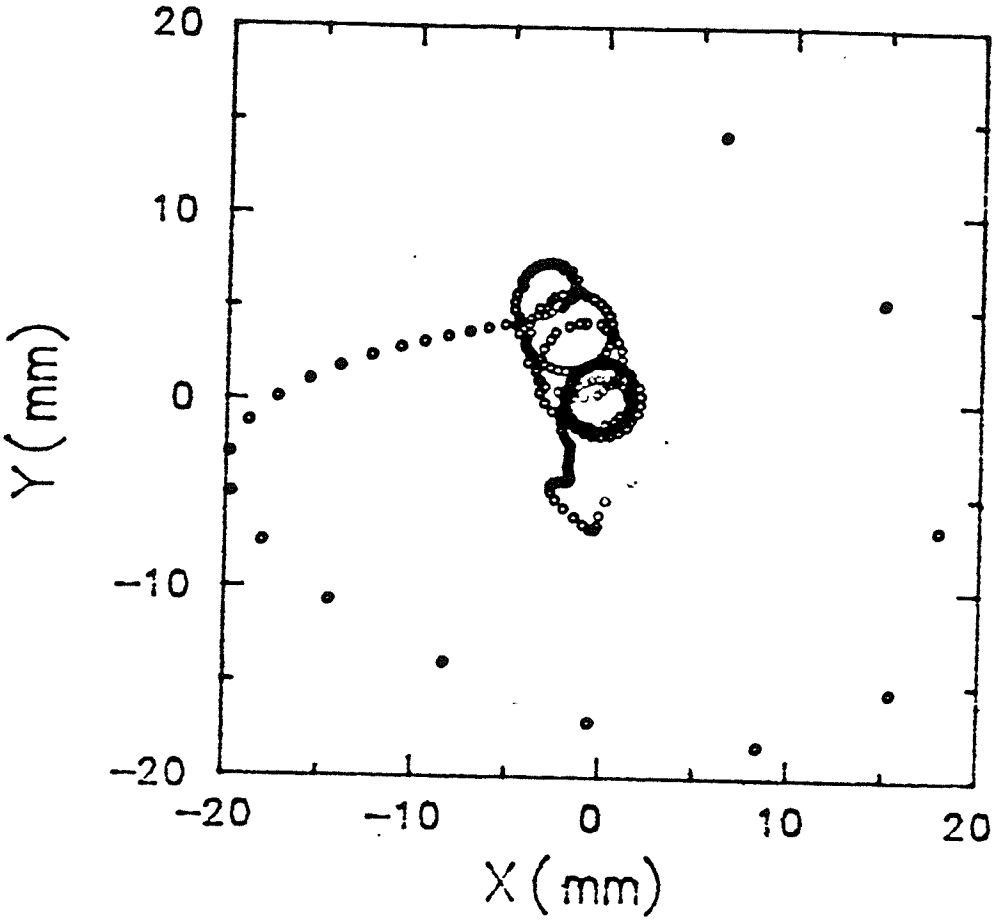

Fig. 8.2.12 The precessional motion of the 12 MeV proton beam's orbit center from the ion source until the extraction region with both the inner first harmonic field of $B_i = 18$ gauss and $\Phi_i = 56°$ and an outer first harmonic field of $B_O = 2$ gauss and $\Phi_o = 140°$ installed. Comparing with fig. 8.2.9, it is seen that the higher outer FH field drives a stronger off-center motion at the extraction region.

Fig. 8.2.13 The turn separation distribution for 12 MeV proton beam after an outer FH field of $B_0 = 2$ gauss and $\Phi_0 = 140°$ was installed at r = 27 inches. Comparing with fig. 8.2.11 it is seen that the higher outer FH field excited a stronger off-center motion so that the turn separation at the entrance to the deflector (about 29 inches) increased up to 18 mm.

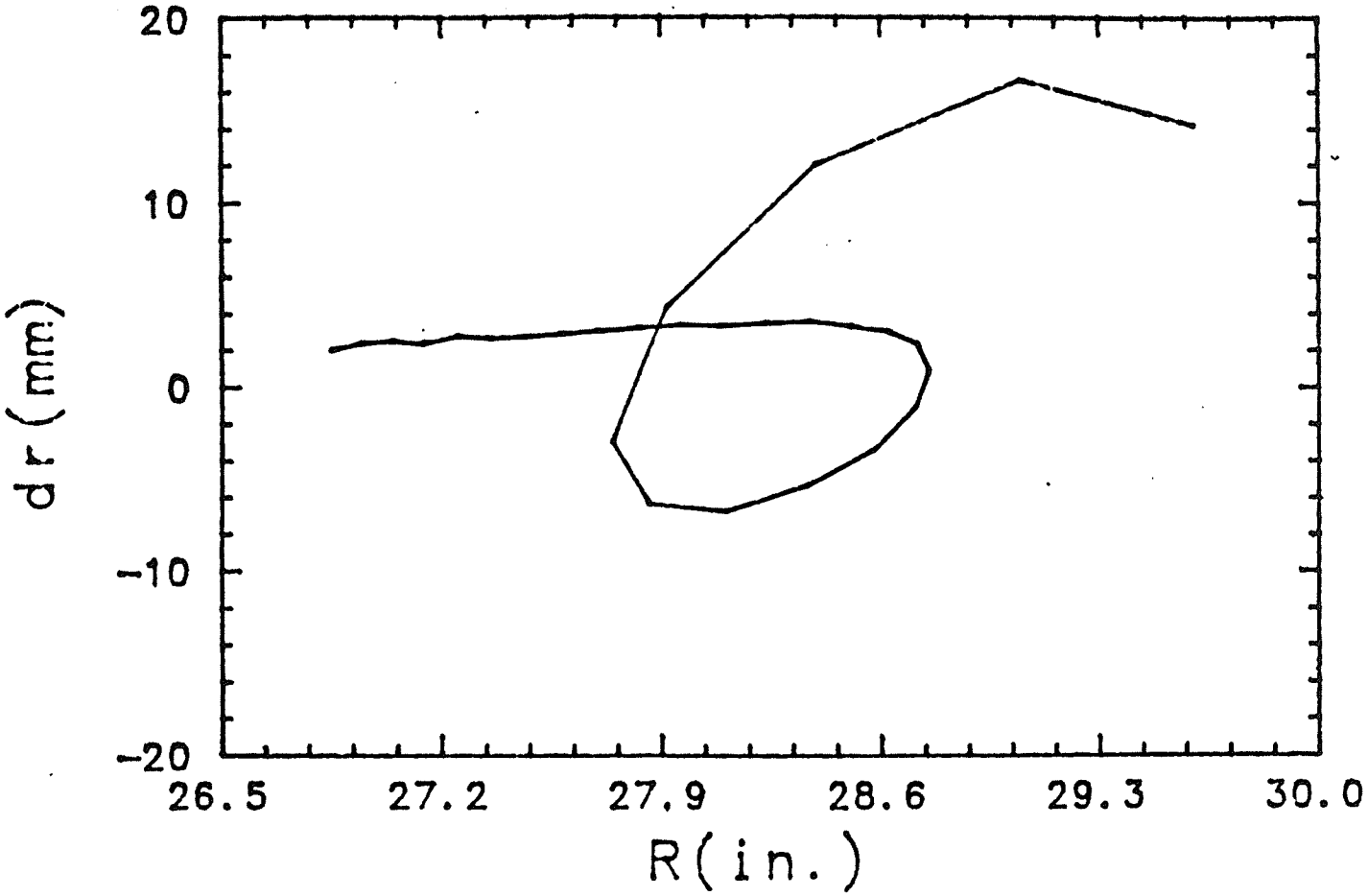
20
10
0
-10
-20
dr (mm)
26.5
27.2
27.9
28.6
29.3
30.0
R(in.)

8.3 Computer Simulation of pre-extraction beam

So far, our studies of beam orbits in the Princeton cyclotron have been based on a single-particle (the reference particle) tracing. However, for more detailed investigations of the optical characteristics of the beam, it is necessary to carry out a more extensive computer simulation of the beam in phase space. These studies have been performed using the upgraded dynamics program NEWEEL. As described in Chapter 7, this program uses the impulse approximation method to replace the calculation of the electric field at the outer orbits ($r > 250cm$). In addition, a nonlinear code, which extends the computation of the main magnetic field components to higher order, has also been included in NEWEEL so that the nonlinear effects which arise in the extraction region can be treated adeguately.

In these studies, a large number of representative particles are chosen from the beam emittance space and are traced through the extraction region. To save computing time, some simplifications have been made. First, we assumed that the motion in the full six-dimensional phase space can be decoupled into three separate parts: radial, axial and longitudinal. Second, in the orbit calculation of the beam in longitudinal phase space, only the initial phase differences among representative particles was included. In the orbit calculation in transverse phase space, only the reference particle was traced from the ion source; all the other particles were traced starting only at a very late orbit turn, and all of their parameters at this turn were assumed to be the same as those of the reference particle except for their differing individual positions on the two-dimensional phase space eigen-ellipse. The computational details and results will now be provided in the following sections.

8.3.1 Calculations of the beam in transverse phase space

The orbit calculations of the beam in transverse phase space were begun at the 175^{th} turn. At this turn, the energy of the reference particle is 8.9 MeV for a 12 MeV proton and 15.5 MeV for a 20 MeV deuteron, respectively, the magnetic field is still isochronous, and the effects of the magnetic fringe field have not yet felt. In the calculations, the two sets of the FH field have been optimized, based on the previous reference particle tracing that was carried out from the ion source all the way out to the extraction region. In addition to the reference particle, two sets of particles were chosen with initial displacements on an (r, r′) and (z, z′) eigen-ellipses, respectively, as shown in Figs. 8.3.1 and 8.3.2. The emittance areas chosen for each set are 3.8 mm-mrad for a 20 MeV deuteron beam and 5.5 mm-mrad for a 12 MeV proton beam. These correspond to an initial emittance area of 120 mm-mrad at a beam energy of $E_0 = 15$ keV. The radial eigen-ellipse was chosen to have a radial width $\Delta r = 2mm$ (about three times the normal radius gain per turn). The axial eigen-ellipse was determined by choosing $\Delta z = 8mm$. A beam height of 8 mm is about the largest expected in the Princeton cyclotron. These conditions should suffice for our design studies.

The results of the radial phase space calculation for the 20 MeV deuteron beam are shown in Fig. 8.3.3. That graph shows the evolution of the r vs. r′ ellipses, through the ν_r=1 resonance to the entrance of the electrostatic deflector. The digits near the last several bunches of the beam denote their turn number. In this diagram the turns prior to N=200 are not shown, since they are well behaved and rather uninteresting, and to avoid confusion through over plotting, one print of each two has been omitted before turn 240. Between turn N=218 and turn N=228, the orbits

Figs. 8.3.1, 8.3.2 The initial distribution of 9 representative particles in radial phase space (top) and axial phase space (bottom) on turn 351. The emittance areas are 3.8 mm-mrad for a 20 MeV deuteron beam and 5.5 mm-mrad for a 12 MeV proton beam.

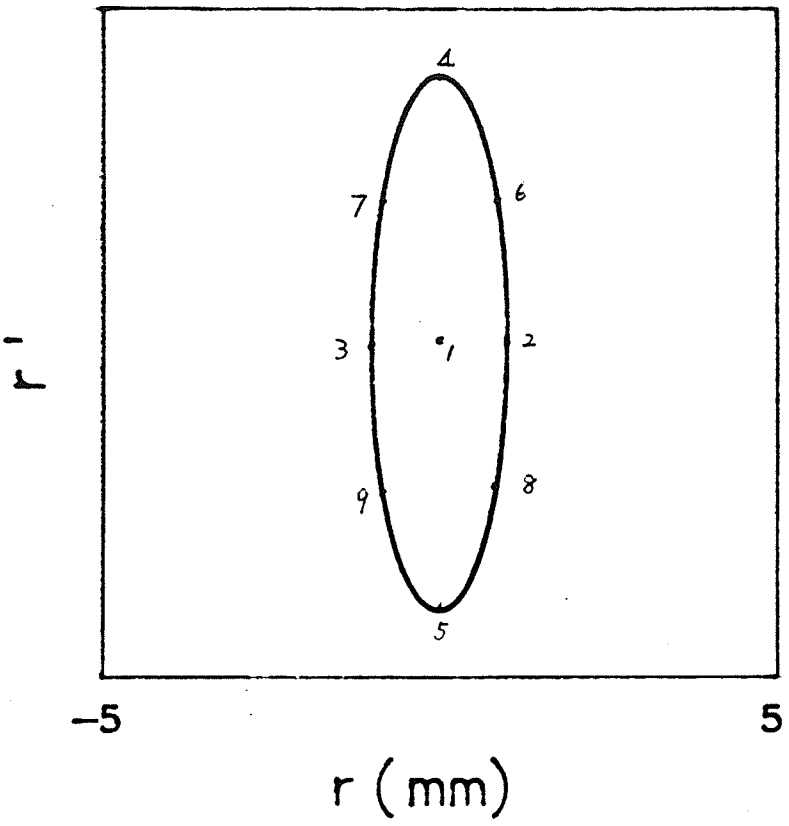
r'
4
7
6
3
1
2
9
8
5
-5
5
r (mm)

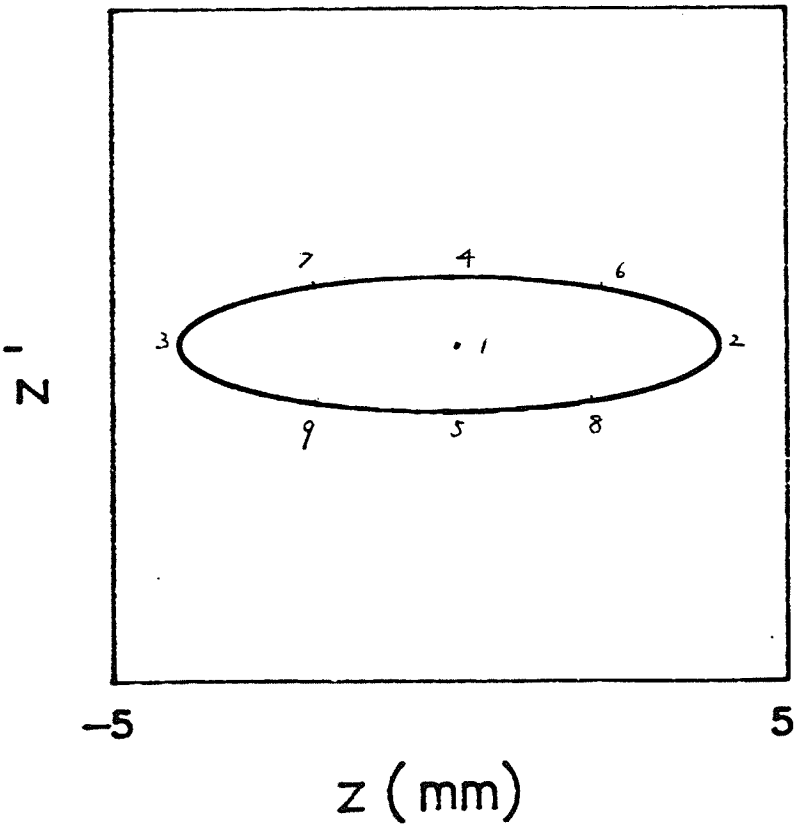
z'
7
4
6
3
1
2
9
5
8
-5
5
z (mm)

pass through the $\nu_r = 1$ resonance and hence are driven off center. As can be seen, the orbits then execute one large precession loop before reaching the final turn. This causes the clearance of successive orbits to increase greatly until the last turn (244), where the clearance is as large as 5 mm, which is wide enough to permit the insertion there of a septum of thickness 0.5 mm.

To exhibit clearly the evolution of the beam envelope in its axial motion, we did not supply here the results of the axial calculation in a phase space(z, z') diagram, instead, instead have directly provided the results for the axial motion of the nine particles described above. Fig. 8.3.4 shows the results of an axial phase space calculation for the 12 MeV proton beam, where the horizontal axis denotes the number of the RF cycle. Since the acceleration of the beam is caused by the second harmonic electric field, two RF cycles are equivalent here to one particle turn. The vertical axis represents the axial departures of the particle from the median plane of the cyclotron. This figure gives the beam envelope in the axial direction for particle orbit turns between N=175 and N=230 It can be seen that with an optimized FH field, the amplitude of the beam is constant in the range of z$\leq$ 4 mm.

8.3.2 Studies of the nonlinear coupling resonance effect

A quick check indicates that, before its extraction, the beam has to pass through the well-known coupling resonance $\nu_r - 2\nu_z$=0. This occurs at E=11.3 MeV and turn number N=216 for 12 MeV protons, and at E=18.9 MeV and N=237 for 20 MeV deuterons. To get a clearer physical picture when the coupling resonance occurs, let us derive a relation between radial and axial oscillation amplitudes for this case.

Fig. 8.3.3 The evolution of r vs. r' ellipses through the $\nu_r = 1$ resonance to the entrance of the electrostatic deflector. The initial coordinates of the 9 representative particles in radial phase space are defined in fig. 8.3.1. The digits near the last several bunches of the beam denote their turn number. To avoid confusion through over plotting, one print of each two has been omitted before turn 240.

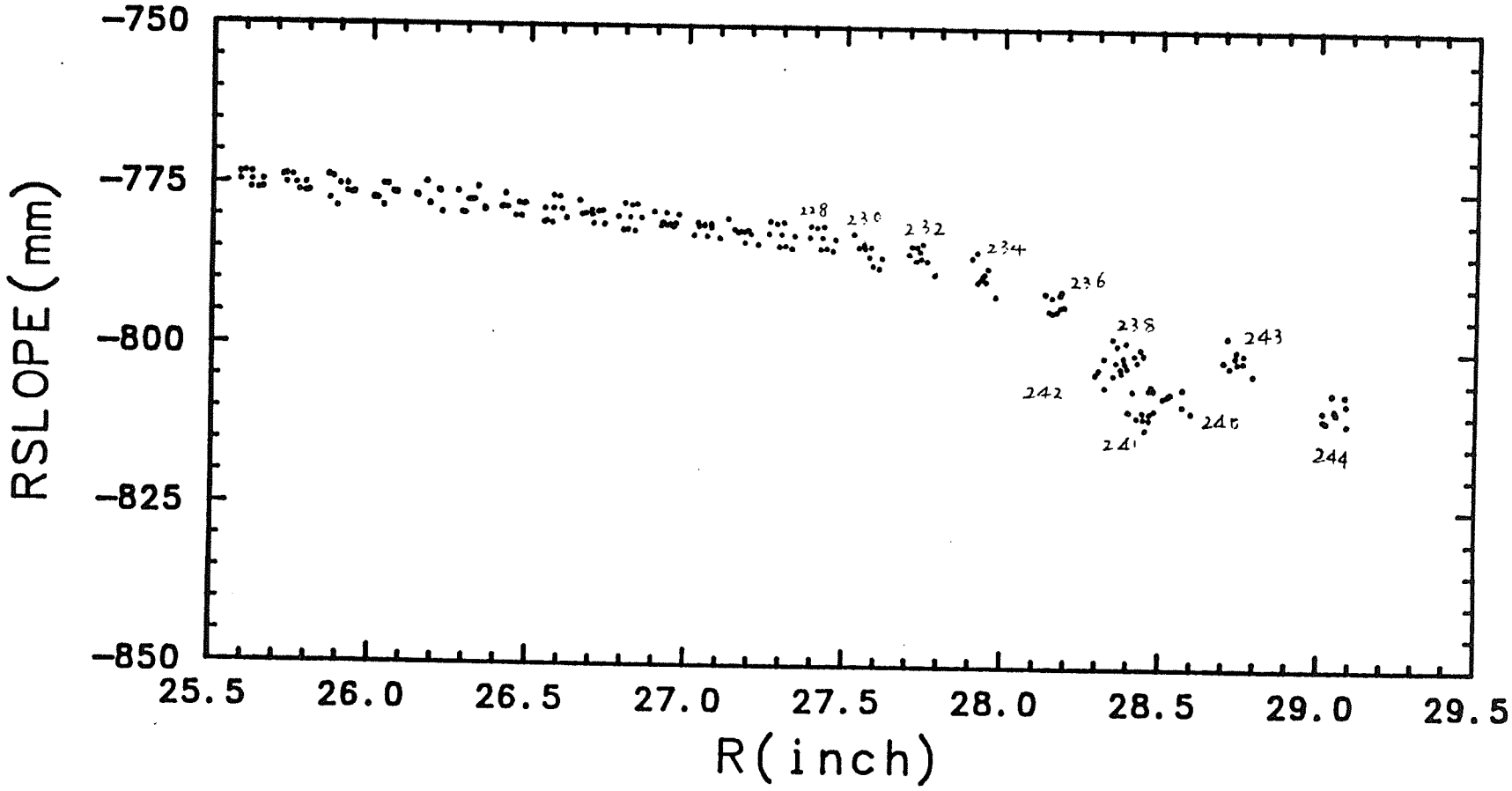
RSLOPE(mm)
-750
-775
-800
-825
-850
25.5
26.0
26.5
27.0
27.5
28.0
28.5
29.0
29.5
R(inch)
238
230
232
234
236
238
243
242
240
241
244

Fig. 8.3.4 The axial oscillation of the 9 particles in axial phase space (see Fig. 8.3.2) for 12 MeV protons. The amplitude of the outer FH field used is 1 gauss. The horizontal axis denotes the number of the RF cycle. Due to the acceleration in the N = 2 mode, two RF cycles here are equivalent to one particle turn. The vertical axis represents the axial departure of the particle's orbits from the median plane of the cyclotron. It can be seen that the envelope of the beam is being kept stable in the range of $z \leq 4$ mm.

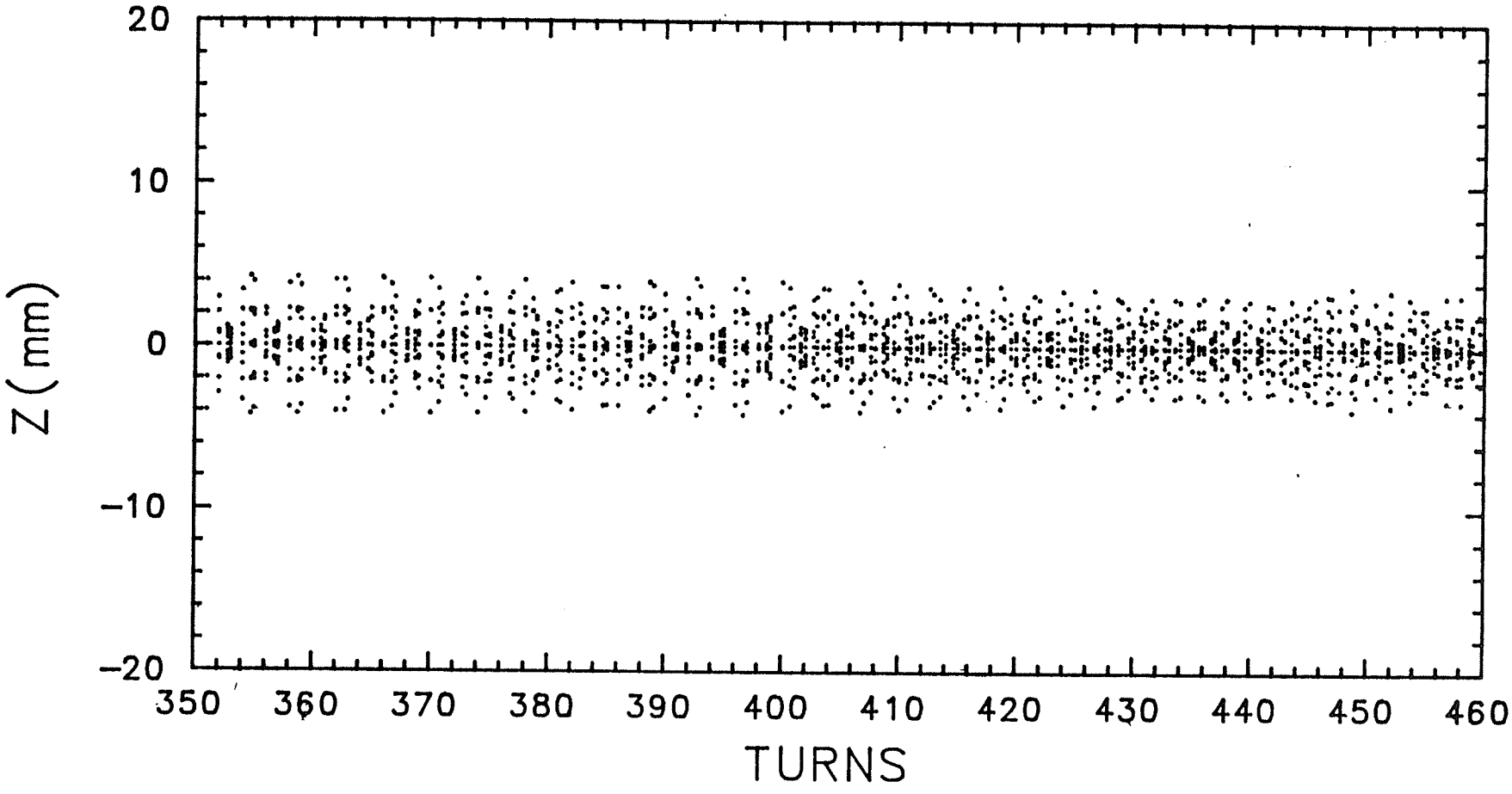
20
10
0
−10
−20
Z (mm)
350
360
370
380
390
400
410
420
430
440
450
460
TURNS

As is well known, the resonance effect is caused by the nonlinear terms in the expansion of the magnetic field. If we keep only the largest nonlinear terms (those of second order) in the magnetic field, and neglect the effect of flutters in eq. (8.2.2), then the equations of motion in the transverse direction can be expressed approximately as

$$\frac{d^2x}{d\theta^2} + \nu_r^2 x = \frac{1}{2}\mu''(y^2 - x^2) \tag{8.3.1}$$

$$\frac{d^2y}{d\theta^2} + \nu_z^2 y = \mu'' xy \quad , \tag{8.3.2}$$

Here, $x = \frac{(r-r_o)}{r_o}$, $y = \frac{z}{r_o}$, and

$$\mu'' = \frac{r_o^2}{B(r_o)} \frac{d^2B(r_o)}{dr_o^2} \quad .$$

Let us now assume that the solutions of eqs. (8.3.1) and (8.3.2) have the form:

$$y = A \sin \nu_z \theta \qquad and \qquad x = B \sin(\nu_r \theta + \phi) \tag{8.3.3}$$

Here, $\sin \nu_z \theta$ and $\sin \nu_r \theta$ should have been written most generally as $\sin \int \nu_z \delta\theta$ and $\sin \int \nu_r \delta\theta$, but since ν_z and ν_r change very slowly, we can omit this change in an approximate analysis.

We now substitute the expressions for x and y and their second order derivatives into eqs. (8.3.1) and (8.3.2). We utilize the condition that the coefficients A and B are slowly varing functions of time(so that their value during one betatron oscillation period may be considered as constant). Then, we can separate equations 8.3.1 and

8.3.2 into two independent parts and select the slowly varing part as follows:

$$\frac{dA}{d\theta}\nu_z - \frac{\mu'' AB}{4}[\cos(2\nu_z\theta - \nu_r\theta - \phi)] \approx 0 \tag{8.3.4}$$

$$\frac{dB}{d\theta}\nu_r - \frac{\mu'' A^2}{8}[\cos(2\nu_z\theta - \nu_r\theta - \phi)] \approx 0 \tag{8.3.5}$$

If $2\nu_z \approx \nu_r$, we have, from the two eqs (8.3.4) and (8.3.5),

$$A\frac{dA}{d\theta} + 4B\frac{dB}{d\theta} = 0 \tag{8.3.6}$$

By integrating eq. (8.3.6), one can get an important expression, namely that

$$A^2 + 2B^2 = A_o^2 + 2B_o^2 = constant, \tag{8.3.7}$$

where A_o and B_o are initial amplitudes, and A and B are the amplitudes at any later time, of the betatron oscillations in the axial and radial directions, respectively. The expression (8.3.7) indicates that if the radial and axial betatron oscillation frequencies satisfy the condition $2\nu_z \approx \nu_r$, then the coupling resonance would take place. One significant characteristic by which this resonance differs from the resonance described by equation (8.2.10), is that it is caused not by the outer perturbing field but rather by the higher-order terms in the main magnetic field. Another property of the coupling resonance is that it is a kind of a "difference" resonance. When this resonance happens, there exists an energy exchange between the radial and axial motions; thus, increase in the oscillation amplitude in one direction must lead to a decrease of the oscillation amplitude in the other direction. Hence, this resonance

can not lead to an infinite increase in the oscillation amplitude. Also, from expression (8.3.7) we can find that if the initial axial amplitude A_o is very small and the initial radial amplitude B_o is very large(that is, if $A_o \ll B_o$), when the resonance happens, then the radial amplitude A might increase up to $\sqrt{2}$ times the initial radial amplitude B_o; otherwise, if $A_o \gg B_o$, then the resonance only leads to the radial amplitude B increasing almost up to $\frac{1}{\sqrt{2}}$ times the initial axial amplitude A_o.

The first of the two situations described above is just the problem about which we are concerned. As stated in section 8.2, we have installed an outer FH field at about r=26 inches in order to excite an off-center motion so that an increasing orbit turn spacing can be attained. Such a large radial oscillation must cause an increment in the axial amplitude due to the subsequent existence of the coupling resonance (at $r \approx 28$ inches). However, according to our analysis, this axial amplitude increment is correlated with the radial amplitude through expression (8.3.7), and as an energy exchange process, a number of turns are always required to build up the oscillation. Therefore, if we properly control the radial amplitude, and consider the very close radial separation between the two points where the unity resonance $\nu_r = 1$ and the nonlinear coupling resonance $\nu_r - 2\nu_z = 1$ happen in the Princeton cyclotron, it is then possible for a beam to passes through the extraction region without notable loss.

Figs. 8.3.5 and 8.3.6 show the axial motion of the nine sample particles of a 12 MeV proton beam, in the phase space(which is described as earlier) with the outer first harmonic field strengths of 1.5 and 2 gauss, respectively. In these figures, the horizontal axis denotes the number of RF cycles, and the vertical axis represents the axial departure from the median plane of the cyclotron, just as in Fig. 8.3.4.